THE *BRUCELLA* EFFECTOR GRHG1 REPROGRAMS THE HOST N-GLYCOME TO SUSTAIN INFECTION

A Dissertation

by

ANA LUCIA CABELLO AGUIRRE

Submitted to the Office of Graduate and Professional Studies of
Texas A&M University
in partial fulfillment of the requirements for the degree of

DOCTOR OF PHILOSOPHY

Chair of Committee,	Thomas A. Ficht
Co-Chair of Committee,	Paul deFigueiredo
Committee Members,	Kristin Patrick
	James Samuel
	Sara Lawhon
Head of Department,	Ramesh Vemulapalli

May 2020

Major Subject: Biomedical Sciences

ABSTRACT

The intracellular bacterium *Brucella* is a globally distributed pathogen that causes brucellosis, a disease of wildlife, domesticated animals, and humans. The *virB* Type IV secretion system (*virB*-T4SS) plays an essential role in bacterial pathogenesis, in part through the secretion into host cells of effector proteins that modulate host cell functions to promote pathogen survival, replication and persistence. To date, several *virB*-T4SS effectors have been identified and characterized in *Brucella abortus,* however no *B. melitensis* effector proteins have been identified or shown to play a role in bacterial pathogenesis. Here, we describe the identification and characterization of a novel effector protein BMEI1482 (Grhg1) that is translocated into macrophages in a *virB*-T4SS dependent fashion. Mechanistic studies revealed that Grhg1 reprograms glycosylation by binding proteins in the oligosaccharide transferase (OST) complex. Importantly, *B. melitensis* Grhg1 gene promotes bacterial replication *in vitro* and *in vivo* demonstrating its important role to sustain infection. Taken together, these findings provide mechanistic insights into *B. melitensis* intracellular lifecycle and demonstrate that this bacterium disrupts cell functions to promote pathogenesis through *virB*-T4SS effector proteins. In addition, this work provides a new paradigm for glycoproteome reprograming as a target for *Brucella* manipulation of host functions to promote disease.

DEDICATION

I dedicate my dissertation work to my husband for his encouragement and support throughout this life process. A special feeling of gratitude to my mother, father and brothers who were always there for me.

ACKNOWLEDGEMENTS

I would like to thank my major professors, Dr. Paul deFigueiredo and Dr. Thomas A. Ficht, for their support and for giving me the opportunity to work with them. Thanks to my committee members. Dr. Kristin Patrick, Dr. Sara Lawhon and Dr. James Samuel for their guidance and help throughout my formation as a PhD and development of my research project.

Special thanks to Dr. Garry Adams for the amazing conversations, advice and words of motivation he was always willing to offer.

A special thanks and love go to my handsome husband Sergio Castillo for his encouragement, patience and love.

Special thanks to my close friends Min Ju, Slim Zriba, Jamie Benn Felix, Omar Khalaf, Elena Gart, Luciana Fachini daCosta, Aseem Pandey, Saugata Mahapatra and Caitlin Older for all the good experiences and great talks we had together. I learned a lot from all of you.

I am extremely thankful to Dr. Delbert Gatlin and to his lab members, Bryan Ray, Fernando Yamamoto, Fernando Giron, Kequan (Paul) Chen, Clement de Cruz, Waldemar Rossi and Alton Burns for accepting me as a member of their lab family and always making me feel welcome.

Thanks to BSL3 team Wendy Wright, David Perez, Todd Wisner, Jessica Cobos, Susan Gater and Christine McFarland for always being there offering trainings, supervision, support and technical advice during my BSL3 work.

Special acknowledgements and thanks go to the Department Head of Veterinary Pathobiology, Dr. Ramesh Vemulapalli, and the graduate academic advisors Dr. Mike Criscitiello, Dr. Ashley Seabury, Dr. David Kessler, Kathie Smith, Demetria Cooper, Eleni Vonda, and Katharina Ojala for their time and support during my studies.

Lastly, I am extremely thankful to the College of Veterinary Medicine & Biomedical Science, Texas A&M University and to CONACYT for giving me the opportunity to accomplish my Ph.D. studies. I'm so proud of this episode in my life.

CONTRIBUTORS AND FUNDING SOURCES

This work was supervised by a thesis committee consisting of advisors Dr. Thomas A. Ficht, of the Department of Veterinary Pathobiology (VTPB) and co-advisor, Dr. Paul deFigueiredo, of the Department of Microbial Pathogenesis and Immunology (MPIM) along with professors Dr. James Samuel (MPIM), Dr. Kristin Patrick (MPIM) and Dr. Sara Lawhon (VTBP).

The S4TE bioinformatic analyses described in Chapter II was conducted by Dr. Damien Meyer and Dr**.** Christophe Noroy from the ASTRE research unit based in Montepellier, France.

The genetic interaction profile analyses (EMAP) described in Chapter III were led by Dr. Kristin Patrick of the Department of Microbial Pathogenesis and Immunology and were published in Cell systems in 2018. The confirmatory immunoprecipitation coupled with mass spectrometry experiments were performed, in part, by M.S. Hui-Qiang Feng and by lab personnel of Dr. William Russell lab, University of Texas Medical Branch. The secretion assay and the N-glycome studies were conducted and analyzed, in part, by Dr. Yuxin Mao and by Dr. Yehia Mechref lab personnel, respectively.

The Ph.D. student used bioinformatic tools to perform bioinformatic analyses that resulted in the selection of *Brucella* effector Grhg1 for further studies. All other biological experiments described in chapter III and the project proposal described in chapter IV were conducted and developed by the PhD student independently.

Graduate study was supported by a fellowship from Consejo Nacional de Ciencia y Teconolgia (CONACYT, Mexico; from 2013-2017) coupled with a Texas A&M university graduate research assistantship (from 2017-2019). The research project was made possible, in part, by funding from NIH, USDA, NSF, TAMU Agrilife Research, Qatar National Research Fund and DARPA.

NOMENCLATURE

B16M	*Brucella melitensis* strain 16M
virB-T4SS	virB Type 4 Secretion System
Grhg1	Global Reprogramming Host Glycome 1
BMEI1482	Gene locus of effector protein Grhg1
ER	Endoplasmic Reticulum
OST complex	OligoSaccharyl-Transferase complex
RPN1	Dolichyl-diphosphooligosaccharide glycosyltransferase subunit 1
RPN2	Dolichyl-diphosphooligosaccharide glycosyltransferase subunit 2
EMAP	Epistasis Mini-Array Profile
CHO	Carbohydrate
BMDMs	Bone Marrow Derived Macrophages
TEM-1 Fusions	Effector proteins labeled with ß-lactamase
TEM-1 Assay	Protein Translocation assay
RFG	Relative Fluorescence Glycan signal

TABLE OF CONTENTS

Page

LIST OF FIGURES

Page

LIST OF TABLES

Page

1. INTRODUCTION

1.1. *Brucella* as the etiological agent of a globally important zoonotic disease

Brucellosis is a widespread disease that affects domestic and wild animals around the globe and is transmissible to humans (Franc et al., 2018; Pappas et al., 2006). Approximately 500,000 new cases per year are reported worldwide, especially in rural areas of Middle-Eastern and Mediterranean countries, Africa, and Central and South America (Atluri et al., 2011). The main etiological agents of human brucellosis (also known as Malta fever, Mediterranean fever or undulant fever) are the Gram-negative intracellular bacteria *Brucella melitensis*, *B. abortus* and *B. suis* (Atluri et al., 2011). Routes of transmission involve 1) ingestion of unpasteurized milk or milk products from goats and cattle, 2) direct contact with infected animals (i.e. cattle, goats, pigs, sheep, dogs) via skin abrasions or mucous membranes or 3) accidental exposure to bacterial cultures in clinical laboratories via inhalation of aerosols (de Figueiredo et al., 2015; Pandey et al., 2016). In addition to wild type strains, current attenuated animal vaccine strains retain sufficient virulence and/or antibiotic resistance to cause considerable human morbidity (Brumell, 2012; Ficht and Adams, 2009).

Brucellosis is considered a systemic infection and since *Brucella* can easily survive intracellularly, chronic infections and relapses are observed. Symptoms in humans can vary from chills, night sweats, undulant fever and headaches. Severe conditions such as focal complications (e.g. joints, spine, and hepatosplenomegaly), cardiac and neurological problems have also been reported (de Figueiredo et al., 2015;

Franc et al., 2018; Pandey et al., 2016). In addition, studies have demonstrated an association between the presence of brucellosis during pregnancy and posterior complications such as spontaneous abortion, intrauterine fetal death, preterm delivery and congenital disorders (Brumell, 2012; Esmaeili, 2014; Vilchez et al., 2015; Voth et al., 2012).

To treat human brucellosis, the World Health Organization recommends a combination of antibiotics (doxycycline and rifampin) for a six-week course. However, studies have demonstrated the occurrence of disease relapses, a finding that indicates an urgent and crucial need for the development of novel alternative strategies for reliable and effective prevention and infection treatment (Atluri et al., 2011). Proposed alternative strategies for brucellosis prevention and treatment include vaccines, phage therapy and antivirulence drugs that specifically target bacterial virulence functions (Atluri et al., 2011). To develop therapies, it is fundamental to increase our knowledge at the molecular level of how *Brucella* manipulates the host to survive by characterizing the activities and contribution to pathogenesis of *vir*B-Type IV Secretion System (*vir*B-T4SS) effector proteins.

1.2. *Brucella* virB-T4SS effector proteins

During infection, *Brucella* is internalized by professional phagocytes via complement receptors, Fc receptors and scavenger receptor A (Jiang, 1992). The pathogen is then transported to sites of systemic infection where it invades nonprofessional phagocytic cells as well (Pei and Ficht, 2011). Once inside the cell,

Brucella can be found to reside within *Brucella*-containing vacuoles (BCVs) (Celli, 2015; Pei and Ficht, 2011). These compartments traffic to and fuse with the endoplasmic reticulum (ER). Mature BCVs are decorated with ER resident proteins (Celli, 2015; Celli et al., 2003). *Brucella* escapes from lysosomal degradation to reach the ER and establish its proliferative niche (Celli, 2015; Starr et al., 2008). The subcellular trafficking of the pathogen from the host plasma membrane to an ER-like compartment includes interactions between BCVs and early endosome, late endosome, and lysosome membranes (Figure 1.1) (Celli, 2015; Starr et al., 2008). The *vir*B-T4SS of the pathogen plays a critical role in directing these subcellular trafficking events. Mutant *Brucella* strains that lack a functional *vir*B-T4SS fail to traffic productively (Atluri et al., 2011; Celli, 2015). Instead, these organisms travel from the plasma membrane to lysosomes, where they are rapidly destroyed by the acidic pH and hydrolytic activities that are present in this organelle (Atluri et al., 2011; Celli, 2015; Lu et al., 2015).

The T4SS is a crucial multi-protein complex widespread in *Bacteria* (Tseng et al., 2009). In *Brucella spp.*, the T4SS is encoded by *vir*B operon which consists of 12 genes (virB1-12) located on chromosome II (Boschiroli et al., 2001). The *vir*B operon expression is regulated by the transcription factor VjbR, a protein that belongs to the family of LuxR quorum sensing (QS) regulators (Delrue et al., 2005). The *virB*-T4SS is an essential virulence factor necessary for *Brucella*'s intracellular survival and virulence (Figure 1.2) (de Jong et al., 2010; de Jong and Tsolis, 2012; Tseng et al., 2009). Based on other well-characterized intracellular bacteria systems (Tseng et al., 2009), it is speculated that *Brucella's vir*B-T4SS translocate effector proteins across the bacterial

membrane into the host cytosol to modulate interactions between *Brucella* and host cells (Byndloss and Tsolis, 2016; Lacerda et al., 2013). To expand our knowledge regarding the intracellular lifecycle of *Brucella*, it is essential to identify and characterize these effector proteins.

In other well-studied microorganisms, such as *Legionella spp*. and *Coxiella spp*., effector proteins disrupt signaling pathways and perpetuate the infection by favoring bacterial growth and pathogenesis (de Felipe et al., 2008; Larson et al., 2015; Newton et al., 2014; Ninio et al., 2009; Weber et al., 2013). A comparison between *Brucella*'s effectors with well-known effector proteins of other microorganisms (i.e. *Coxiella spp.* and *Legionella spp*.) suggests that, during infection, *Brucella*'s effectors might be involved in events such as 1) inhibition of enzymatic degradation by exclusion of specific markers that recruit lysosomes, 2) resistance to the severe intracellular environment of host cells, 3) transport to the ER by acquisition of ER markers, 4) and interaction and/or regulation of secretory and immune pathways (de Felipe et al., 2008; Larson et al., 2015; Newton et al., 2014; Ninio et al., 2009; Weber et al., 2013).

Although it is well-known that *vir*B-T4SS is necessary to sustain bacterial infection, since *Brucella spp.* strains lacking a functional *vir*B-T4SS are highly attenuated *in vitro* (macrophages) and *in vivo* (mouse model) (Foulongne et al., 2000; Hong et al., 2000; O'Callaghan et al., 1999), the attribution of biological roles to *Brucella's vir*B-T4SS effector proteins still remain a topic in progress (de Barsy et al., 2011; Dohmer et al., 2014; Herrou and Crosson, 2013; Keestra-Gounder et al., 2016; Marchesini et al., 2011; Marchesini et al., 2016; Miller et al., 2017). Using a

combination of bioinformatic and biochemical approaches, authors have begun to identify and characterize effectors (Ke et al., 2015). To date, some effector proteins secreted by *virB*-T4SS have been identified in *B. abortus* **(**Table 1) (Ke et al., 2015), however the biological function during bacterial infection has been attributed to only a few of them (Table 1).

VceC (BAB1_1058) an effector protein that is co-regulated with the *vir*B operon during *Brucella abortus* infection binds to BiP and elicits an IRE1 alpha-dependent response that contributes to evoking innate immune responses through downstream activation of NOD1 and NOD2 (de Jong et al., 2013; Keestra-Gounder et al., 2016). RicA (BAB1_1279), an effector with similarities to acetyltransferases of the gamma carbonic anhydrase-like family, recruits active (GTP-bound) Rab2 to the BCVs and modulates bacterial intracellular trafficking (de Barsy et al., 2011). BPEI123 (BAB2_0123), a small hypothetical protein with a central coiled coil motif is associated to BCV's and interacts with a human alpha-enolase (ENO-1) to promote intracellular replication (Marchesini et al., 2011; Marchesini et al., 2016). BspB (BAB1_0712), contains a SCOP structural domain (d2gsaa) present in pyridoxal phosphate (PLP)-dependent transferases flanked by 2 predicted transmembrane (TM) domains (Myeni et al., 2013). BspB interacts with the conserved oligomeric Golgi (COG) tethering complex and redirects Golgi-derived vesicles to the BCV, contributing to *Brucella* replication (Miller et al., 2017). BtpA (BAB1_0279) and BtpB (BAB1_0756) effectors contain toll-interleukin-like receptor (TIR) domains and inhibit the maturation of dendritic cells (Salcedo et al., 2013b; Salcedo et al., 2008). BtpA specifically targets the host signaling

adapter protein, MyD88 adapter-like (MAL)/TIRAP, through a BB loop region within TIR domain and inhibits toll-like receptor (TLR) signaling via MyD88 (Radhakrishnan and Splitter, 2010; Radhakrishnan et al., 2009; Salcedo et al., 2013b; Salcedo et al., 2008). Whereas TcpB, the *B.melitensis* BtpA homolog, induces the upregulation of UPR target genes (Smith et al., 2013). SepA (BAB1_1492) an effector localized in horizontally transmitted pathogenic islands (Dohmer et al., 2014), is necessary to efficiently invade host cells and is involved in the exclusion of the lysosomal marker (LAMP-1) (Dohmer et al., 2014). Since many molecular aspects of *Brucella* pathogenesis remain unknown, the identification of novel *virB*-T4SS effectors and the characterization of their biological and molecular functions, as well as their target host pathways, will significantly expand our understanding of the intracellular lifecycle of *Brucella spp.*

1.3. Research relevance and overall goals

Brucella has evolved a variety of specific adaptations to survive and replicate inside the host (de Figueiredo et al., 2015). An important mechanism that *Brucella* uses for virulence is a macromolecular machine, the T4SS, encoded by the *virB* operon (de Jong and Tsolis, 2012). This secretion system translocates effector proteins that are essential to establishment of a replicative niche (rBCV) by modulating host functions to the pathogen's advantage (Ke et al., 2015). Understanding the mode of action of bacterial effectors has been key to deciphering the pathogenic molecular mechanisms of many intracellular bacteria, as well as their normal function in uninfected cells (Welch,

2015). Only a handful of *Brucella* effectors have been discovered and shown to target specific host mechanisms including secretory pathways and the host immune response (de Barsy et al., 2011; de Jong et al., 2013; de Jong et al., 2008; Dohmer et al., 2014; Keestra-Gounder et al., 2016; Marchesini et al., 2011; Marchesini et al., 2016; Miller et al., 2017; Myeni et al., 2013; Salcedo et al., 2013b; Salcedo et al., 2008). Molecular mechanisms have been poorly characterized, impeding a better understanding of the intracellular lifecycle of *Brucella* (de Figueiredo et al., 2015). To develop novel interventions to address brucellosis, researchers must gain a better understanding of how the pathogen interacts with host cells. Therefore, the overall goal of this work is to identify novel *virB*-T4SS effector proteins and to elucidate their molecular and biological functions using *B. melitensis* for these studies. Hence, this dissertation identifies and characterizes novel *virB*-T4SS effector proteins found in *B. melitensis* and demonstrates the molecular mechanism of a selected effector with the purpose of improving our understanding of *Brucella* pathogenesis, a zoonotic disease of major importance, threatening animal and human health worldwide.

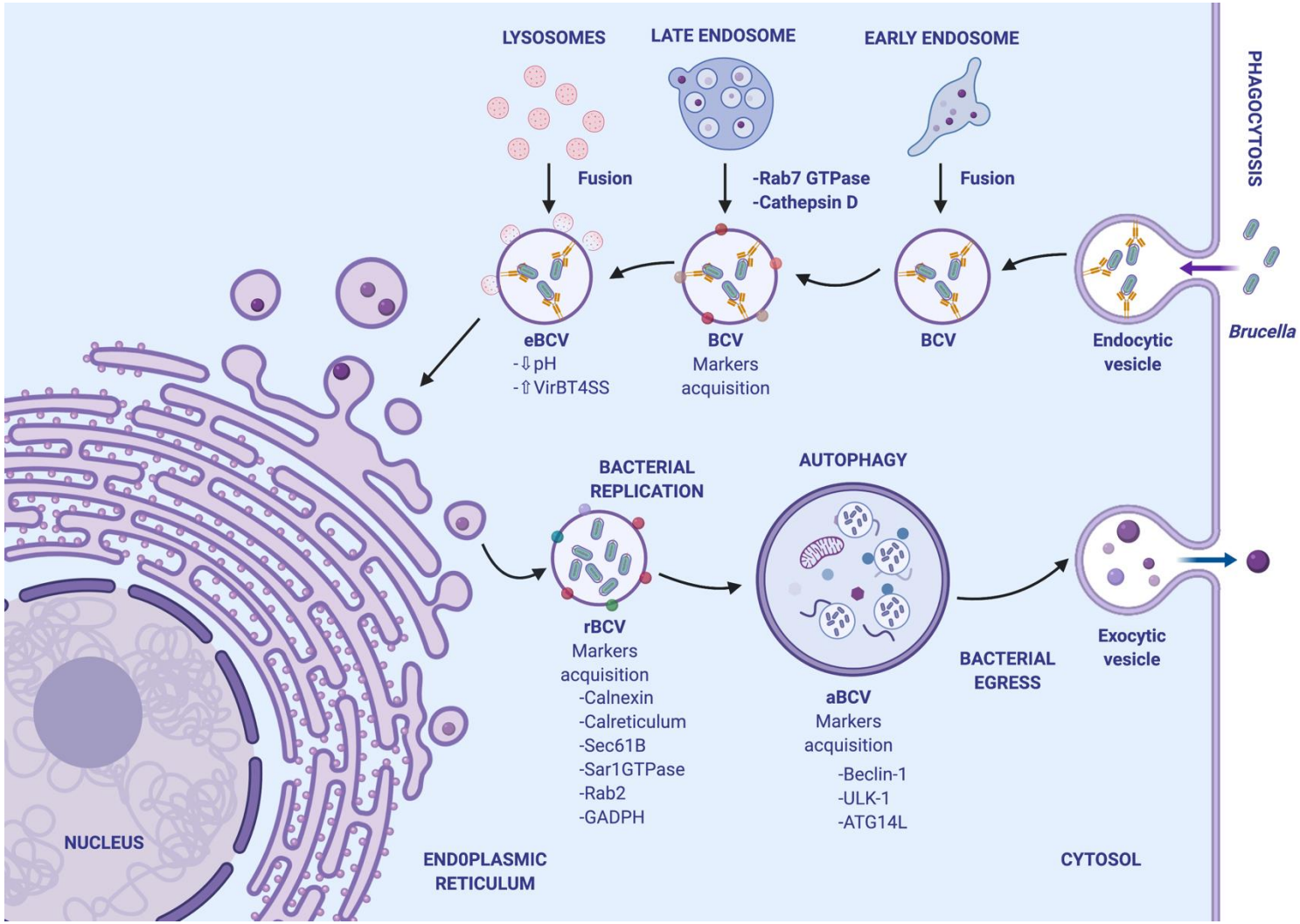

Figure 1.1 Model of *Brucella* intracellular trafficking in mammalian cells adapted from (Celli, 2015).

Table 1.1 Description of the 15 *virB*-T4SS effectors secreted by *Brucella abortus*. Each column summarizes results from studies performed with each effector. Adapted from (Ke et al., 2015).

T4SS-EP[x]	ORF in Ba*	ORF in Bm†	Mice Phenotype	Mice IR[x]	MØ^ Phenotype	MØ^ IR[x]	Cellular localization	Host target	Function
VceA	BAB1_1652	BMEI0390	N/A	N/A	N/A	N/A	N/A	N/A	N/A
VceC	BAB1_1058	BMEI0948	C57BL/6 mice. No replication deficiency (14 d p.i.)	IL-6 and spleen weight reduced	No Phenotype (Test: 24h p.i.)	TNF-α and IL-6 decreased	ER	BiP/Grp78, NOD1/NOD2	Activates UPR and pro-inflammatory response
RicA	BAB1_1279	BMEI0736	N/A	N/A	N/A	N/A	Cytosol	Rab2	Regulates vesicle trafficking
BtpA	BAB1_0279	BMEI1674	BALB/c mice. No replication deficiency (30, 60, 90, 130 d p.i.)	No phenotype	No Phenotype (Test: 48h p.i.)	TNF-α increased	N/A	MAL	Inhibits TLR pathway
BtpB	BAB1_0756	BMEI1216	BALB/c mice. No replication deficiency (30, 60, 90, 130d p.i.)	Higher number of granulomas in spleen	No Phenotype (Test: 48h p.i.)	IL-12 increased	N/A	N/A	Inhibits TLR pathway
BspA	BAB1_0678	BMEI1290	C57BL/6 mice. Liver, spleen. No replication deficiency (42d p.i.)	N/A	No Phenotype (Test: 24h p.i.)	N/A	N/A	Not tested	Inhibits secretory pathway
BspB	BAB1_0712	BMEI1259	C57BL/6 mice. Liver, spleen. Replication deficiency (42d p.i.)	N/A	Bacterial replication deficiency (Test: 24h p.i.)	N/A	ER	COG complex	Inhibits secretory pathway, delayed rBCV biogenesis
BspC	BAB1_0847	BMEI1135	N/A	N/A	N/A	N/A	Golgi	N/A	N/A
BspE	BAB1_1671	BMEI0372	N/A	N/A	N/A	N/A	Perinuclear	N/A	N/A
BspF	BAB1_1948	BMEI0199	C57BL/6 mice. No replication deficiency (42d p.i.)	N/A	No Phenotype (Test: 24h p.i.)	N/A	Cytosol and plasma membrane	N/A	Inhibits secretory pathway
BPE005	BAB1_2005	BMEI0067	N/A	N/A	N/A	N/A	N/A	N/A	N/A
BPE043	BAB1_1043	BMEI0961	N/A	N/A	N/A	N/A	N/A	N/A	N/A
BPE275	BAB1_1275	BMEI0739	N/A	N/A	N/A	N/A	N/A	N/A	N/A
BPE123	BAB2_0123	BMEII1111	N/A	N/A	THP1 cells. Replication deficiency (Test: 24h p.i.)	N/A	N/A	N/A	N/A
SepA	BAB1_1492	BMEI0539	C57BL/6 mice. Spleen. No replication deficiency (15d p.i.)	N/A	ΔSepA replication deficency (Test: 24h p.i.)	N/A	N/A	N/A	Inhibits BCV fusion with lysosome

T4SS-EP[x]: TSS effector proteins; ORF: Open reading frame; Ba[*]: *Brucella abortus*, Bm[†]: *Brucella melitensis*; MP[♦]: mouse phenotype; IR[♣]: Immune response; MØP[◊]macrophage phenotype; MØ^: Macrophage, CL[Φ]: cellular localization (Ke et al., 2015).

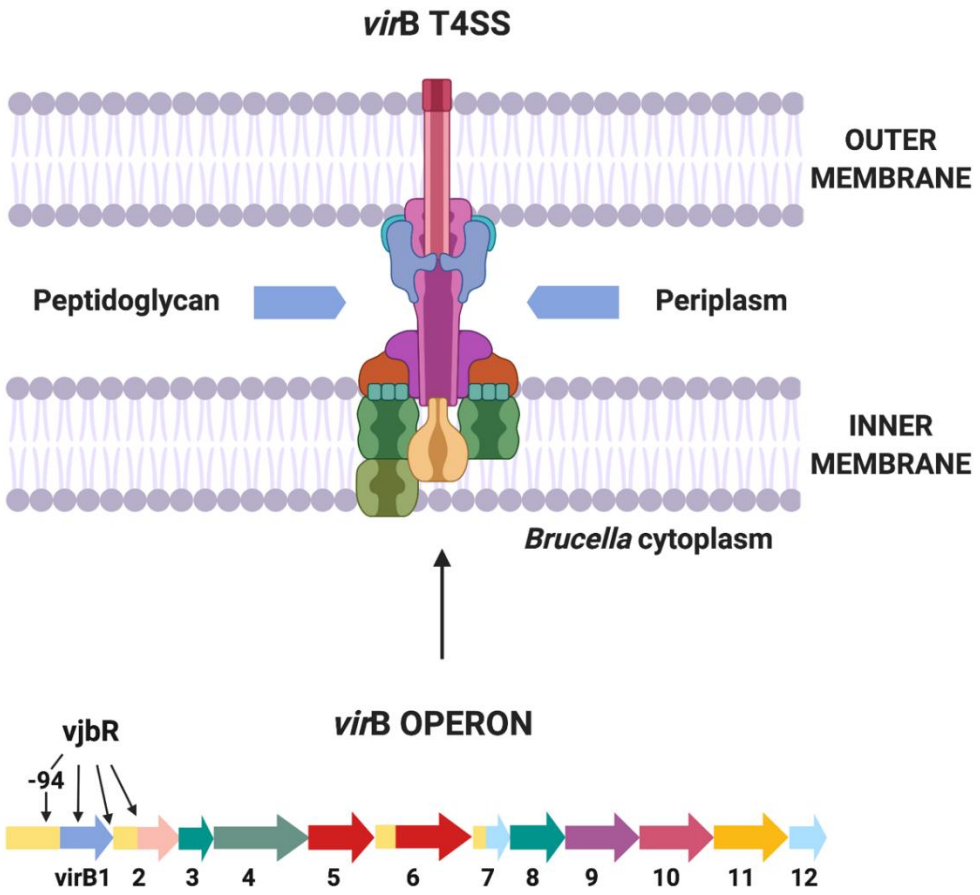

Figure 1.2 Schematic representation of *Brucella's* T4SS encoded by *virB* operon (virB1-12) regulated by the transcription factor VjbR. VjbR: Lux QS family transcription factor, -94: denotes virB promoter box, virB1-12: genes conforming virB operon. Adapted from (de Jong and Tsolis, 2012).

2. IDENTIFICATION AND CHARACTERIZATION OF NOVEL *BRUCELLA MELITENSIS VIRB*-T4SS-EFFECTOR PROTEINS

2.1. Introduction

The type IV secretion system (T4SS) in *Brucella* is a crucial multi-protein complex encoded by the *virB* operon (genes virB1 to 12), which delivers effector proteins into host cells to prevent bactericidal responses and perpetuate infection (Atluri et al., 2011). To date, 15 *Brucella abortus* effector proteins secreted by *virB*-T4SS have been identified using different methodologies that were successfully applied to other intracellular pathogens (e.g. *Legionella pneumophila, Coxiella burnetii, Agrobacterium tumefaciens* and *Bartonella henselae*) (Ke et al., 2015). This collection represents a significantly smaller number of effectors than in other intracellular bacterial vacuolar pathogens; for example, more than 330 and 133 T4SS substrates are described in *L. pneumophila* and *C. burnetii*, respectively (Chen et al., 2010; Ninio et al., 2009). Common screening strategies used to identify *Brucella* effector proteins include: a) *in silico* screening for proteins with C-terminal features (positive charge, alkaline or hydrophobic), arginine-rich motifs, Sec-dependent secretion signals and eukaryotic-like domains (Marchesini et al., 2011; Myeni et al., 2013); b) co-regulation with the *virB* operon (de Jong et al., 2008); and c) *in vitro* screening for interaction with mammalian proteins associated with phagosomes, or with other host proteins (de Barsy et al., 2011). However, some major disadvantages of current screening methods for identification of candidate effector proteins are 1) failure to screen for all known effector protein features,

2) infeasibility of screening the complete bacterial genome, and 3) challenges associated with performing high throughput screening with a BSL3/select agent pathogen. Each of these factors limit the number of candidate effector proteins that can be identified. To tackle these problems, a search algorithm for T4SS effectors (S4TE) was developed by Meyer *et al*. (Meyer et al., 2013). The S4TE program can computationally analyze a broad spectrum (i.e. α- and γ- proteobacteria) of the bacterial genome and proteome allowing its use as a method for rapidly identifying candidate T4SS effector proteins (Meyer et al., 2013). The authors validated S4TE with experimentally confirmed T4SS effectors of *L. pneumophila*. Subsequently, validated T4SS effectors were found in genomes of α- and γ- proteobacteria as well (i.e. *B. abortus, Erlichia chaffeensis, Anaplasma marginale* and *C. burnetti*) (Meyer et al., 2013). Therefore, we hypothesized that novel *virB*-T4SS effectors could be identified in *B. melitensis* by using this bioinformatic approach. This chapter describes the bioinformatics pipeline that resulted in the identification and characterization of relevant candidate *virB*-T4SS effectors of *B. melitensis*. Taken together, this work defined novel candidate effector proteins that potentially play significant roles during *Brucella* intracellular parasitism.

2.2. Results and discussion

2.2.1. Identification of candidate *Brucella* virB-T4SS effector proteins

The S4TE bioinformatics suite was applied to generate a ranked list of *Brucella* candidate effector proteins (Table 2.2). This analysis was carried out in the two most globally prevalent strains that affects humans, *B. melitensis* strain 16M and *B. abortus*

strain 2308; as well as in *B. abortus* strain 19, a vaccine strain which has been used in brucellosis eradication programs in developing countries, that sustains some residual virulence to animals and that can cause disease in humans as well (Pandey et al., 2016). The analysis revealed a total of 321 candidate effector proteins from which 38 candidates are specific to *B. melitensis* 16M, 44 candidates are specific to *B. abortus* 2308, and 48 candidates are specific to *B. abortus* S19. Moreover, 45 candidate effectors are common to all three *Brucella* strains (Table 2.3, Figure 2.2). Because differences in intracellular trafficking, survival and replication have been observed among *Brucella* species (Salcedo et al., 2013a), only candidate effector proteins common to all three *Brucella* strains were selected for further analyses (n=45). The common effector sequences were selected with the purpose of learning biological roles of effector proteins that are homogenous among *Brucella* species.

An examination of the selected hit list (n=45) revealed that the program S4TE identified 7 out of 15 previously reported effectors translocated by *vir*B-T4SS of *B. abortus* during bacterial infection (Ke et al., 2015). Then, 3 (VceC, RicA and BPE123) out of the 7 are characterized at the biological level (Ke et al., 2015). The hit list revealed proteins with assorted combinations of T4SS effectors hallmarks (Table 2.3). For example, BMEI0948, the homolog of VceC a well-studied T4SS effector (de Jong et al., 2013; de Jong et al., 2008; Keestra-Gounder et al., 2016), contained E-block (glutamate-rich sequence EEXXE), C-ter basicity and global hydrophilicity features. BMEII1111, the homolog of BPE123 (Marchesini et al., 2011; Marchesini et al., 2016), contained *de novo* regulatory motif (a *cis*-acting regulatory sequence found in *Legionella*

to regulate numerous effectors), coiled coil domain, and C-ter basicity. BMEI0736, the homolog of RicA, an effector that has a role in BCV trafficking (de Barsy et al., 2011; Herrou and Crosson, 2013; Nkengfac et al., 2012), contained C-ter charge and C-ter basicity. However, no protein contained all the hallmarks of T4SS effectors, a finding that is consistent with T4SS effector proteins from other bacterial systems (Alvarez-Martinez and Christie, 2009).

2.2.2. A sequence analysis of candidate virB-T4SS effectors showed genetic variations among *B. melitensis* strains 16M, 2308 and S19

To determine how genetically conserved are the selected candidate effectors (n=45) across analyzed *Brucella melitensis* strain 16M, *B. abortus* strains 2308 and S19, nucleic acid and amino acid sequences were obtained from PATRIC (Wattam et al., 2017) and analyzed using CLC genomic workbench software (v.10.1.1). Out of 45 analyzed genes, 10 were highly conserved across *Brucella* species since no mutations were present at nucleic acid and amino acid levels (BMEI0304, BMEI0610, BMEI0736, BMEI0908, BMEI1279, BMEI1445, BMEI1751, BMEII0116, BMEII0659, BMEII1013) (Figure 2.3). 8 genes had at least a single nucleotide mutation in *B. melitensis*; however, such changes led to no amino acid substitution (BMEI0359, BMEI0527, BMEI0810, BMEI1044, BMEI1531, BMEI1577, BMEII1067, BMEII0041) (Figure 2.3). 3 genes (BMEI1968, BMEI0328, BMEI658) had a single nucleotide mutation in *B. melitensis* that led into a substitution of valine for alanine amino acid; however, its chemistry was conserved because both amino acids are non-polar (Figure

2.3). The remaining 24 genes presented a high frequency of single nucleotide point mutations in *B. melitensis* that led into relevant amino acid substitutions, as well as, gene deletions and insertions that might lead into an alternative or even non-functional protein structure. Genes BMEI0321 and BMEI0370 were the only two genes that presented gene insertions in *B. abortus* 2308 but were highly conserved across *B. melitensis* 16M and *B. abortus* S19 strains (Figure 2.3).

2.2.3. An analysis of candidate effectors across Brucella spp. reference strains revealed a high frequency of genetic variation

Next, the selected candidate effector nucleotide sequences were obtained from PATRIC (Wattam et al., 2017) and analyzed with CLC workbench v.10.1.1 using the nucleotide sequence alignment tool. The sequence alignment analysis was performed to search for 1) gene deletions, 2) gene insertions, 3) single nucleotide polymorphism (SNPs) across *Brucella* species.

The analysis of reference strains revealed that 25 out of 45 candidate effectors presented relevant gene deletions in all *Brucella* species (BMEI0948, BMEI0359, BMEI1057, BMEI1837, BMEI0610, BMEI0321, BMEI0908, BMEI1751, BMEI1088, BMEI1694, BMEI1895, BMEI0238, BMEI0657, BMEI1298, BMEI1445, BMEI0740, BMEI0379, BMEII1111, BMEII0533, BMEII0314, BMEII1013, BMEII0297, BMEII0041, BMEI1482, BMEI1361) (Figure 2.4). The species with the highest amount of candidate effectors carrying gene deletions (10 out of 25) was *B. ovis.* The species with the lowest amount of candidate effectors carrying gene deletions (2 out of 25) was *B. abortus* 2308 (Figure 2.4). Also, gene insertions were found in 5 out of 45 candidate

effectors across most of *Brucella* species, except for *B. melitensis* 16M (BMEI0370, BMEI0908, BMEI0321, BMEI0238 and BMEII0116); where *B. neotomae* and *B. suis* presented the highest amount of candidate effectors with gene insertions (3 out of 5) (Figure 2.4). Finally, 43 out of 45 candidate effector genes had single nucleotide polymorphisms (SNPs) across all reference *Brucella* species. Only genes BMEI1279 and BMEII0659 were highly conserved, since no species presented any type of mutation. In *B. ovis,* the gene BMEI0908 had the highest amount of SNP's. In *B. suis* 1330, *B. microti* and *B. canis* the gene BMEI1694 was absent. In *B. pinnipedialis* and *B. ceti* the gene BMEI1658 was absent (Figure 2.4). All the previously observed genetic changes led into frameshift mutations with altered and/or potentially nonfunctional candidate effector proteins.

2.2.4. A sequence analysis of *Brucella melitensis* clinical isolates revealed candidate effectors prevalence

Using the protein comparison service from PATRIC (Wattam et al., 2017) genetic prevalence of selected 45 candidate effectors across clinical isolates of *B. melitensis* was evaluated. The analysis of 121 clinical isolates of *B. melitensis* revealed that 11 out of 45 candidate effectors were absent in at least one clinical isolate (BMEI1658, BMEII0314, BMEI1577, BMEII0297, BMEI1057, BMEI1694, BMEI0321, BMEI0948, BMEI0736, BMEI1751, BMEI1837) (Figure 2.5). The gene that presented the highest absence rate was BMEI1658 (absent in 75 out of 121 strains), whereas genes BMEI1751 and BMEI1837 were absent in only 1 out of 121 strains

(Figure 2.5). The absence of gene BMEI1658 was more frequent in human (47 out of 75) and sheep (12 out of 28) clinical isolates. An interesting feature found in human clinical isolates that lacked BMEI1658 was the absence of additional genes such as BMEI1057, BMEII0314, BMEI0321, BMEI1694, BMEI0948 and BMEI0736. Finally, another gene that was absent, although in less frequency (9 out of 121), was BMEI1577 coupled with an absence of BMEII0297 and BMEI0736 (Figure 2.5). These results indicate that BMEI1658 gene is highly specific to animal strains, which makes it a potential candidate marker to differentiate among animal and human *B. melitensis* strains for diagnostic purposes.

2.2.5. An analysis of bacterial pathogens genomes revealed candidate virB-T4SS effector proteins specific to *Brucella melitensis*

Lastly, an additional bioinformatics analysis was performed to further refine the list of candidate effectors, aiming to generate a list of high priority genes to pursue in future biological experiments. The protein comparison service from PATRIC was used (Wattam et al., 2017) to learn genetic specificity of selected 45 candidate effectors across available reference strains of a diverse spectrum of pathogens (n=82). The pathogens used in the analysis consisted of a set of bacterial species that express secretion systems and belonged to the classes α-, β-, δ-, ε-proteobacteria, actinomycetales, chlamydiales, bacilli, clostridia and spirochaetales. Homology was determined by their sequence coverage (>30%) and percentage of identity (>10%) (Wattam et al., 2017). Analysis showed that 41 candidate effectors presented at least one

homologous sequence to other bacterial pathogens. Significative homologous sequences to candidate effector BMEI0321 and BMEII0659 were frequently observed in analyzed pathogen genomes (82 out of 82 and 79 out of 82, respectively). This indicates a lack of candidate effector specificity to *B. melitensis* 16M strain. Genes BMEI1279, BMEI1658, BMEI1694, BMEI1361 were highly specific to *B. melitensis* 16M strains since no pathogen genome showed significative homologous sequences to these genes (0 out of 82) (Table 2.4). Based on: 1) the genetic conservation of effectors among *B. melitensis* 16M, *B. abortus* 2308 and *B. abortus* S19, 2) prevalence of candidate effectors among *B. melitensis* clinical isolates and 3) candidate effectors specificity to *B. melitensis* (low frequency of homologous sequences in other bacterial pathogens), 6 effectors were selected for further analyses (Figure 2.6).

Membrane proteins serve as highly active mediators of cell pathways that take place between organelles and the cytosol. Since bacterial effectors can either mimic or modify activity of endogenous host cell proteins, majority of effectors that carry transmembrane eukaryotic-like domains are involved in protein-protein interactions and interfere with host cellular processes to facilitate bacterial replication (Kahsay et al., 2005). Based on this hypothesis and to facilitate the selection of a single effector for an in-depth biological analysis, a bioinformatics approach was explored to find transmembrane sequence domains. Briefly, the 6 selected hits were analyzed using TMHMM 2.0 server, a tool that predicts transmembrane helices in proteins based on a hidden Markov model and developed by Anders Krogh and Erik Sonnhammer (Kahsay

et al., 2005). Analysis showed BMEI1482 candidate as the only protein with 7 transmembrane domains (Figure 2.6).

2.2.6. Candidate virB-T4SS effector BMEI1482 is localized in host endoplasmic reticulum

To gain insight into the biological functions of the BMEI1482 *vir*B-T4SS candidate effector, the subcellular localization in cells was determined. HeLa cells have proven a useful model system for elucidating interactions between *Brucella* and host cells (de Jong et al., 2013; Myeni et al., 2013). Ectopically expressed BMEI1482-eGFP displayed an ER-like staining, a very similar pattern to the one found in the well-studied effector VceC (BMEI0948) (Figure 2.7). VceC is known to localize in ER and interact with components of ER stress (de Jong et al., 2013). In addition to these findings, bioinformatics analysis revealed that a DUF domain found in BMEI1482 by S4TE, is homologous to TMEM208, a protein domain found in eukaryotic resident proteins involved in ER stress and autophagy (Graham et al., 2016; Zhao et al., 2013). Based on that, the ER and nucleus were stained to learn subcellular localization of BMEI1482. Data showed that BMEI1482-eGFP colocalized with calreticulin, an ER-resident protein, suggesting a specific localization in this cellular compartment (Figure 2.7). These results indicate that BMEI1482 is part of the growing number of *Brucella* effectors that targets the ER (Ke et al., 2015), such observations suggest that BMEI1482 might be involved in secretory pathway disruption to sustain infection.

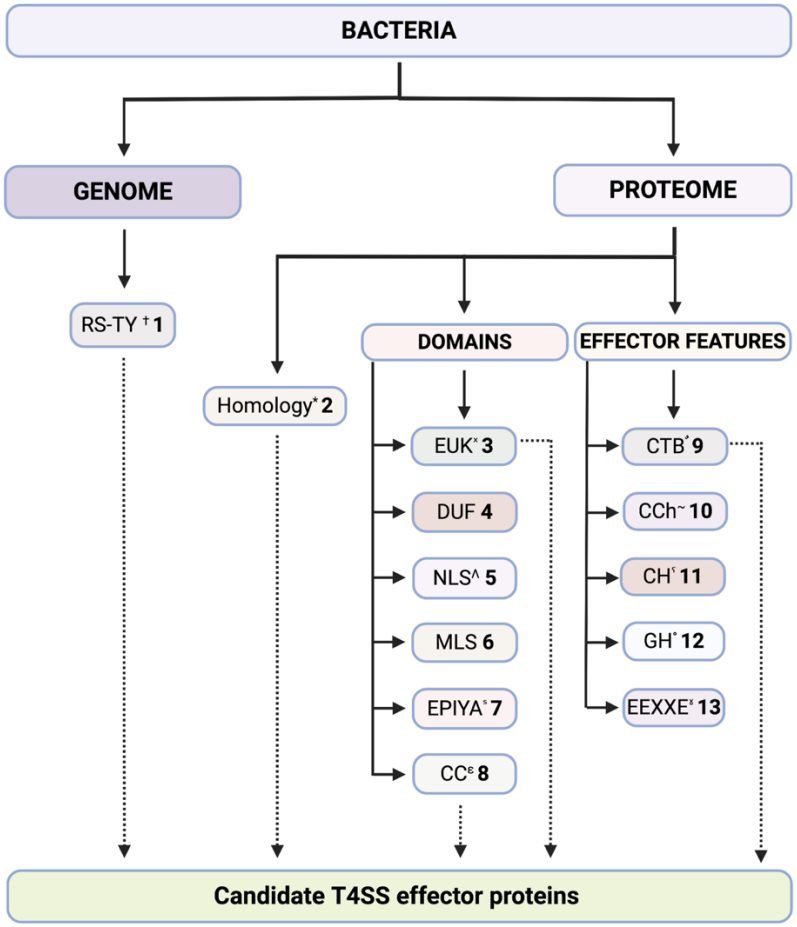

Figure 2.1 Flowchart of S4TE program representing effector hallmarks searched during genome and proteome screening of candidate effectors. Adapted from (Meyer et al., 2013). Detailed description of effector features is shown in table 2.1.

Table 2.1 Description of the 13 effector features considered in S4TE program to screen a bacterial proteome and genome. Adapted from (Meyer et al., 2013).

Abbreviation	Feature number	Description
RS-TY†	1	De novo motif search: RRRSNTTTTY motif in the -300 bp
Homology*	2	Homology: Sequence identity to a known effector molecule; Blast against effector database (e-value = 10^{2})
EUK^{x}	3	Euk-like domains: Presence of eukaryotic domain: 58 eukaryotic domains
DUF	4	Prok-like domains: 3617 Domain of Unknown Function (DUF) domains
NLS$^{\wedge}$	5	NLS (nuclear localization signal): Monopartite NLS; K-[KR]-[KR]-[KR]-[KR]-[KR] and bipartite NLS; K-[KR]-X(6,20)- [KR]-[KR]-[KR]
MLS	6	MLS (mitochondrial localization signal): Probability of a sequence containing mitochondrial targeting peptide (P > 0.95)
EPIYA^{s}	7	Prenylation domain: CaaX at the C-terminal; “C” represents a cysteine residue, “a” denotes an aliphatic amino acid and “X” is one of four amino acids
CC‡	8	Secondary structure - Coiled coils: Probability of a coiled-coil structure for windows of 28 residues through a protein sequence (P > 0.95)
CTB*	9	C-ter basicity: ≤ 3 [HRK] in the C-terminal 25 amino acids
CCh~	10	C-ter charges: Charge of C-terminal 25 amino acids ³2; C-ter charge = number of [HRK]-number of [ED]-1 (COO^{-})
CH$^{\varsigma}$	11	C-ter hydrophobicity: Hydrophaty of C-terminal 25 amino acids; hydrophobic reside at the -3rd or -4th position
GH°	12	Global hydrophilicity: Hydropathy of total protein < -200
EEXXE$^{\gamma}$	13	E-block: EEXXE in the C-terminal 30 amino acids

Feature number*: used to describe flowchart of Figure 3.

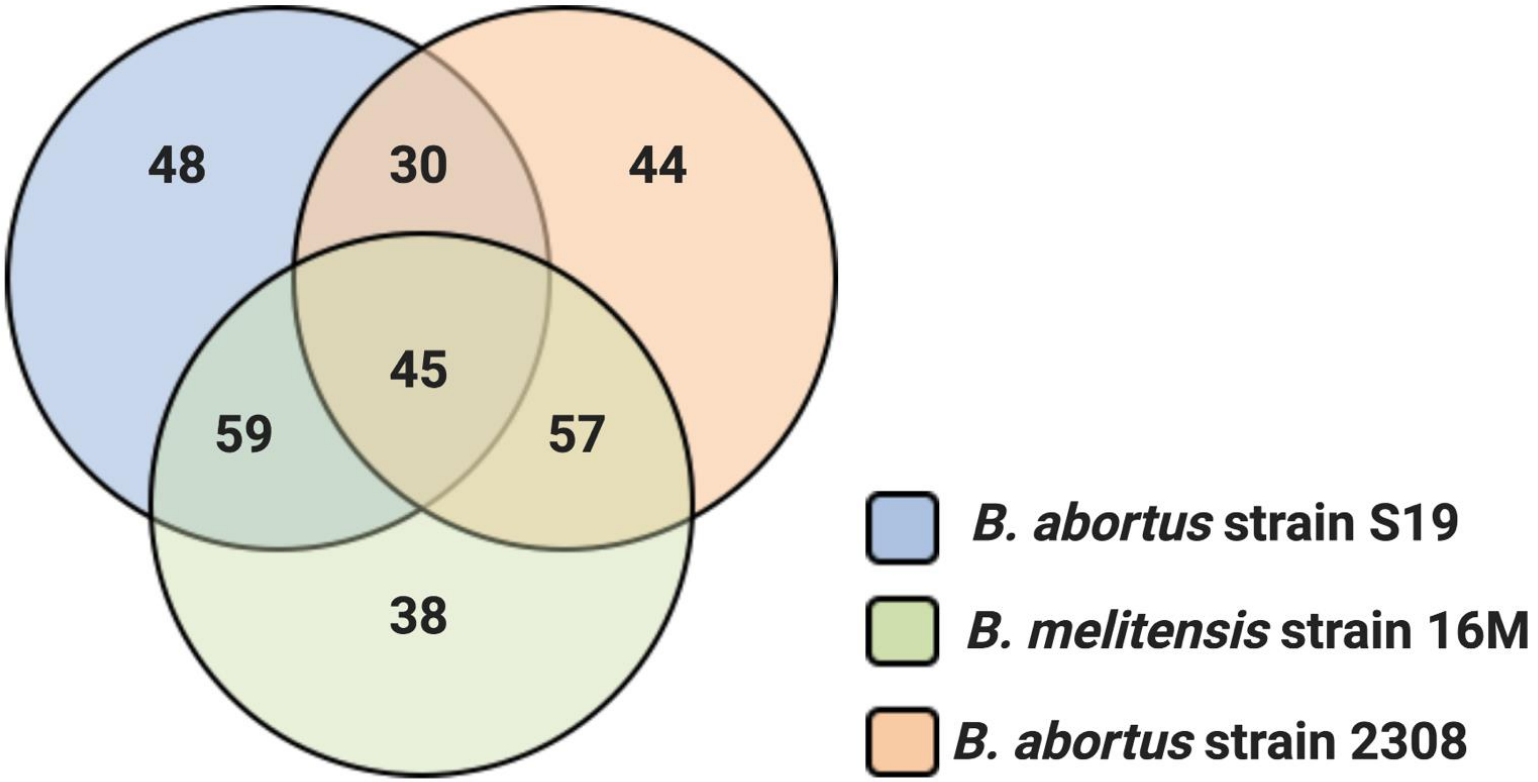

Figure 2.2 Venn diagram representing candidate effector proteins found in each *Brucella* strain. Each color indicates a strain: S19 blue, 16M green, 2308 red. Overlapping colors indicates candidate effector genes shared among the color-coded strains.

Table 2.2 Ranked list of candidates T4SS effector proteins. Each column represents a *Brucella* strain: 16M, S19 and 2308. Candidate T4SS effectors are color-coded according to presence or absence among the three analyzed species.

Brucella strain		
16M	2308	S19
		BAbS19_I00100
		BAbS19_I01350
		BAbS19_I01790
		BAbS19_I02070
		BAbS19_I03160
		BAbS19_I04450
		BAbS19_I04460
		BAbS19_I05030
		BAbS19_I06000
		BAbS19_I06290
		BAbS19_I08500
		BAbS19_I10460
		BAbS19_I11070
		BAbS19_I12100
		BAbS19_I12550
		BAbS19_I12830
		BAbS19_I13500
		BAbS19_I14070
		BAbS19_I14270
		BAbS19_I14830
		BAbS19_I15580
		BAbS19_I16400
		BAbS19_I17080
		BAbS19_I17150
		BAbS19_I17490
		BAbS19_I17500
		BAbS19_I17530
		BAbS19_I18030
		BAbS19_I18630
		BAbS19_I18800
		BAbS19_I19030
		BAbS19_I19650
		BAbS19_I20070
		BAbS19_I20130
		BAbS19_I20260
		BAbS19_II0030
		BAbS19_II0335
		BAbS19_II0456
		BAbS19_II0489
		BAbS19_II0527
		BAbS19_II0581
		BAbS19_II0585
		BAbS19_II0593
		BAbS19_II0619
		BAbS19_II0652
		BAbS19_II0818
		BAbS19_II0851
		BAbS19_II1073
	BAB1_0010	
	BAB1_0143	
	BAB1_0146	
	BAB1_0175	
	BAB1_0188	
	BAB1_0220	
	BAB1_0288	
	BAB1_0346	
	BAB1_0361	
	BAB1_0508	
	BAB1_0537	
	BAB1_0640	
	BAB1_0672	
	BAB1_0910	
	BAB1_1344	
	BAB1_1444	
	BAB1_1508	
	BAB1_1530	

Brucella strain		
16M	2308	S19
	BAB1_1567	
	BAB1_1586	
	BAB1_1665	
	BAB1_1834	
	BAB1_1868	
	BAB1_1873	
	BAB1_1922	
	BAB1_2005	
	BAB1_2032	
	BAB1_2089	
	BAB1_2146	
	BAB1_2152	
	BAB1_2165	
	BAB2_0031	
	BAB2_0321	
	BAB2_0395	
	BAB2_0519	
	BAB2_0529	
	BAB2_0559	
	BAB2_0626	
	BAB2_0635	
	BAB2_0662	
	BAB2_0889	
	BAB2_0922	
	BAB2_1031	
	BAB2_1074	
BMEI0067		
BMEI0141		
BMEI0195		
BMEI0288		
BMEI0450		
BMEI0451		
BMEI0553		
BMEI0684		
BMEI0739		
BMEI0803		
BMEI0824		
BMEI1087		
BMEI1094		
BMEI1121		
BMEI1296		
BMEI1302		
BMEI1692		
BMEI1759		
BMEI1867		
BMEI1934		
BMEI1965		
BMEI1978		
BMEI1984		
BMEI1997		
BMEI2010		
BMEII0022		
BMEII0105		
BMEII0413		
BMEII0430		
BMEII0523		
BMEII0565		
BMEII0654		
BMEII0734		
BMEII0793		
BMEII0895		
BMEII0930		
BMEII1042		
BMEII1132		
	BAB1_0151	BAbS19_I01440
	BAB1_0279	BAbS19_I02540

Brucella strain		
16M	2308	S19
	BAB1_0477	BAbS19_I04420
	BAB1_0534	BAbS19_I04980
	BAB1_0630	BAbS19_I05900
	BAB1_0706	BAbS19_I06590
	BAB1_0747	BAbS19_I06990
	BAB1_0891	BAbS19_I08310
	BAB1_1100	BAbS19_I10210
	BAB1_1153	BAbS19_I10710
	BAB1_1162	BAbS19_I10790
	BAB1_1183	BAbS19_I11000
	BAB1_1275	BAbS19_I11890
	BAB1_1565	BAbS19_I14630
	BAB1_1611	BAbS19_I15070
	BAB1_1615	BAbS19_I15110
	BAB1_1693	BAbS19_I15840
	BAB1_1705	BAbS19_I15950
	BAB1_1751	BAbS19_I16370
	BAB1_1756	BAbS19_I16410
	BAB1_1832	BAbS19_I17130
	BAB1_1856	BAbS19_I17360
	BAB1_1867	BAbS19_I17480
	BAB1_2121	BAbS19_I19830
	BAB1_2129	BAbS19_I19910
	BAB2_0077	BAbS19_II0072
	BAB2_0099	BAbS19_II0092
	BAB2_0208	BAbS19_II0198
	BAB2_0319	BAbS19_II0302
	BAB2_0665	BAbS19_II0622
BMEI0050		BAbS19_I18950
BMEI0121		BAbS19_I18240
BMEI0140		BAbS19_I18040
BMEI0242		BAbS19_I16960
BMEI0275		BAbS19_I16640
BMEI0311		BAbS19_I16250
BMEI0423		BAbS19_I15100
BMEI0417		BAbS19_I15150
BMEI0530		BAbS19_I14000
BMEI0532		BAbS19_I13990
BMEI0589		BAbS19_I13460
BMEI0596		BAbS19_I13390
BMEI0654		BAbS19_I16500
BMEI0749		BAbS19_I11790
BMEI0750		BAbS19_I11780
BMEI0789		BAbS19_I11390
BMEI0876		BAbS19_I10480
BMEI0887		BAbS19_I10370
BMEI0888		BAbS19_I10360
BMEI0915		BAbS19_I10140
BMEI0920		BAbS19_I10100
BMEI0961		BAbS19_I09680
BMEI1027		BAbS19_I09020
BMEI1069		BAbS19_I08570
BMEI1137		BAbS19_I07870
BMEI1200		BAbS19_I07260
BMEI1239		BAbS19_I06860
BMEI1243		BAbS19_I06810
BMEI1258		BAbS19_I06660
BMEI1365		BAbS19_I05540
BMEI1380		BAbS19_I05380
BMEI1439		BAbS19_I04860
BMEI1582		BAbS19_I03410
BMEI1607		BAbS19_I03150
BMEI1823		BAbS19_I01160
BMEI1831		BAbS19_I01090
BMEI1836		BAbS19_I01040
BMEI2001		BAbS19_I19920

Brucella strain		
16M	2308	S19
BMEI2023		BAbS19_I19690
BMEI2036		BAbS19_I19590
BMEII0011		BAbS19_II0076
BMEII0012		BAbS19_II0075
BMEII0040		BAbS19_II0047
BMEII0051		BAbS19_II0038
BMEII0250		BAbS19_II0937
BMEII0329		BAbS19_II0255
BMEII0361		BAbS19_II0283
BMEII0462		BAbS19_II0384
BMEII0466		BAbS19_II0388
BMEII0529		BAbS19_II0451
BMEII0666		BAbS19_II0594
BMEII0676		BAbS19_II0606
BMEII0742		BAbS19_II0662
BMEII0791		BAbS19_II0707
BMEII0867		BAbS19_II0760
BMEII0950		BAbS19_II0833
BMEII0910		BAbS19_II0799
BMEII1043		BAbS19_II0184
BMEII1118		BAbS19_II0709
BMEI0050	BAB1_2022	
BMEI0121	BAB1_1946	
BMEI0140	BAB1_1923	
BMEI0242	BAB1_1815	
BMEI0275	BAB1_1781	
BMEI0311	BAB1_1740	
BMEI0417	BAB1_1621	
BMEI0423	BAB1_1614	
BMEI0530	BAB1_1499	
BMEI0532	BAB1_1498	
BMEI0589	BAB1_1439	
BMEI0596	BAB1_1432	
BMEI0654	BAB1_1766	
BMEI0749	BAB1_1264	
BMEI0750	BAB1_1263	
BMEI0789	BAB1_1223	
BMEI0876	BAB1_1130	
BMEI0887	BAB1_1118	
BMEI0888	BAB1_1117	
BMEI0915	BAB1_1093	
BMEI0920	BAB1_1089	
BMEI1027	BAB1_0966	
BMEI1069	BAB1_0917	
BMEI1137	BAB1_0845	
BMEI1200	BAB1_0777	
BMEI1239	BAB1_0733	
BMEI1243	BAB1_0728	
BMEI1258	BAB1_0713	
BMEI1365	BAB1_0593	
BMEI1380	BAB1_0577	
BMEI1439	BAB1_0522	
BMEI1582	BAB1_0370	
BMEI1607	BAB1_0345	
BMEI1823	BAB1_0122	
BMEI1831	BAB1_0114	
BMEI1836	BAB1_0109	
BMEI2001	BAB1_2130	
BMEI2023	BAB1_2105	
BMEI2036	BAB1_2092	
BMEII0011	BAB2_0081	
BMEII0012	BAB2_0080	
BMEII0040	BAB2_0053	
BMEII0051	BAB2_0041	
BMEII0361	BAB2_0299	
BMEII0466	BAB2_0413	

Brucella strain		
16M	2308	S19
BMEII0529	BAB2_0477	
BMEII0598	BAB2_0555	
BMEII0666	BAB2_0636	
BMEII0676	BAB2_0649	
BMEII0742	BAB2_0709	
BMEII0791	BAB2_0762	
BMEII0867	BAB2_0821	
BMEII0910	BAB2_0865	
BMEII0950	BAB2_0904	
BMEII1043	BAB2_0194	
BMEII1118	BAB2_0764	
BMEI0197	BAB1_1866	BAbS19_I17470
BMEI0238	BAB1_1819	BAbS19_I17000
BMEI0304	BAB1_1748	BAbS19_I16340
BMEI0321	BAB1_1729	BAbS19_I16160
BMEI0328	BAB1_1720	BAbS19_I16080
BMEI0359	BAB1_1685	BAbS19_I15770
BMEI0370	BAB1_1673	BAbS19_I15660
BMEI0379	BAB1_1664	BAbS19_I15570
BMEI0390	BAB1_1652	BAbS19_I15450
BMEI0527	BAB1_1501	BAbS19_I14020
BMEI0610	BAB1_1416	BAbS19_I13230
BMEI0657	BAB1_1367	BAbS19_I12770
BMEI0736	BAB1_1279	BAbS19_I11920
BMEI0740	BAB1_1274	BAbS19_I11880
BMEI0810	BAB1_1199	BAbS19_I11160
BMEI0948	BAB1_1058	BAbS19_I09810
BMEI1042	BAB1_0948	BAbS19_I08870
BMEI1044	BAB1_0946	BAbS19_I08850
BMEI1057	BAB1_0930	BAbS19_I08700
BMEI1088	BAB1_0897	BAbS19_I08370
BMEI1279	BAB1_0690	BAbS19_I06460
BMEI1298	BAB1_0669	BAbS19_I06260
BMEI1361	BAB1_0597	BAbS19_I05580
BMEI1445	BAB1_0515	BAbS19_I04790
BMEI1482	BAB1_0478	BAbS19_I04430
BMEI1531	BAB1_0430	BAbS19_I03950
BMEI1577	BAB1_0375	BAbS19_I03460
BMEI1658	BAB1_0294	BAbS19_I02540
BMEI1694	BAB1_0258	BAbS19_I02410
BMEI1751	BAB1_0197	BAbS19_I01860
BMEI1837	BAB1_0108	BAbS19_I01030
BMEI1895	BAB1_0045	BAbS19_I00430
BMEI1968	BAB1_2162	BAbS19_I20230
BMEII0041	BAB2_0051	BAbS19_II0046
BMEII0110	BAB2_1145	BAbS19_II1068
BMEII0116	BAB2_1138	BAbS19_II1062
BMEII0297	BAB2_0233	BAbS19_II0222
BMEII0314	BAB2_0252	BAbS19_II0241
BMEII0533	BAB2_0481	BAbS19_II0455
BMEII0659	BAB2_0628	BAbS19_II0587
BMEI0908	BAB1_1099	BAbS19_I10200
BMEII0996	BAB2_0952	BAbS19_II0881
BMEII1013	BAB2_0223	BAbS19_II0212
BMEII1067	BAB2_0170	BAbS19_II0161
BMEII1111	BAB2_0123	BAbS19_II0114

Table 2.3 Assorted T4SS effector hallmarks observed on the selected candidate effector genes list (n=45). Each column represents a *Brucella* strain: 16M, 2309 and S19, score and features found by S4TE. Abbreviations are described in table 2.

Brucella strain			S4TE 2.0 Features												
16M	2308	S19	Score	Homology*	RS TY†	EUK‹	DUF	NLS^	EEXXE›	CC'	EPIYA»	CH‹	CCh~	CTB˙	GH°
BMEI0948	BAB1_1058	BAbS19_I09810	169	VceC											
BMEI1968	BAB1_2162	BAbS19_I20230	164	CBU-1434											
BMEI0359	BAB1_1685	BAbS19_I15770	162	lpg0257											
BMEI1044	BAB1_0946	BAbS19_I08850	162	CBU_1769											
BMEI1057	BAB1_0930	BAbS19_I08700	145												
BMEI1837	BAB1_0108	BAbS19_I01030	140												
BMEI0610	BAB1_1416	BAbS19_I13230	137												
BMEI1577	BAB1_0375	BAbS19_I03460	132												
BMEI0527	BAB1_1501	BAbS19_I14020	128	Lpg2359/CBU_1594											
BMEI0390	BAB1_1652	BAbS19_I15450	128	VceA											
BMEI0321	BAB1_1729	BAbS19_I16160	122	CBU_1566											
BMEI0328	BAB1_1720	BAbS19_I16080	109	Lpg2222/CBU_1457											
BMEI0908	BAB1_1099	BAbS19_I10200	109	lpg1426											
BMEI1751	BAB1_0197	BAbS19_I01860	104	CBU_1043											
BMEI0736	BAB1_1279	BAbS19_I11920	104	RicA											
BMEI0810	BAB1_1199	BAbS19_I11160	100	lpg2628											
BMEI1279	BAB1_0690	BAbS19_I06460	98												
BMEI1042	BAB1_0948	BAbS19_I08870	95												
BMEI1088	BAB1_0897	BAbS19_I08370	92												
BMEI1694	BAB1_0258	BAbS19_I02410	91												
BMEI1895	BAB1_0045	BAbS19_I00430	87												
BMEI0370	BAB1_1673	BAbS19_I15660	78												
BMEI0238	BAB1_1819	BAbS19_I17000	76												
BMEI0657	BAB1_1367	BAbS19_I12770	76												
BMEI0197	BAB1_1866	BAbS19_I17470	76												
BMEI1531	BAB1_0430	BAbS19_I03950	76												
BMEI1298	BAB1_0669	BAbS19_I06260	74												
BMEI1445	BAB1_0515	BAbS19_I04790	74												
BMEI0740	BAB1_1274	BAbS19_I11880	73												
BMEI0379	BAB1_1664	BAbS19_I15570	72												
BMEI0304	BAB1_1748	BAbS19_I16340	39												
BMEI1361	BAB1_0597	BAbS19_I05580	27												
BMEI1482	BAB1_0478	BAbS19_I04430	26												
BMEI1658	BAB1_0294	BAbS19_I02540	20												
BMEII1111	BAB2_0123	BAbS19_II01140	151	BPE123											
BMEII0533	BAB2_0481	BAbS19_II04550	133	lpg0257											
BMEII0314	BAB2_0252	BAbS19_II02410	108	lpg2826											
BMEII1013	BAB2_0223	BAbS19_II02120	104	BAB1_1652											
BMEII0659	BAB2_0628	BAbS19_II05870	98	CBU_1043											
BMEII1067	BAB2_0170	BAbS19_II01610	84												
BMEII0110	BAB2_1145	BAbS19_II10680	82												
BMEII0996	BAB2_0952	BAbS19_II08810	79												
BMEII0297	BAB2_0233	BAbS19_II02220	76												
BMEII0041	BAB2_0051	BAbS19_II00460	74												
BMEII0116	BAB2_1138	BAbS19_II10620	73												

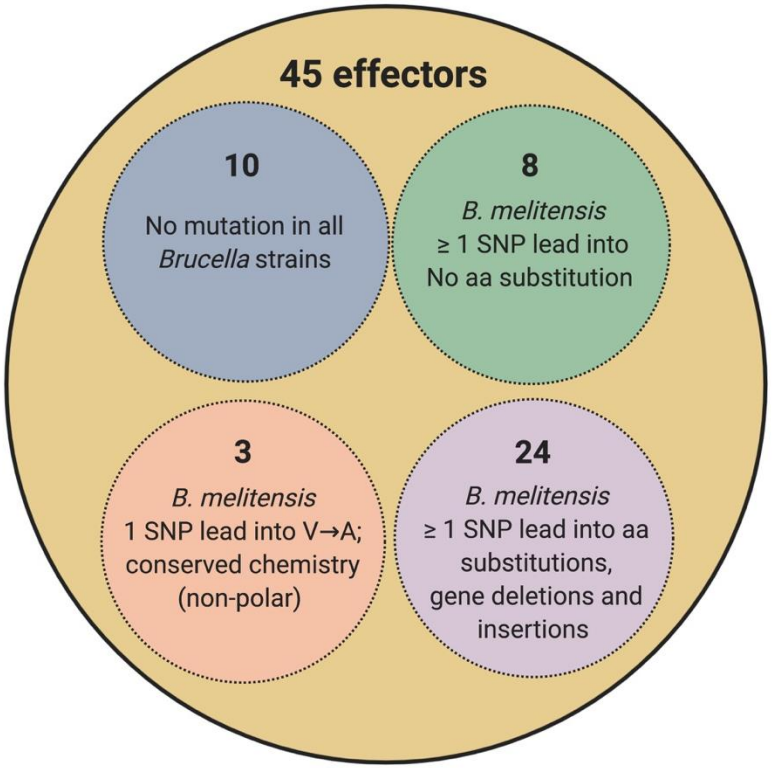

Figure 2.3 Genomic and proteomic analyses of 45 candidate T4SS effectors common to three *Brucella* strains (16M, 2308, S19). Analyses showed that some genes are highly conserved while others presented high frequency of genetic variations defined as single nucleotide polymorphism (SNP), gene deletions and gene insertions. Genetic variations were translated into amino acid (aa) substitutions or changes in chemistry.

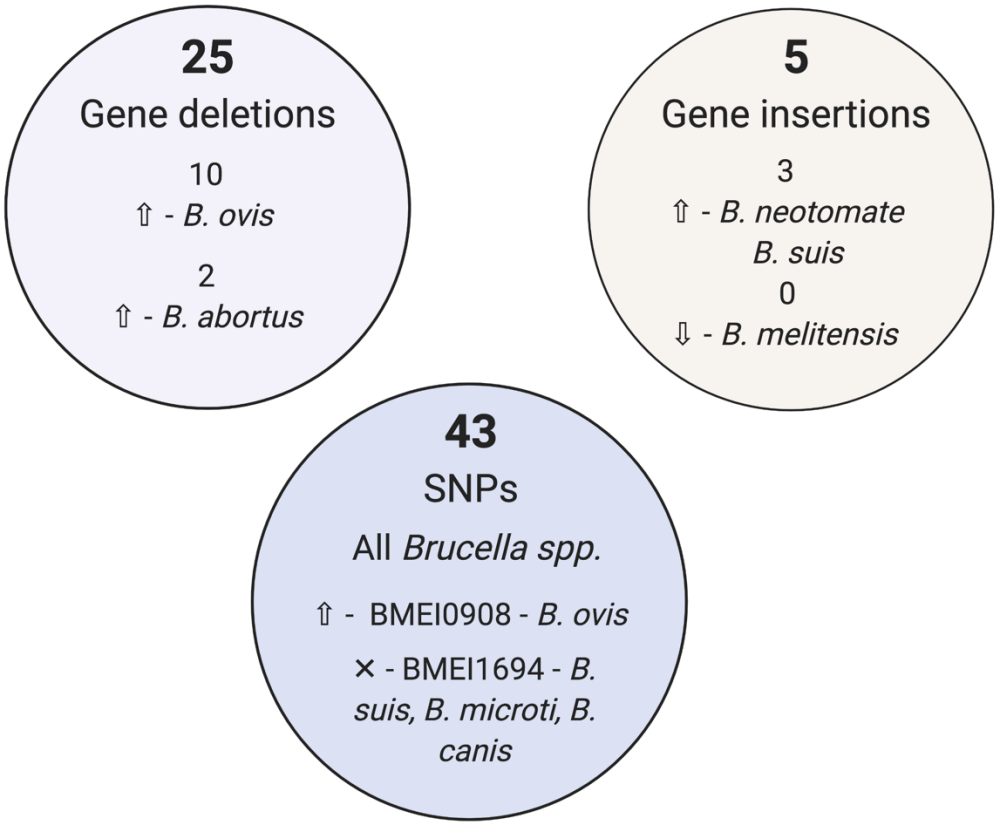

Figure 2.4 Genetic conservation of *Brucella* candidate T4SS effectors among all *Brucella* representative species. Reference sequences from each representative *Brucella* specie were obtained from PATRIC database. Each circle represents genetic variations observed among all candidate T4SS effectors across species: 1) gene deletions, 2) gene insertions and 3) single nucleotide polymorphism (SNPs). Arrows indicates either the highest or the lowest frequency of the indicated genetic variation related to candidate effector genes across bacterial species. Cross mark indicates the candidate effector and the bacterial species with no mutations.

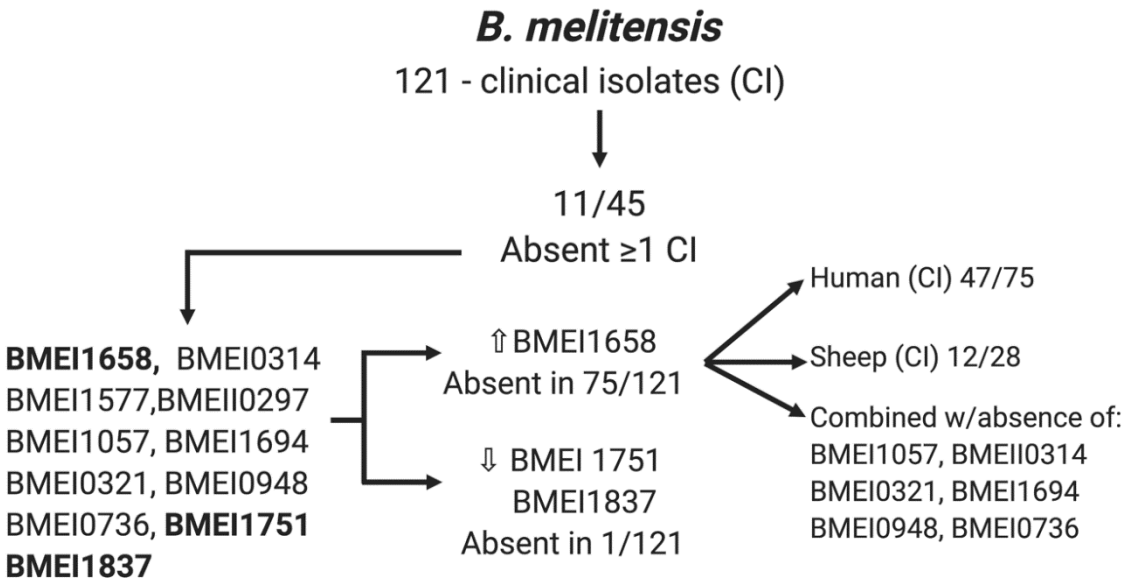

Figure 2.5 Genetic prevalence of candidate T4SS effectors in *B. melitensis* clinical isolates. Reference genomes from 121 *Brucella melitensis* clinical isolates were obtained from PATRIC. Data was analyzed using genome comparison tool (PATRIC) to determine whether candidate T4SS effectors were present or absent across clinical isolates. Arrows indicates either high absence or low absence frequencies of indicated candidate effectors.

Table 2.4 Proteome comparison of *B. melitensis* candidate *vir*B-T4SS effectors. Green color denotates significant homologous sequences found in bacterial pathogens (>30% sequence coverage coupled with >10% sequence identity).

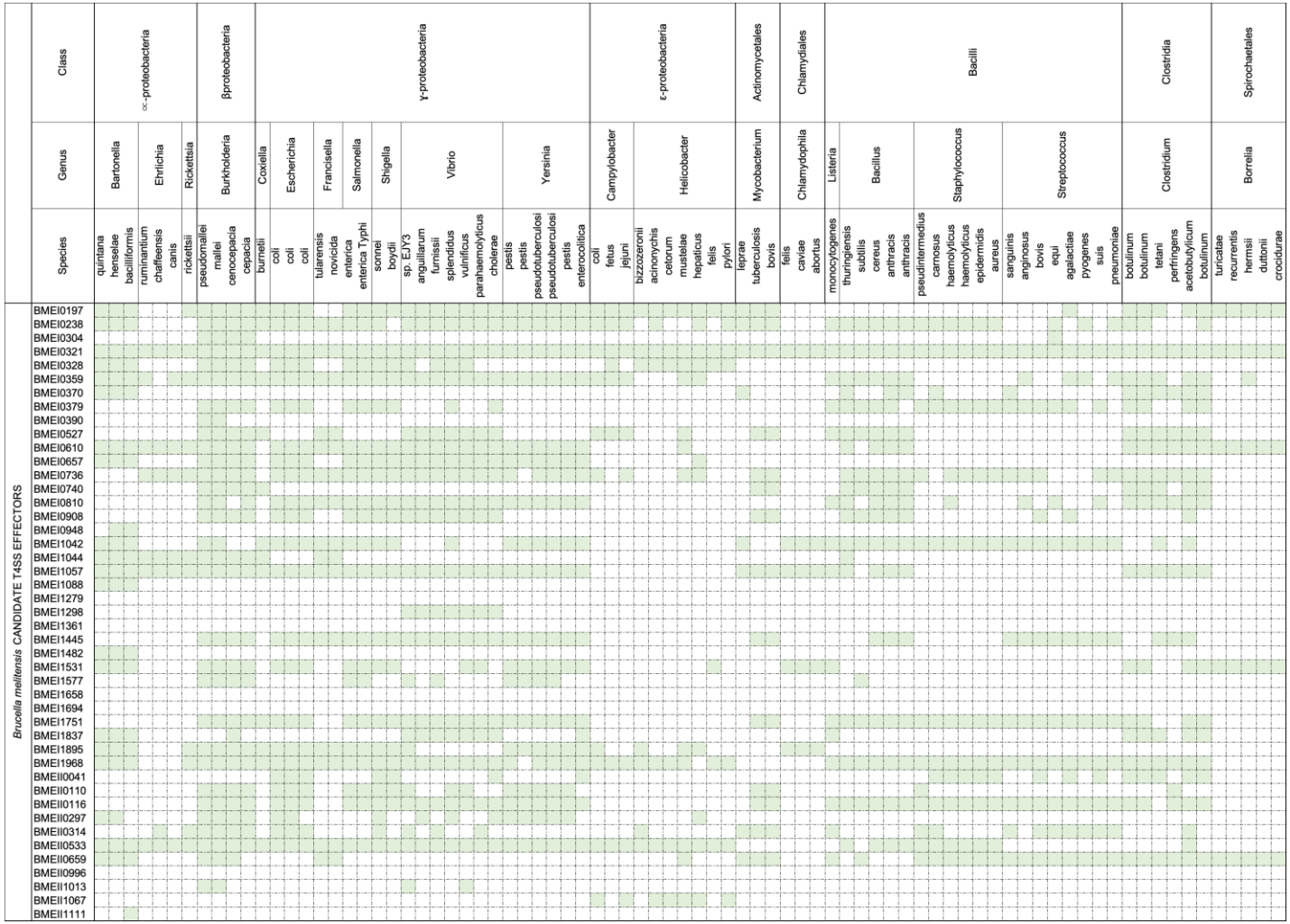

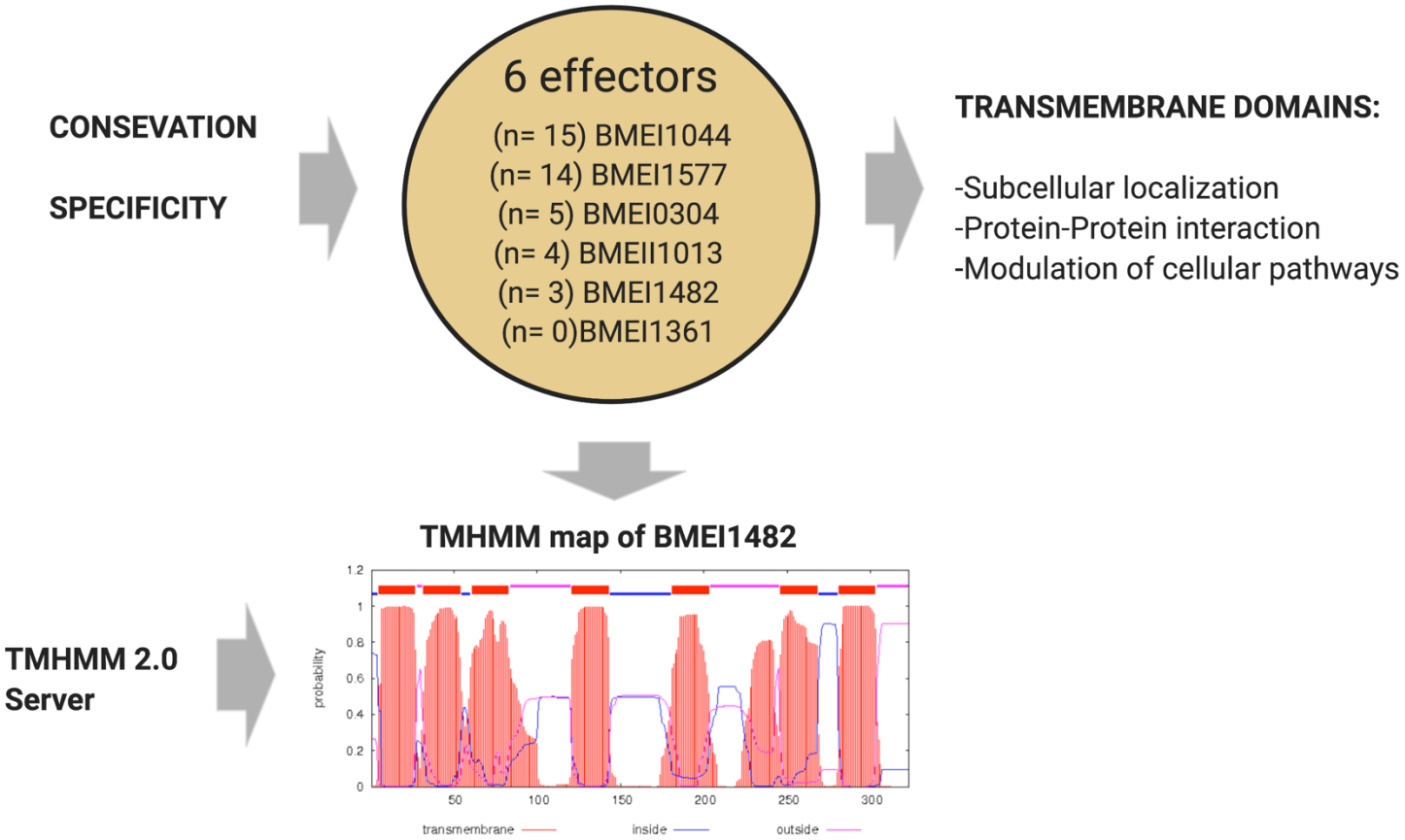

Figure 2.6 Final list of candidates T4SS effectors. Genes specific to *B. melitensis* and genetically conserved among *B. melitensis* clinical isolates were analyzed for transmembrane domains. TMHMM map of BMEI1482 shows that effector has seven transmembrane domains (represented in red peaks), which makes it a suitable effector for functional biology studies.

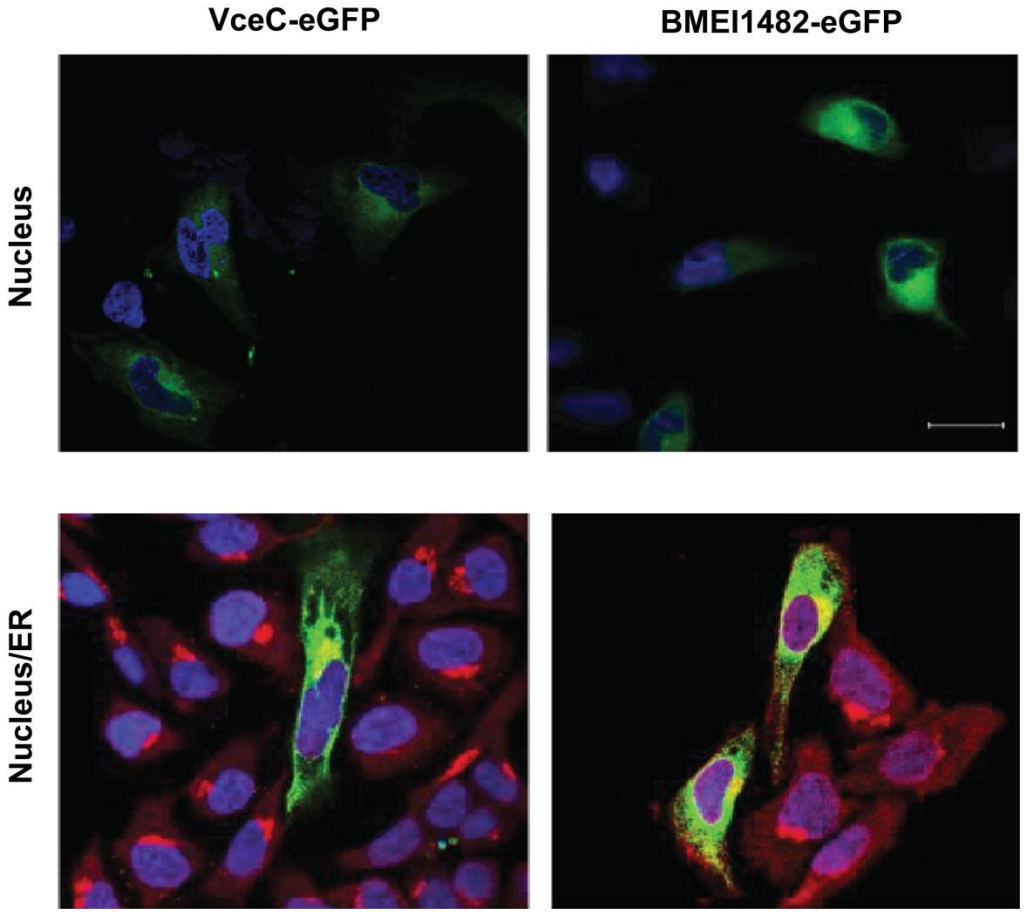

Figure 2.7 Representative confocal micrographs of HeLa cells transfected for 24 h with plasmids expressing either (BMEI0948) VceC-eGFP or BMEI1482-eGFP. HeLa cells expressing eGFP-tagged *Brucella* effectors and grown in coverslips, were immunostained using an anti-calnexin antibody (red) to visualize ER and 1X Hoescht to visualize nucleus (blue). Scale bar, 10 μm.

2.3. Materials and Methods

2.3.1. *In silico* analysis of novel candidate *Brucella* spp. virB-T4SS effector proteins

To identify novel candidate *virB*-T4SS effector proteins of *Brucella*, a PERL-based command line bioinformatics tool S4TE was used (Meyer et al., 2013). The S4TE algorithm for identifying T4SS effectors is broadly based on: 1) presence of eukaryotic-like domains, 2) subcellular localization signals and secretion signals, 3) homology with known effectors (e.g. *L. pneumophila, C. burnetii, A. tumefaciens, B. abortus, Bartonella spp., Anaplasma spp.* and *Ehrlichia spp*.), and 4) homology to effector features such as positive charge, basicity, hydrophobicity, glutamate-rich sequence (E-block) on C-terminal and global hydrophilicity of total protein (Anderson and Frank, 2012; Backert and Meyer, 2006; Hicks and Galan, 2013; Mattoo et al., 2007; Meyer et al., 2013). The program searches all considered criteria in an independent manner and compiles all outputs to generate a score to rank T4SS effector candidates, describing positive features found in each protein. S4TE sets the selection default threshold cutoff at 5. In addition, the program provides a GC content analysis and a local gene density analysis (Table 2.1 and Figure 2.1). Importantly, the S4TE tool has proven valuable in identifying T4SS effectors in assorted α- and γ- proteobacterial systems, including *L. pneumophila* and *E. chaffeensis* (Meyer et al., 2013). The genome and proteome sequences of three different species of *Brucella* reported pathogenic in humans. *B. melitensis* 16M, a strain isolated from diseased goats; *B. abortus* 2308, a standard laboratory strains virulent for cattle; and *B. abortus* strain 19, a spontaneously attenuated strain broadly used as vaccine to prevent brucellosis in cattle were analyzed.

2.3.2. Selection of novel candidate *Brucella spp*. virB-T4SS effector proteins

Additional bioinformatics analyses were performed to further refine a list of candidate effectors, aiming to generate a high priority gene set to pursue in biological experiments. Proteome comparison tools from Pathosystems Resource Integration Center (PATRIC) (Wattam et al., 2017) coupled with nucleotide alignment using CLC workbench v.10.1.1 were used to determine: 1) genetic conservation of candidate effectors across the three analyzed species (*B. melitensis* 16M, *B. abortus* 2308 and S19), 2) genetic conservation and prevalence of candidate effectors across all reference *Brucella* species and *B. melitensis* clinical isolates reported in PATRIC, and 3) genetic specificity of candidate effectors to *B. melitensis* determined by identification of significative homologous sequences found in other bacterial pathogens that are reported in PATRIC database.

For proteome comparison analysis, the PATRIC settings used were a minimum of 30% sequence coverage coupled with a minimum sequence identity of 10% of query and subject, and a maximum BLAST E value of 1e-5. Bacterial protein sequences that presented less than 30% of sequence coverage with less than a 10% of sequence identity, would more likely play a role as novel effectors of *Brucella melitensis* (Wattam et al., 2017). For nucleotide alignment analysis, the CLC workbench settings used were gap open cost of 10.0, gap extension cost of 1.0 and the very accurate alignment option was selected. Bacterial gene sequence alignments were used to search for gene deletions, gene insertions and SNP's that were coupled to protein sequence changes. Taken

together, these analyses generated a list of high priority candidate *virB*-T4SS effectors, each of which carried hallmarks of effector functions.

2.3.3. Selection of a candidate T4SS effector for biological analyses

By combining both screening using S4TE program and bioinformatic analyses, the candidate T4SS effector BMEI1482 was selected based on 1) genetic conservation among *Brucella* strains (16M, 2308 and S19 but also among all known *Brucella* reference strains), 2) genetic prevalence among *B. melitensis* clinical isolates, 3) genetic specificity to *B. melitensis* when compared to other bacterial proteomes, 4) presence of transmembrane domains as an indicative of subcellular localization, protein-protein interaction and possible modulation of cellular pathways, 5) localization at ER, the *Brucella* replicative niche, so the selected effector most likely will have a role in brucella pathogenesis.

2.3.4. Subcellular localization of candidate virB-T4SS effector BMEI1482

For these experiments, a set of vectors that express proteins of interest fused to enhanced GFP were generated. VceC (BMEI0948) a known control (de Jong et al., 2013; de Jong et al., 2008), and BMEI1482 were cloned into BglII and SalI digested pEGFP-C1 plasmid to be expressed in frame with eGFP and under CMV promoter. HeLa cells were seeded on 12-mm coverslips in 24-well plates a 1 x10^5 cells per well. Next day, cells were transfected with pEGFP-C1-BMEI1482 (Grhg1), pEGFP-C1-VceC (BMEI0948) and pEGFP-C1. Briefly, transfection mixture was prepared by mixing

0.75µl plus reagent, 500ng-1µg plasmid DNA and 1µl Lipofectamine into 100µl of DMEM without FBS (no antibiotic). Then, plasmid transfection mixture was added to cells and incubated at 37°C for 4-6h. Afterwards, mixture was removed and fresh 500µl of DMEM with 10% FBS were added. At 24 hours post transfection (h.p.t.), cells were washed three times with 1XPBS and fixed with 4% paraformaldehyde (PFA) during 15min. Then, the fixing solution was removed, and cells were again washed three times with 1XPBS. Expression of VceC (BMEI0948)-eGFP and BMEI1482-eGFP was observed at 24 hours post-transfection using confocal microscopy according to (de Jong et al., 2013). To learn subcellular localization of effectors, cells were treated with 0.1% Triton-100, incubated at RT for 3-5 min and washed three times with 1XPBS. Then, cells were blocked with 1%BSA and incubated at RT for 30 min or overnight at 4°C. Afterwards, BSA solution was removed and primary mouse anti-calnexin antibody was added (1:1000 dilution) and incubated at RT for 1h. Antibody solution was removed from wells by aspiration to wash cells times with 1XPBS and 1%BSA was added to cells and incubated at RT for 30 min. 1%BSA solution was removed and secondary anti-mouse Alexa Fluor 594 antibody was added (1:10,000 dilution) along with 1X Hoechst (1:250 dilution) as a nuclear marker. Plates were incubated at room temperature for 1h. Finally, antibody solution was removed, and cells were washed five times with 1XPBS. Wells were mounted with prolong anti-fade and observed at 24 hours post-transfection using confocal microscopy as previously described (Pandey et al., 2018).

3. THE *BRUCELLA MELITENSIS* EFFECTOR GRHG1 REPROGRAMS THE HOST N-GLYCOME TO SUSTAIN INFECTION

3.1. Introduction

Intracellular bacteria encode specialized secretion systems that deliver bacterial effector proteins into host cells to promote bacterial survival and replication. To achieve bacterial success, translocated effectors must target a subcellular compartment to interact with specific protein machinery and modulate biochemical activities within the host cell. Such "biochemical modulations" are translated into manipulation of cell processes including cytoskeleton dynamics, cell cycle progression, transcription, signal transduction, endocytic and secretory pathways (Hicks and Galan, 2013).

The endoplasmic reticulum (ER) is an essential organelle involved in protein synthesis and transport, protein folding, lipid synthesis, carbohydrate metabolism and calcium storage (Schwarz and Blower, 2016). Studies demonstrate that ER is a major organelle targeted by bacterial effectors with the purpose of modulating cellular processes within the endocytic and secretory pathways; such as, endocytosis, vesicular trafficking, unfolded protein response (UPR), autophagy, and nutrient acquisition to promote formation of the bacterial niche (Celli, 2015; Schwarz and Blower, 2016; Weber and Faris, 2018).

In the secretory pathway, a fundamental protein folding procedure, also known as a post-translational modification, involves the addition of glycans to asparagine residues, a process called N-linked glycosylation. This process is a key enzymatic quality control

mechanism to ensure properly folded proteins are stable during traffic through the Golgi apparatus up to their release, achieving their functional purpose (Wong et al., 2018), and plays important biological roles in protein folding regulation, response to stress, cell signaling and immune response (Loke et al., 2016; So, 2018). The N-glycome represents the glycan structures present on a given tissue, cell type or molecule population; in fact, changes in N-glycome pattern are linked to infectious disease and inflammation (Kreisman and Cobb, 2012). Studies revealed that host-pathogen interaction modulates host glycosylation machinery, which translates into changes in N-glycome patterns to allow bacterial invasion (i.e. *Salmonella typhimurium*) (Park et al., 2016) or to promote immune response as a bacterial infection strategy (i.e. *Mycobacteriuum tuberculosis*) (Hare et al., 2017; Walters et al., 2013). Using *M. tuberculosis* (Mtb) as a model, studies indicated an increase in N-glycan density, a change in cellular N-glycoproteome, and an upregulation of both glycosylation enzymes and a cluster of proteins forming the multi-subunit oligosaccharyl-transferase (OST) complex, all combined correlated with an activation of immune pro-inflammatory response during Mtb infection (Hare et al., 2017; Walters et al., 2013). However, the molecular mechanisms by which pathogens modulate host glycosylation remain unclear.

The OST is a multi-subunit enzyme complex integrated into the ER protein translocon and containing either STT3A or STT3B as catalytic subunits, and RPN1, RPN2, OST48, DAD1, N33 or IAP and OST4 as accessory subunits (Lu et al., 2018; Pfeffer et al., 2015). OST complex transfers a preassembled oligosaccharide ($Glc_3Man_9GlcNAc_2$) from a lipid-linked oligosaccharide (LLO) donor substrate to an

asparagine contained in a N-X-S(T) sequon of the polypeptide substrate (Mohorko et al., 2011).

The mechanism by which OST activity is regulated remains poorly understood. However, recent reports indicate that the unfolded protein response (UPR), a mechanism to tackle ER stress, can drive changes in the host N-glycome (Wong et al., 2018). Briefly, the UPR signals through the stress transmembrane sensors IRE1α, ATF6, and PERK to detect protein misfolding. The central stress sensor is IRE1α, which possess endonuclease activity to catalyze the splicing of XBP1 mRNA, generating XBP1 transcription factor to control the expression of ER chaperones and other proteins that mitigate the harmful consequences of unfolded protein accumulation (Lamriben et al., 2016; Walter and Ron, 2011). Studies demonstrated that XBP1s activation alters the composition of the N-glycome in a cell type- and proteome-dependent manner (Dewal et al., 2015; Wong et al., 2018). XBP1s activation increases levels of oligomannose, core fucosylation and tetraantennary N-glycans. This activation also decreases levels of sialylation and bisecting GlcNAc (N-acetylglucosamine) in both cell membrane and secretome. The observed N-glycome pattern is coupled with changes in expression of specific transcripts encoding enzymes involved in N-glycosylation such as RPN1, RPN2, STT3A, subunits of the OST complex and in N-glycan maturation such as GFPT1, PGM3, SLC35A3 and UAP1, all involved in regulating UDP-GlcNAc availability (Wong et al., 2018). These observations suggest a mechanism to translate intracellular stress signaling due to congenital or infectious diseases.

Brucella infection induces sustained ER stress that translates into an unfolded protein response (UPR) coupled with an inflammatory response. Studies show that *B. melitensis* infection upregulates the expression of UPR target genes, induces XBP1 mRNA splicing (Smith et al., 2013) and depletion of IRE1α dramatically reduces *Brucella's* replication. These observations demonstrate that IRE1α is critical to sustain *Brucella* parasitism (Pandey et al., 2018; Qin et al., 2008; Taguchi et al., 2015).

Previous work by (Patrick et al., 2018) used an epistasis mini-array profile (EMAP), a synthetic genetic interaction assay, to identify conserved eukaryotic pathways that are targets of effector proteins from a set of bacteria that expresses secretion systems: *Coxiella, Salmonella* and *Brucella* (Figure 3.1A). The study revealed that our selected candidate *virB*-T4SS effector protein BMEI1482 presented a strong correlation with components of translocon, glycosylation and GPI biosynthesis biology ($z > 5$) localized in the ER, suggesting that BMEI1482 plays an important mechanistic role in the ER biology (Patrick et al., 2018) (Figure 3.1B). In support of this observation, analyses performed with S4TE software (Meyer et al., 2013) revealed that BMEI1482 possesses effector protein hallmarks such as an RS-TY motif, a cis-regulatory element required for expression of T4SS encoding genes in *L. pneumophila*, and a DUF domain that is homolog to an evolutionary highly conserved eukaryotic protein domain TMEM208 involved in ER stress and autophagy (Graham et al., 2016; Zhao et al., 2013).

Taken all data and literature together, in the present dissertation work, we subjected BMEI1482 to biological analyses to demonstrate translocation by *virB*-T4SS,

its biological function and its virulence in *in vitro* and *in vivo* host cell models. We observed that our *virB*-T4SS effector contributes to bacterial infection and reprograms host N-glycome, for this reason we named it "Global reprogramming host glycome or "Grhg1". Therefore, this chapter describes the first link between Grhg1 N-glycome modulation and its contribution to bacterial pathogenesis.

3.2. Results

3.2.1. BMEI1482 is translocated into the host cytosol by *virB*-T4SS during infection

To test whether the BMEI1482 is translocated into host cells during infection, a TEM1 β-lactamase protein translocation reporter assay was used (Charpentier and Oswald, 2004). This translocation assay has previously been useful for identifying translocated substrates in other bacterial pathosystems (Burstein et al., 2015; Chen et al., 2010; Wolters et al., 2015). First, expression plasmids were constructed carrying effectors of interest in-frame to β-lactamase gene (TEM-1 fusions), and then these were inserted in *B. melitensis* strain 16M. Because the *virB*-T4SS translocation signals are not well known in *Brucella*, it is not possible to predict whether N- or C-terminal fusions to specific effectors will perturb translocation into host cells. To overcome this, "BlaM-N" terminal and "C-BlaM" terminal in-frame fusions to BMEI1482 (TEM-1 fusions) were generated. As controls, expression plasmids were constructed carrying BlaM-N in-frame to BMEI0948 and C-BlaM in-frame to BMEII1111, both genes homologous to known *B. abortus virB*-T4SS effectors VceC and BPE123 (Figure 3.3) (de Jong et al., 2008; Marchesini et al., 2011). The effector proteins were placed under control of isopropyl-ß-

D-thiogalactopyranoside (IPTG)-inducible *Ptac* promoter, thereby allowing immediate TEM-1 fusion induction before testing in an infection assay, this approach has worked well in previous studies (Myeni et al., 2013). PCR analysis and presence of kanamycin resistance revealed that strains carried the pTEM plasmids with effector fusions. In addition, TEM-1 fusions were detected by Western blot analysis using anti-β-lactamase (Figure 3.6).

To test translocation of candidate effector proteins, RAW 264.7 macrophage-like cells were infected with wild type *Brucella* strains expressing effector TEM-1 fusions at a MOI of 1000 for 16 h and then loaded with β-lactamase substrate CCF2/AM. When excited at 409 nm, this substrate emits green fluorescence (520 nm) due to fluorescence resonance energy transfer (FRET) between the coumarin and fluorescein fluorophores. However, when β-lactam ring of CCF2/AM is cleaved, the two fluorophores are released, and the fluorescence emission changes from green to blue (447 nm). Therefore, infection harboring bacteria, which translocate effector fusions into host cells, induce a readily detectable blue fluorescence signal in host cells. The ratio of blue to green fluorescence is quantified using appropriate excitation and emission filters in fluorescence microscopy (de Felipe et al., 2008).

The candidate effector protein BMEI1482 was reproducibly found to be translocated into host cells by *B. melitensis* 16M. As expected, our positive control effector VceC (BMEI0948) for N-terminal and BPE123 (BMEII1111) for C-terminal were found to be efficiently translocated into host cells, and our empty vector used as a negative control failed to give a positive signal (Figure 3.7).

To determine whether BMEI1482 was translocated in a *vir*B-T4SS-dependent manner, translocation efficiencies by a *virB*-T4SS deficient strain (B16MΔ*virB*2) and WT strain (B16M) were examined and compared. The translocation of control effectors (VceC and BPE123) was impaired in the *virB* mutant as expected (de Jong et al., 2013; Marchesini et al., 2011), moreover, BMEI1482 translocation was impaired as well, confirming that effector is a *virB*-T4SS substrate (Figure 3.7). Taken together, these results demonstrate that *in silico*-identified BMEI1482 is translocated by *B. melitensis* during infection and the position of the BlaM tag at either the N- or C-terminus of the protein did not influence translocation in this assay.

3.2.2. BMEI1482 effector decreases bacterial replication in BMDMs

The experiments presented above indicated that BMEI1482 is translocated into host cells by the *vir*B-T4SS. We therefore tested whether BMEI1482 plays a critical role in the intracellular lifestyle of the pathogen. First, *B. melitensis* deletion mutant of BMEI1482 (ΔBMEI1482) and complemented mutant that ectopically express BMEI1482 (CΔBMEI1482) strains were generated. Then, the ability of the strains to be internalized and replicated in BMDMs cells was tested. To generate mutant strains, plasmids were created carrying upstream and downstream operon sequences to allow with SacB gene and kanamycin gene for colony selection (Kahl-McDonagh and Ficht, 2006). To demonstrate that the targeted gene was ablated from the genome of the bacterium, PCR directed strategies coupled with DNA sequencing were used. This effort

verified that the mutant strain had a clean deletion at the targeted genomic loci (BMEI1482), and that the operon structure was not perturbed by genetic manipulations.

To determine whether the mutant strain displayed alterations in interactions with host cells, an infection of BMDM cells was performed to measure internalization and replication of the pathogen (Kahl-McDonagh and Ficht, 2006). When BMDMs were infected with either B16M and ΔBMEI1482, no differences were observed during bacterial invasion and intracellular replication. Similar findings have been observed with previously studied *B. abortus* effector proteins mutant strains (i.e. VceC, BPE123) (de Jong et al., 2013; Myeni et al., 2013). However, when effector BMEI1482 was exogenously expressed (CΔBMEI1482), bacterial replication was significantly impaired (Figure 3.8). Thus, our data suggests that exogenous expression of BMEI1482 inhibits *B. melitensis* intracellular replication.

3.2.3. BMEI1482 interacts with components of N-glycosylation machinery, the OST complex

A successful strategy to understand the mode of action of effector proteins in *Brucella* pathogenesis is to identify important targeted host factors (Marchesini et al., 2011). To learn the molecular mechanism of BMEI1482 and understand its role during infection, biochemical analysis of factors that interact with the ectopically expressed protein was performed. Briefly, HEK293T cells were transfected with pEGFP-C1-BMEI1482 (Grhg1), pEGFP-C1-BMEI0948 (VceC, as control) and pEGFP-C1 (empty vector), harvested at 36 h.p.t. and processed for immunoprecipitation. To select host

factors specifically targeted by BMEI1482, LC-MS analysis of the precipitated materials was performed scaffold v.4 software, and BMEI1482 hits were manually filtered and annotated. The hits were ranked according to score based on amino acid sequence coverage against database. The data showed that BMEI1482 specifically co-immunoprecipitated with a group of proteins between 50.8-80.5 KDa that are known to localize to the ER (Table 3.2) (Cherepanova et al., 2016). Hits were identified as RPN1 (score of 168.47), RPN2 (score of 83.86), DDOST (OST48) (score of 44.80) and STT3A (score of 22.37) subunits of the mammalian oligosaccharyl-transferase complex (OST). The OST complex is integrated into the ER protein translocon and has eight to nine subunits. OST exists as one of two major isoforms with either STT3A or STT3B catalytic subunits, and accessory subunits RPN1, RPN2, OST48, DAD1, N33 or IAP and OST4. OST transfers oligosaccharides from lipid-linked oligosaccharides (LLOs) to asparaginyl residues of Asn-X-Ser/Thr acceptor sequons, a mechanism known as N-linked glycosylation (Lu et al., 2018; Mohorko et al., 2011). Co-immunoprecipitation of BMEI1482 with hits RPN1 and RPN2 was confirmed and consistent with the localization of BMEI1482 in the host ER (Figure 3.9).

3.2.4. *B. melitensis* modulates the host N-glycoproteome

It has been revealed that bacteria modulate glycosylation as strategy to infect host and establish a replicative niche (Hare et al., 2017; Kreisman and Cobb, 2012; Park et al., 2016). To gain an insight into whether N-glycoproteome is altered during *Brucella* infection, BMDMs infected with B16M, ΔBMEI1482 and CΔBMEI1482 strains were

processed. Lectin microarray is a technology that utilizes a panel of lectins immobilized on well-defined substrate for a high-throughput analysis of glycans and glycoproteins. Lectins are glycan-binding proteins with high affinity and specificity to monosaccharides and oligosaccharides that are present in complex glycan structures attached to proteins (Hu and Wong, 2009). An array of 70 lectins was used to define a glycopattern profile during bacterial infection. To allow a broad interpretation of data, lectins were categorized in groups based on their affinity to an specific monosaccharides: 1) GalNAc: N-Acetylglactosamine, 2) GlcNAc: N-Acetylglucosamine, 3) Gal: D-Galactose, 4) Glc: D-Glucose, 5) Fuc: L-Fucose, 6) Lac: Lactose, 7) Man: Mannose and 8) Nac: N-Acetylneuraminic acid.

Interestingly, relative fluorescence glycan signal (RFG) of mannose, N-acetylgalactosamine and N-acetylglucosamine and with less frequency glycans N-acetylneurmainic acid, glucose and fucose were significantly increased by effector gene-deletion (ΔBMEI1482) but significantly decreased by ectopically expression of effector BMEI1482 (CΔBMEI1482). A characteristic glycoproteome pattern was observed in wild type BMEI1482 expression levels (B16M), with a significant decrease in RFG signal specific to mannose. Interesting changes in RFG signal specific to galactose were observed among the three strains, where wild type BMEI1482 expression levels (B16M) showed a signal decrease while effector gene-deletion (ΔBMEI1482) presented and increased signal. Finally, ectopically expression of effector BMEI1482 (CΔBMEI1482) showed no significative galactose signal differences. These findings demonstrate that *Brucella* infection modulates host glycoproteome and most importantly, data suggests

that effector BMEI1482 plays a specific role on glycoproteome reprogramming to sustain bacterial infection (Figure 3.10).

3.2.5. BMEI1482 reprograms the host N-glycome abundance and glycan isomer distribution

The study of glycomics allows to understand the changes on biological function as a result of congenital, innate immune-related or infectious diseases (Kreisman and Cobb, 2012). To date, few reports have linked modulation of glycosylation genes, glycoproteins and host glycome distribution to bacterial strategies to sustain infection (Hare et al., 2017; Krishnan et al., 2014; Lu et al., 2015; Park et al., 2016). LC-MS/MS has been the most common technique used to study glycomics since it gives an enriched structural information with high sensitivity and resolution (Peng et al., 2019), and approach that independent of affinity, specificity and sensitivity of protein-protein interactions.

To test whether ectopically expression of 1482-eGFP results in altered N-glycome abundance and changes in glycan isomer distribution, HEK293Ts cells transfected with pEGFP-C1-BMEI1482 and pEGFP-C1 were processed, and N-glycan isomers were determined. Overall 90 N-glycans were identified and quantified. The total glycan abundance was calculated by summing up all individual glycan abundances. A statistically significant decrease of the overall N-glycan expression was observed with ectopically expression of 1482-eGFP (Figure 3.11A). After grouping N-glycans by categories, it was possible to observe a statistically significant decrease in high-mannose

and sialyated structures, while a significant increase was observed in fucosylated and fucosylated+sialylated structures during ectopically expression of 1482-eGFP (Figure 3.11B). The data indicates that protein BMEI1482 has a direct “effect” (effector protein) on N-glycome abundance but most interestingly, it influences N-glycome patterns favoring specific categories of glycan structures.

3.2.6. BMEI1482 disturbs secretion by retaining cargo at Golgi

Given that BMEI1482 interacts with components of the N-glycosylation, a post-translational modification process that takes place in the secretory pathway, we investigated whether ectopically expressed BMEI1482 disrupts the classical secretory pathway function. To test this hypothesis, HeLa-M (C1) cell line (given by Andrew A. Peden at Cambridge University) (Gordon et al., 2010) was used as a model to measure constitutive secretion. The cell line expresses a reporter construct or cargo (eGFP-FM4-FCS-hGH) that forms ligand-reversible dimers. When dimers of reporter cargo are linked to one another they form large aggregates in ER and cannot be secreted unless treated with rapamycin, which solubilizes and synchronizes their secretion. This model has been used to study host factors that are required in ER-Golgi transport. C1 cells were transfected with GalT-mCherry, a marker of the *trans*-Golgi network [4-galactosyltransferase (GalT)], with pENTRY-HA-BMEI1482 and with HA-empty vector. Then, transfected cells were treated with rapamycin to synchronize cargo secretion (eGFP-FM4-FCS-hGH). Data showed a similar trafficking kinetics of cargo eGFP-FM4-FCS-hGH after rapamycin treatment in both HA-BMEI1482 and HA-empty

vector transfected C1 cells. In both cases, the fluorescent intensity reached a maximum peak at about 20 min post rapamycin treatment (Figure 3.12B,C). However, the secretion of the cargo from the Golgi apparatus is apparently delayed in C1 cells expressing HA-BMEI1482 when compared to HA-empty vector C1 cells (Figure 3.12D). When the amount of the cargo accumulated at the Golgi area was quantified, fluorescence was 20% higher in HA-BMEI1482 C1 cells than in HA-empty vector C1 cells at each time point after the 20 min fluorescence peak (30, 40, 50, 60 min). These results demonstrate that ectopically expressed effector BMEI1482 interaction disturbs the secretion kinetics of cargo eGFP-FM4-FCS-hGH.

3.2.7. BMEI1482 sustains bacterial replication during infection in the mouse model

Mice provide a convenient and established model system for studying *Brucella* colonization of animals (Grilló et al., 2012; Silva et al., 2011). In fact, mice have proven particularly useful for elucidating the role that specific effector proteins play in regulating bacterial invasion and virulence (Keestra-Gounder et al., 2016). With this in mind, the murine model was exploited to test whether BMEI1482 effector protein is involved in bacterial colonization of mouse tissue (Grillo, 2012; Silva et al., 2011). For these experiments, groups of five mice were intraperitoneally inoculated with 10^6 CFU of B16M, ΔBMEI1482 and CΔBMEI1482 strains and then, at 7- days post-infection (d.p.i.), animals were euthanized according to ethical standards. Spleen, liver, uterus, lung, kidney, heart and brain were aseptically harvested to assess inflammation and bacterial colonization (Figure 3.13). Interestingly, differences in bacterial replication

were observed among all strains and tissues (Figure 3.14). At 7 d.p.i., B16M and CΔBMEI1482 strains showed no significant differences in bacterial replication in spleen and heart, while ΔBMEI1482 replication significantly decreased in uterus, kidney, lungs and brain and increased in liver when compared to B16M. Impressively, ectopically expression of BMEI1482 (CΔBMEI1482) significantly decreased the bacterial replication in liver, uterus, kidney, lungs and heart (Figure 3.14). Taken together, these data suggest that expression levels of BMEI1482 effector might play an important role in modulating the bacterial replication in a mice-tissue specific manner.

Table 3.1 Strains, plasmids, primers and antibodies provided and developed in this study.

Strains	Relevant characteristic(s)	Source
Brucella melitensis 16M (B16M)	Wild type (WT): *Brucella melitensi*s bv. 1 (16M) was obtained from ATCC and reisolated by this lab from an aborted goat fetus.	Kahl-McDonagh M.M. and Ficht T.A. (2006)
B16M ΔvirB2	WT::ΔvirB2	Kahl-McDonagh M.M. and Ficht T.A. (2006)
B16M ΔBMEI1482	WT::ΔBMEI1482	This work
B16M::pTEM-N-BMEI1482 (Grhg1)	WT strain expressing BlaM-BMEI1482	This work
B16M::pTEM-C-BMEI1482 (Grhg1)	WT strain expressing BMEI1482-BlaM	This work
B16M::pTEM-N-VceC (BMEI0948)	WTstrain expressing BlaM-VceC	This work
B16M::pTEM-C-BPE123 (BMEII1111)	WT strain expressing BPE123-BlaM	This work
B16M ΔvirB2::pTEM-N-BMEI1482	WT strain::ΔvirB2 expressing BlaM-BMEI1482	This work
B16M ΔvirB2::pTEM-C-BMEI1482	WT strain::ΔvirB2 expressing BMEI1482-BlaM	This work
B16M ΔvirB2::pTEM-N-VceC	WT strain::ΔvirB2 expressing BlaM-VceC	This work
B16MΔvirB2::pTEM-C-BPE123	WT strain::ΔvirB2 expressing BPE123-BlaM	This work
Escherichia coli DH5α	fhuA2 lac(del)U169 phoA glnV44 Φ80' lacZ(del)M15 gyrA96 recA1 relA1 endA1 thi-1 hsdR17	Invitrogen
HeLa cell line		Weber M.M, et al. (2013)
HeLa-M1 (C1)		Andrew A. Peden at Cambridge University
Raw264.7 cell line		Patrick K, et al. (2018)
HEK293T cell line		Patrick K, et al. (2018)

Table 3.1 Continued.

Plasmids	Characteristics (*)	Source
pKM244	pKM244 containing LacIq-Ptac and BlaM fragments, Cam^R	Weber M.M, et al. (2013)
pBBR1MCS-2	Broad-host range cloning vector, Kan^R	Martin Roop
pTEM	pBBR1MCS-2 containing functional LacIq-Ptac fragment, Kan^R	This work
pTEM-B16MBPE123-BCV	pTEM encoding full length BPE123 C-terminal labeled with BlaM, Kan^R	This work
pTEM-B16MVceC-ER	pTEM encoding full length VceC N-terminal labeled with BlaM, Kan^R	This work
pTEM-N-BMEI1482	pTEM encoding full length BMEI1482 N-terminal labeled with BlaM, Kan^R	This work
pTEM-C-BMEI1482	pTEM encoding full length BMEI1482 C-terminal labeled with BlaM, Kan^R	This work
pEGFP-C1	Broad-host range encodes the GFP mut variant as C-terminal, Kan^R	Weber M.M, et al. (2013)
pEGFP-C1-VceC (BMEI0948)	pEGFP-C1 encoding full length of B16MVceC-ER C-terminal EGFP, Kan^R	This work
pEGFP-C1-BMEI1482	pEGFP-C1 encoding full length of BMEI1482 C-terminal EGFP, Kan^R	This work
pENTRY-HA	AmpR	Patrick K, et al. (2018)
pENTRY-HA-BMEI1482	AmpR	This work
pNPTS138	Bacterial Expression; Bacterial allelic exchange vector with sacB; KanR	Martin Roop
pNPTS138-BMEI1482	pNPTS138 encoding upstream and downstream fragments of BMEI1482 with sacB and KanR	This work
pBBR1MCS-2-VirB-N3XFlag	pBBR1MCS-2 containing functional VirB promoter and 3XFlag, KanR	This work
pBBR1MCS-2-VirB-N3XFlag-BMEI1482	pBBR1MCS-2-VirB-N3XFlag encoding full lenght BMEI1482, KanR	This work

Table 3.1 Continued.

Primers	Sequence (5'-3')	Source
LacIq-Fwd	TGAAAAATACCATGCTCAGAAAAGG	IDT
Ptac-Rev	TTCCACACATTATACGAGCCGA	IDT
LacIq-Ptac-Frag.Rev	GTGTGAAATTGTTATCCGCTCACAATTCCACACATTATACGAGCCGATGA	IDT
LacIq-Ptac-Frag.Fwd	AATTAATGTGAGTTAGCTCACTCATTGAAAAATACCATGCTCAGAAAAGGCTTAACA	IDT
CAP-pBBR1MCS-2-Fwd	ATGAGTGAGCTAACTCACATTAATTGCG	IDT
LacOperator-Rev	TTGTGAGCGGATAACAATTTCACAC	IDT
LacIq-Ptac-Vector.Fwd	CCTTTTCTGAGCATGGTATTTTTCAATGAGTGAGCTAACTCACATTAATTGCG	IDT
LacIq-Ptac-Vector.Rev	TCATCGGCTCGTATAATGTGTGGAATTGTGAGCGGATAACAATTTCACAC	IDT
LacZa-pBBR1MCS-2-Fwd	CAGCTTTTGTTCCCTTTAGTGAGGGTTAAT	IDT
LacZa-pBBR1MCS-2-Rev	CAATTCGCCCTATAGTGAGTCGTAT	IDT
BlaM-Fwd	ATGAGTATTCAACATTTCCGTGTCG	IDT
BlaM-TAA-Rev	TTACCAATGCTTAATCAGTGAGGC	IDT
BlaM-Rev	CCAATGCTTAATCAGTGAGGCACCTA	IDT
Seq pBBR1MCS-2-LacIqPtac-Fwd	CAGCTTTTGTTCCCTTTAGTGAG	IDT
Seq pBBR1MCS-2-LacIqPtac-Rev	GCGCAACGCAATTAATGTGAG	IDT
M13-Fwd	TGTAAAACGACGGCCAGT	IDT
M13 (-21) F	TGTAAAACGACGGCCAGT	Sigma
M13-Rev	CAGGAAACAGCTATGAC	IDT
SalI-N-BlaM-Fwd	CCCCCGTCGACatgagtattcaacat	IDT
BamHI-C-BlaM-Rev	CCCCCGGATCCttaccaatgcttaat	IDT
N-VceC-Frag1.Fwd	TAGGTGCCTCACTGATTAAGCATTGGatgaaggaatggctcagcgg	IDT
BamHI-N-VceC-Rev	CCCCCGGATCCctaattgcgggtttc	IDT
N-VceC-Frag2.Rev	gatgatgccgctgagccattccttcatCCAATGCTTAATCAGTGAGGCACC	IDT

Table 3.1 Continued.

Primers	Sequence (5'-3')	Source
SalI-C-BPEI123-Fwd	CCCCCGTCGACatgagcttgttgctg	IDT
C-BPE123-Frag2.Rev	CGACACGGAAATGTTGAATACTCATtgcctgtcccgccag	IDT
C-BPE123-Frag1.Fwd	aaccgttgaactggcgggacaggcaATGAGTATTCAACATTTCCGTGTCGC	IDT
N-BMEI1482-Frag1.Fwd	TAGGTGCCTCACTGATTAAGCATTGGatgaaattcaacggaaccatcatcggtatcgg	IDT
BamHI-N-BMEI1482-Rev	CCCCCGGATCCttattgattgtcagc	IDT
N-BMEI1482-Frag2.Rev	cgatgatggttccgttgaatttcatCCAATGCTTAATCAGTGAGGCACC	IDT
SalI-C-BMEI1482-Fwd	CCCCCGTCGACatgaaattcaacgga	IDT
C-BMEI1482-Frag2.Rev	CGACACGGAAATGTTGAATACTCATttattgattgtcagcacccggaatt	IDT
C-BMEI1482-Frag1.Fwd	gaaaattccgggtgctgacaatcaaATGAGTATTCAACATTTCCGTGTCGCCCTTATTCC	IDT
VirB1-Fwd	ccagtaaaaaaacgacagcc	IDT
VirB3-Rev	gctataggcggatgcccg	IDT
pEGFP-C1-BMEI1482-Fwd	CCAGATCTATGAAATTCAACGGAACCATCATCG	IDT
pEGFP-C1-BMEI1482-Rev	CCGTCGACTTGATTGTCAGCACCCGGAATT	IDT
pEGFP-C1-BMEI0948-Fwd	CCAGATCTATGAAGGAATGGCTCAGCGGCA	IDT
pEGFP-C1-BMEI0948-Rev	CCGTCGACATTGCGGGTTTCTCCCTTGG	IDT
pGFP-Seq-F	CACTCTCGGCATGGACGAGC	IDT
pGFP-Seq-R	TGGTGCAGATGAACTTCAGG	IDT
pNPTS-1482-PA-Fwd	cttctctgcaggatatctggatccggcaagttcggtaaggtc	Sigma
pNPTS-1482-PD-Rev	taaggccttgactagaggGTCGACGgccgatcctgataagag	Sigma
Bru1482-PC-Fwd	catgaaattcaacggaaccatcatcggtatcgaaaattccgggtgctgac	Sigma
Bru1482-PB-Rev	gataccgatgatggttccgttgaatttcatgaacttcgctgtcctgctc	Sigma
N-Term-Seq-Fwd	ACAACACTACCCAATAATGACCG	Sigma
pVirb-KpnL-F	GTTCGGGGTACCTGCCGCCTTGTTCACCGGCT	Sigma

Table 3.1 Continued.

Primers	Sequence (5'-3')	Source
pVirB - 3XFLAG - XhoI - R	GGGCCGCTCGAGCTTGTCATCGTCATCCTTGTAGTCGATGTCATGATCTTTATAATCAC CGTCATGGTCTTTGTAGTCCATGGATCGTCTCCTTCTCAGAG	Sigma
pVirB - Xho - R	GGGCCGCTCGAGGGATCGTCTCCTTCTCAGAG	Sigma
(C)3xFLAG-XbaI-F	CGCCGCTCTAGAGACTACAAAGACCATGACG	Sigma
(C)3xFLAG-SacI-R	GGGCCCGAGCTCCTACTTGTCATCGTCATCCTTGT	Sigma
BMEI1482-XhoI-F	GGGCCGCTCGAGATGAAATTCAACGGAACCATC	Sigma
BMEI1482-BamH-NF-R	CGCCGCGGATCCTTATTGATTGTCAGCACCCG	Sigma
Antibodies	**Characteristics (*)**	**Source**
monoclonal IgG anti-β-lactamase	Mouse IgG uncojugated, primary antibody (8A5.A10)	Santa Cruz Biotechnology
polyclonal anti-mouse IgG HRP	Donkey IgG HRP conjugated, secondary antibody (sc-231)	Santa Cruz Biotechnology
monoclonal anti-HA High Affinity	Rat IgG unconjugated, primary antibody (3F10)	Roche
polyclonal anti-rat IgG HRP	Goat IgG (H+L) HRP conjugated, secondary Antibody (AB_228356)	Thermo Scientific
monoclonal anti-calnexin	Mouse IgG unconjugated, primary antibody (AF18)	Thermo Scientific
polyclonal anti-mouse IgG Alexa Fluore 594	Goat IgG (H+L) Alexa Fluor 594 conjugated, secondary antibody (AB_2534073)	Thermo Scientific
Hoechst 33342	Blue fluorescent stain specific for DNA (i.e., nuclei of eukaryotic cells)	Thermo Scientific

(*) Cam^R, Cloramphenicol resistance; Kan^R, Kanamycin resistance; Amp^R, Ampicillin resistance.

Figure 3.1 Genetic interaction profile of effector protein BMEI1482 expressed in *S. cerevisiae*. A) Schematic diagram of the EMAP screening approach. Bacterial effector (BMEI1482) expressing query strains were mated with the *S. cerevisiae* non-essential gene deletion library according to (Patrick et al., 2018). S-scores denotate the quantified genetic interactions between bacterial effector (BMEI1482) and *S. cerevisiae* mutant strains (Collins et al., 2006). Z-scores denotate the effector-host genetic interaction profile correlated to host-host profiles (*S. cerevisiae* genetic profile library) to reveal functional biology of BMEI1482 effector. B) STRING analysis of EMAP hits (z>5) associated to BMEI1482 effector. STRING analysis reports functional modules (protein-protein associations) (von Mering et al., 2005). Green circle denotates proteins associated to translocon and glycosylation biology. Blue circle denotates proteins associated to GPI biosynthesis biology.

Figure 3.1 Continued.

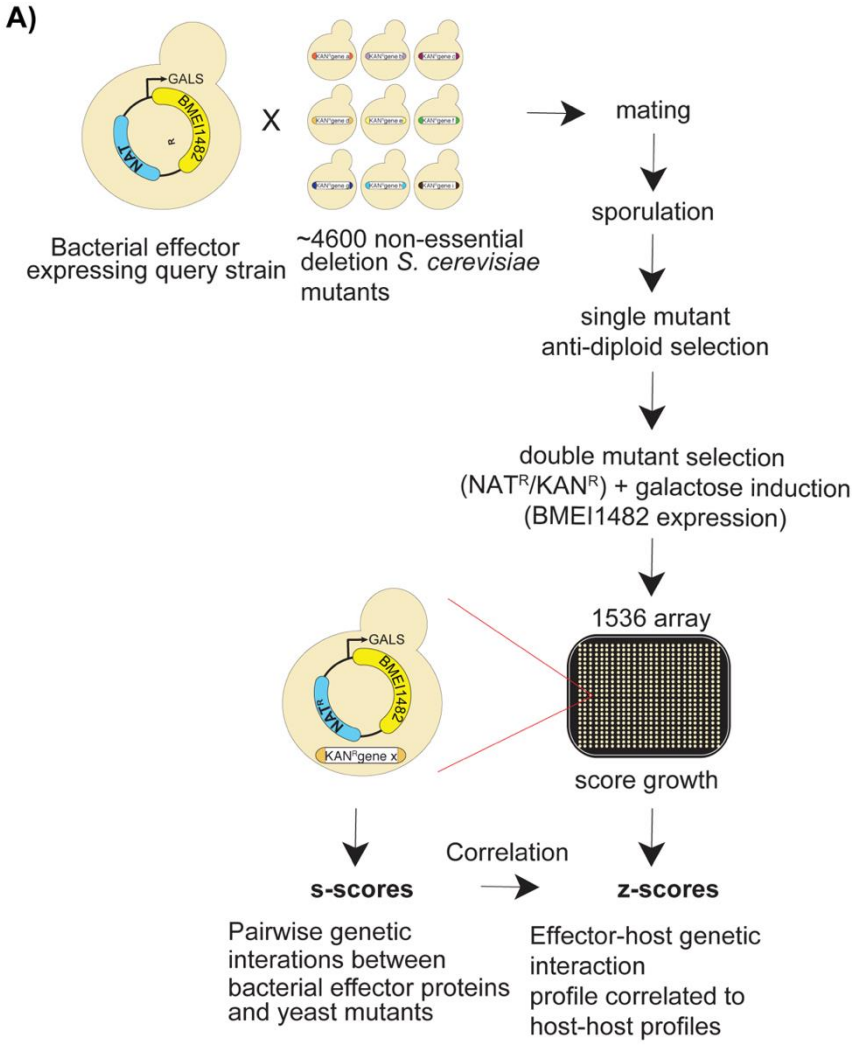

Figure 3.1 Continued.

B)

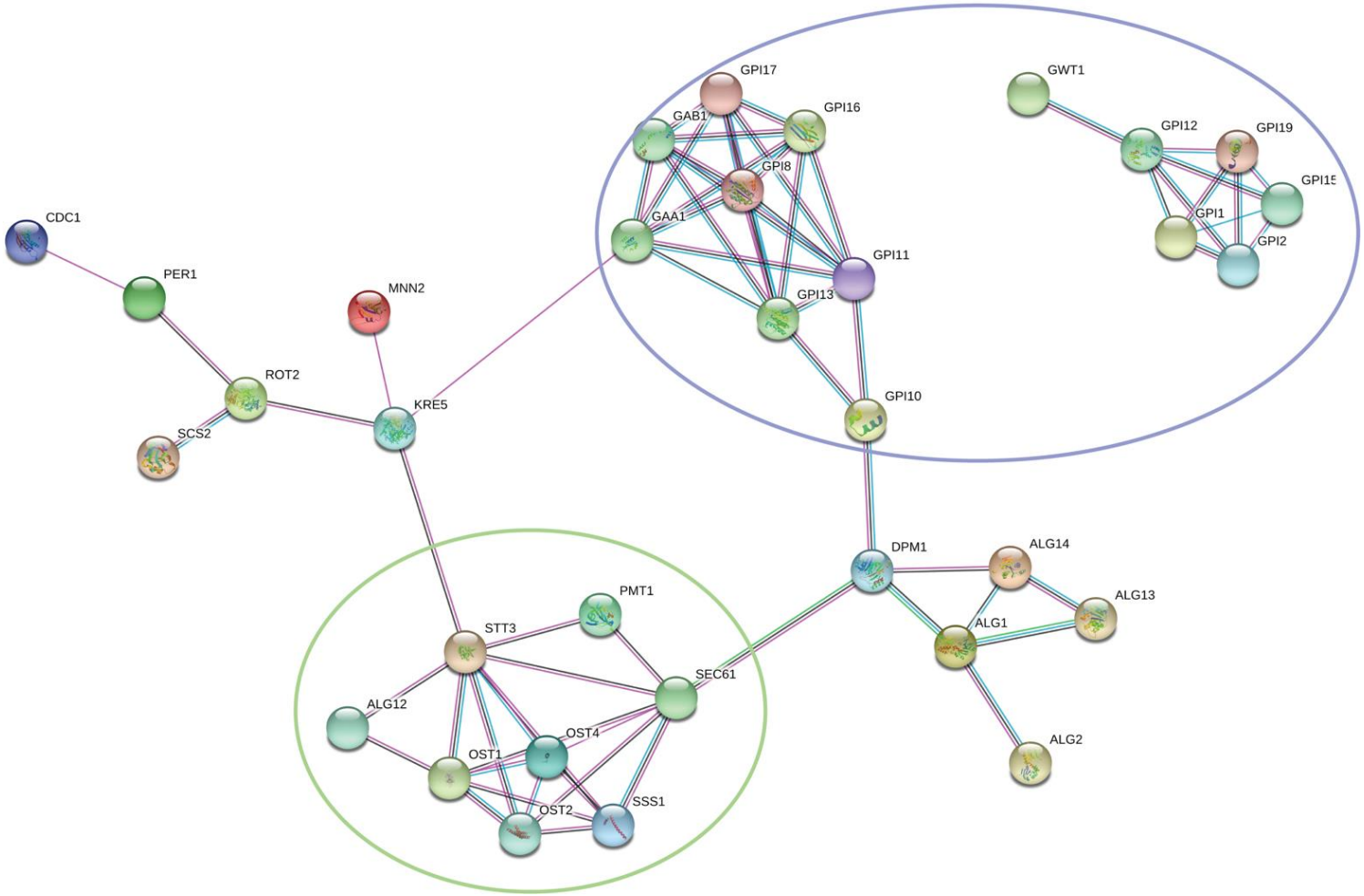

Figure 3.2 Construction of pTEM-1 backbone. A) pBBR1MCS-2 was linearized by PCR and LacIqPtac fragment was PCR amplified from pKM244 plasmid. LacIqPtac was cloned into linearized pBBR1MCS-2 to replace Lac promoter. B) Agarose gel images shows PCR linearized pBBR1MCS-2 (5,144 bp) and PCR fragment LacIqPtac (1,701 bp).

Figure 3.2 Continued.

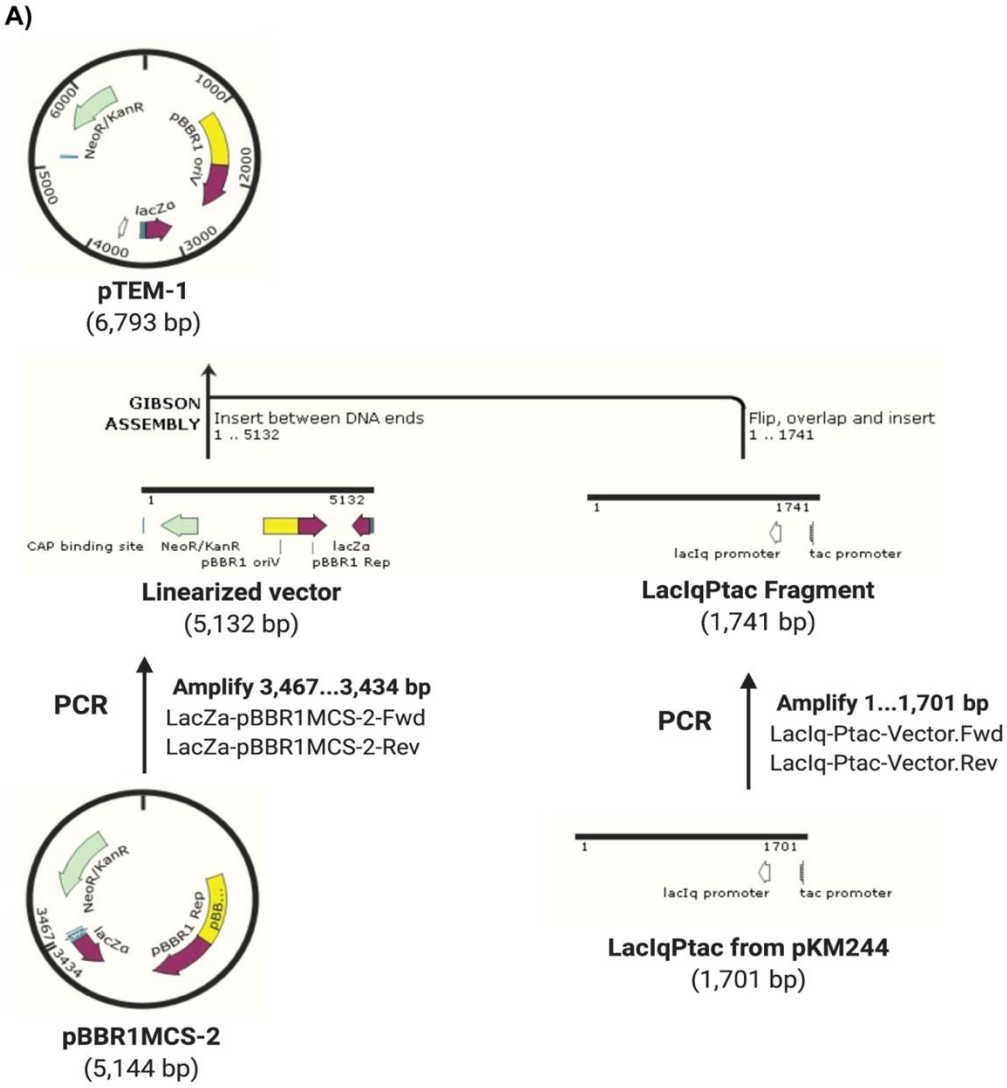

Figure 3.2 Continued.

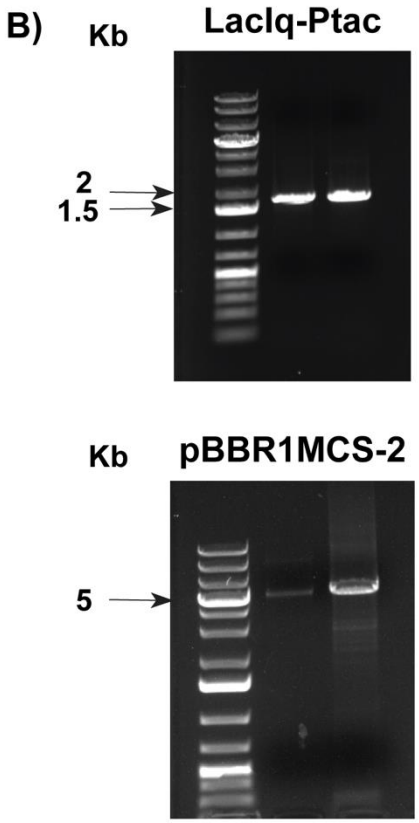

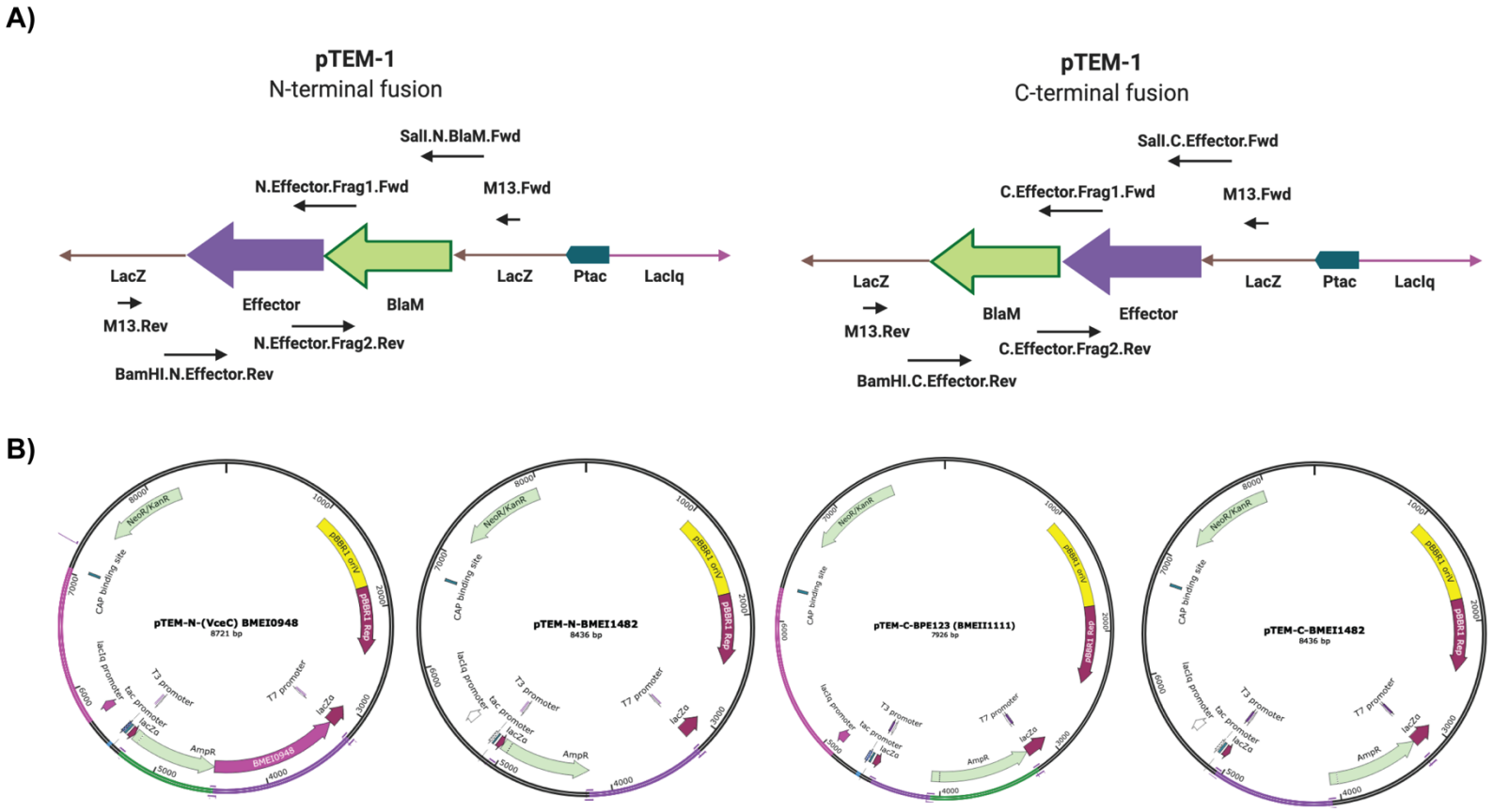

Figure 3.3 Diagram representing pTEM plasmids expressing *B. melitensis* effector proteins VceC (BMEI0948) and BMEI1482. A) Representation of fusion PCR to obtain TEM-1constructs. Briefly, β-lactamase gene (BlaM) was used to label effector gene at both N- and C-terminal. B) Maps of pTEM plasmids expressing effector proteins.

Figure 3.4 Schematic description of vector construction and mutant creation. A) Flowchart representing BMEI1482 operon, vector construction and downstream analyses. To delete BMEI1482 gene, UPstream fragment was PCR amplified using primers 1482-PA-Fwd and 1482-PB-Rev and DNstream fragment was PCR amplified using primers 1482-PC-Fwd and 1482-PD-Rev, using *B. melitensis* genomic DNA. The UPstream and DNstream fragments were used to obtain a single UP-DN fragment through fusion PCR (1,534 bp). UP-DN fragment digested with XbaI and XmaI was cloned into pNPTS138 to obtain pNPTS138-BMEI1482. B) Clone selection and PCR analysis using primers 1482-PA-Fwd and 1482-PD-Rev primers. Agarose gel shows bands that represent: 1) presence of gene BMEI1482 (~2.4Kb) and 2) absence of gene BMEI1482 (~1..5Kb). Clones with red arrows were selected based on PCR result coupled with presence of bacterial growth on TSASuc10 and absence of bacterial growth on TSAKan50, indicating that homologous recombination ocurred.

Figure 3.4 Continued.

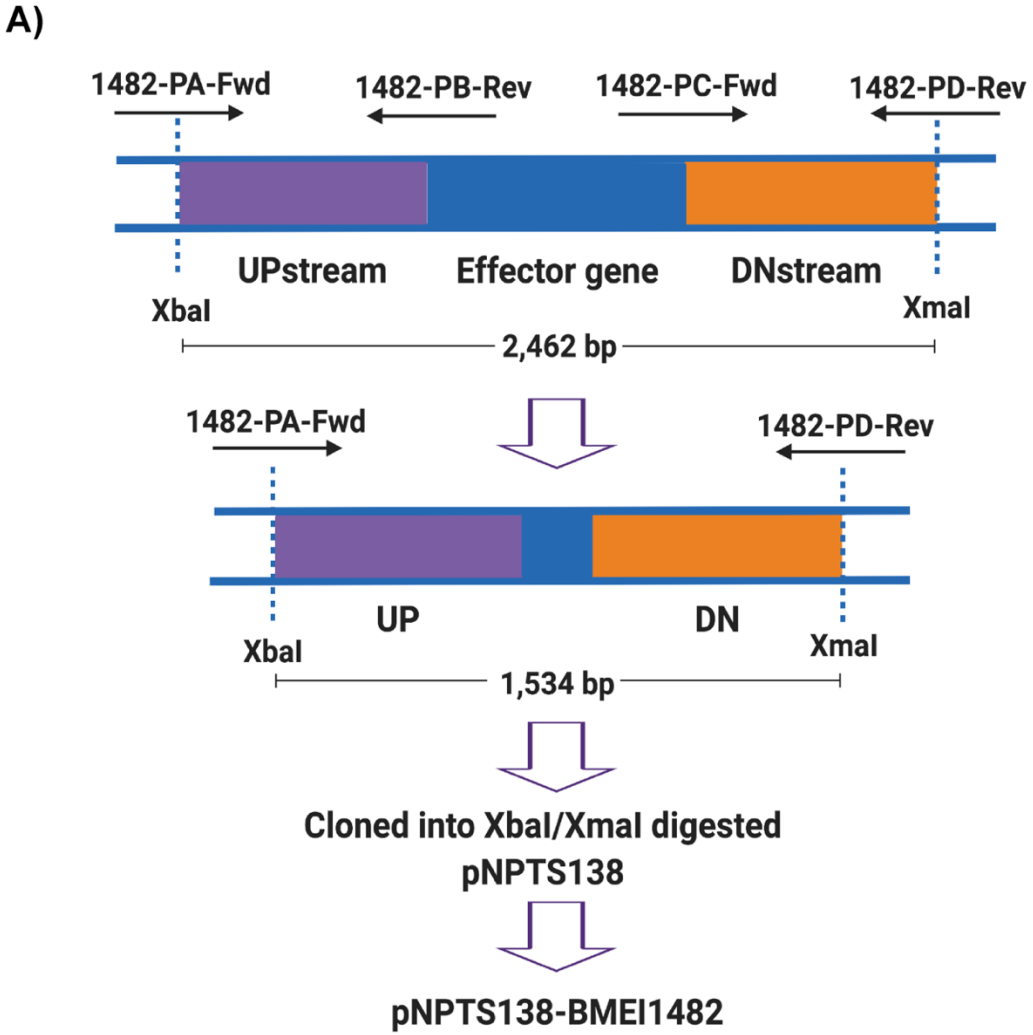

Figure 3.4 Continued.

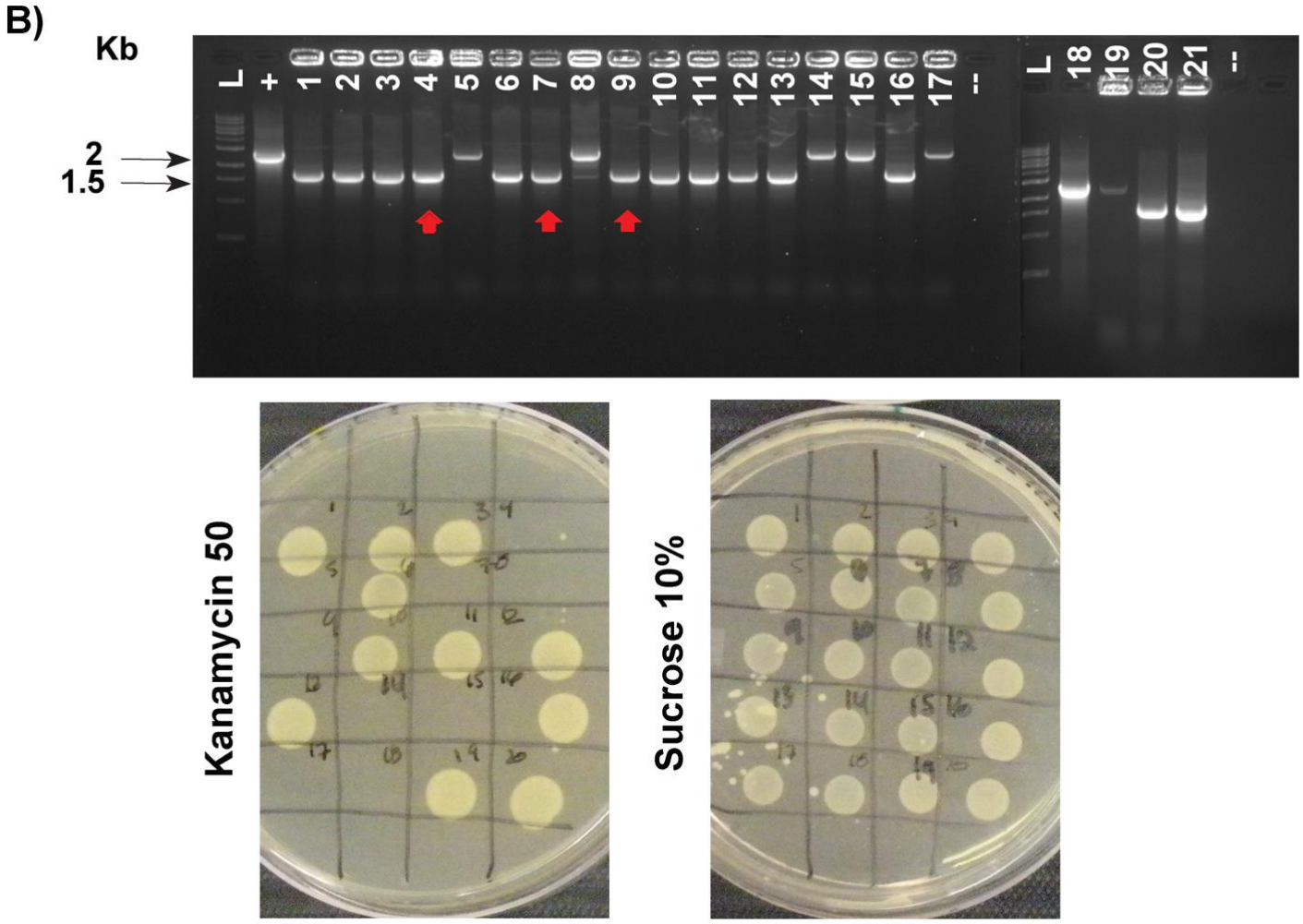

Figure 3.5 Schematic description of vector construction for ectopic expression of BMEI1482 and complemented mutant strain creation. A) Flowchart representing fragments of VirB promoter and BMEI1482 effector gene. Genomic DNA from *B. melitensis* was used to PCR amplify the virB promoter using primers pVirb-KpnL-Fwd and pVirB-3XFLAG-XhoI-Rev (500bp) and to PCR amplify the BMEI1482 effector gene using primers BMEI1482.XhoI.F and BMEI1482.BamH.NF.R (972 bp). VirB promoter fragment was cloned into KpnL and XhoI digested backbone pBBR1MCS-2 to obtain plasmid pCVirB-N3XFlag. Then, BMEI1482 gene was cloned into XhoI and BamHI digested pCVirB-N3XFlag to obtain pCVirB-N3XFlag.BMEI1482. B) Description of clone selection and PCR analysis using the represented primers on the left. Agarose gel shows bands that represent: 1) presence of gene BMEI1482 (~2.4Kb) (control WT, +), 2) absence of gene (~1.5Kb) (control mutant, C1.P2#7) and 3) presence of exogenous gene BMEI1482 (~1.2Kb and ~1.1Kb) using different primers sets (indicated on the left) indicative of gene mutation (pNPTS-1482-PA-Fwd and pNPTS-1482-PD-Rev) and plasmid complementation (N-Term-Seq-Fwd with M13-Rev and N-Term-Seq-Fwd with BMEI1482-BamH-NF-R). C1.P2#7 represents *B. melitensis* strain mutant of effector BMEI1482 gene (B16MΔBMEI1482).

Figure 3.5 Continued.

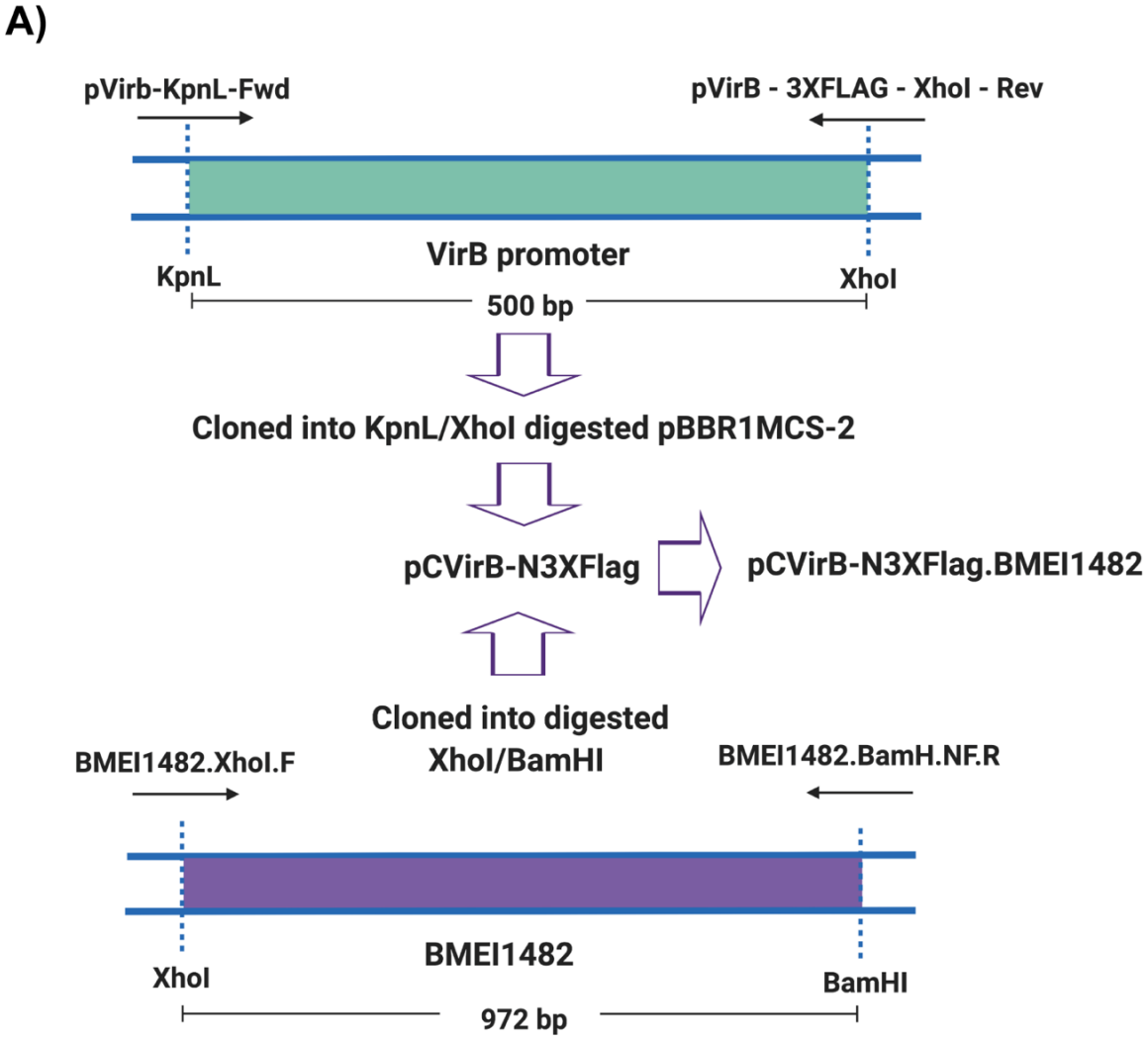

Figure 3.5 Continued.

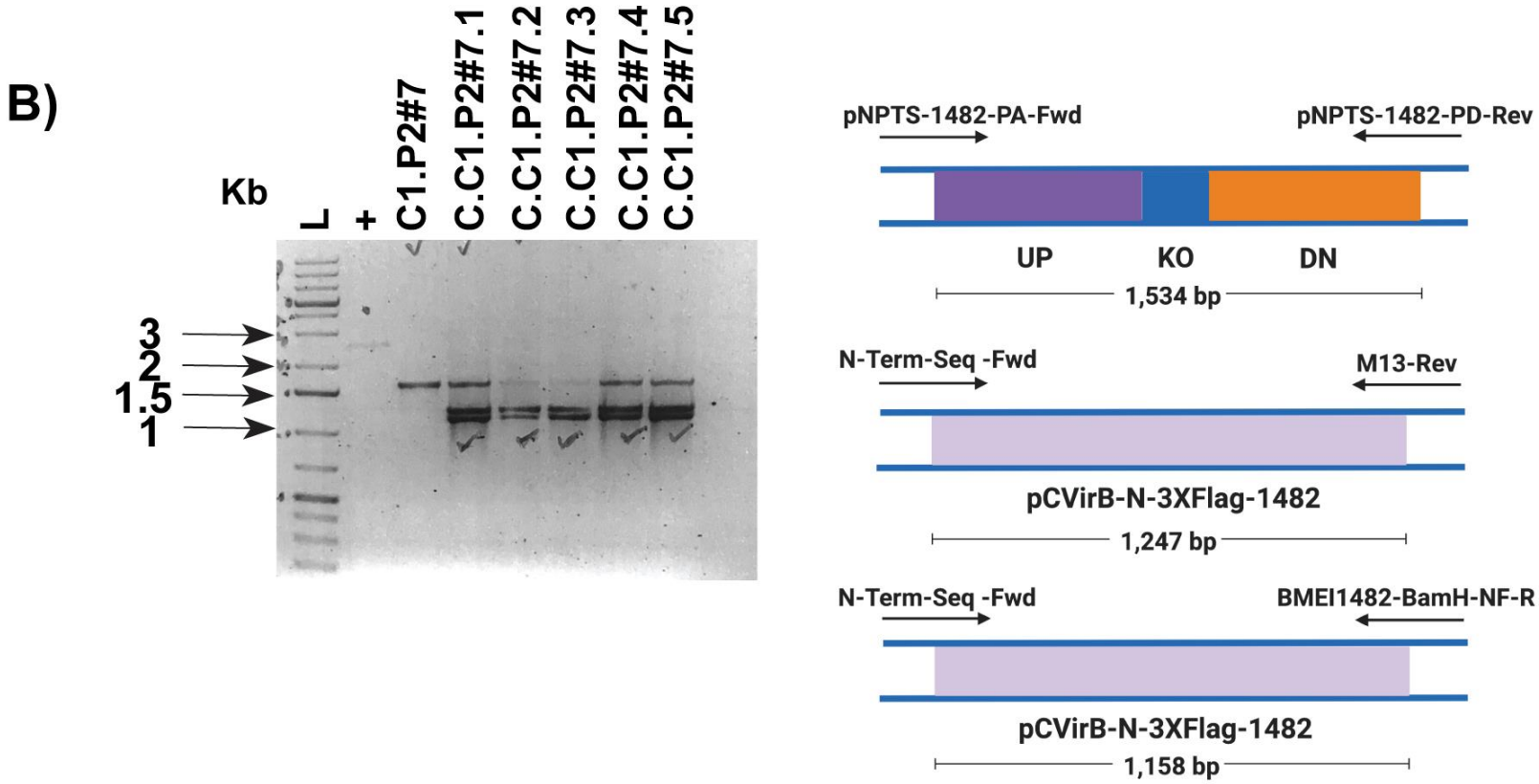

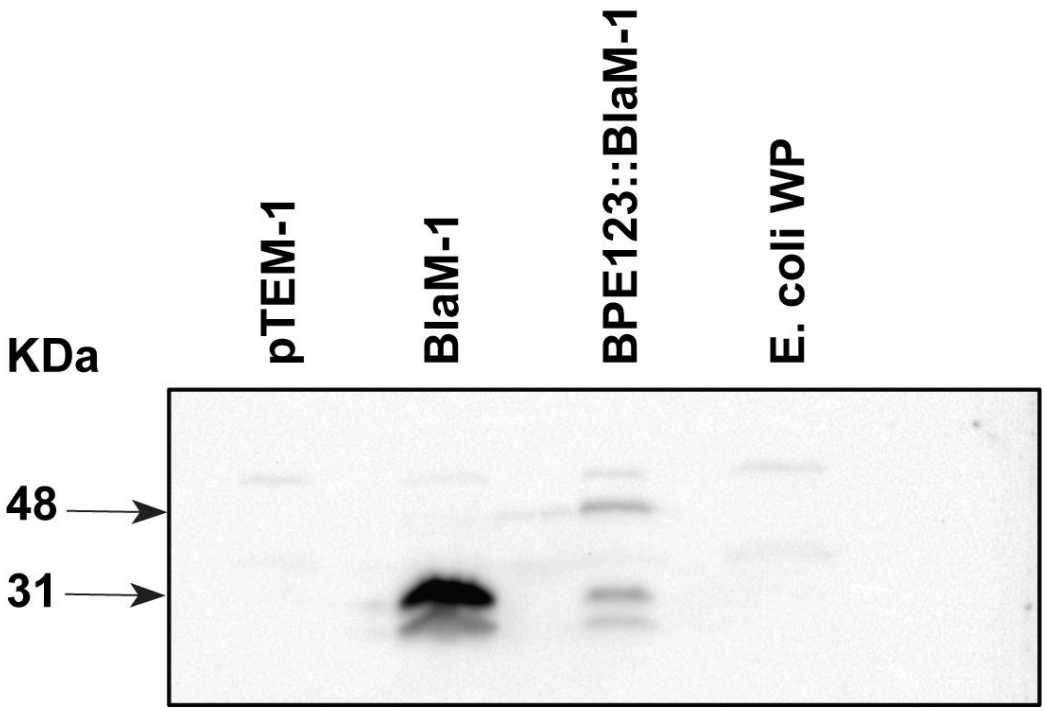

Figure 3.6 Representation of effector protein-BlaM tagged expression for protein translocation (TEM-1) assay. *E. coli* strains carrying plasmid pTEM-1 variants were treated with IPTG to induce effector protein expression. Samples were processed for protein isolation and western blot analysis was performed using mouse anti-β lactamase antibody and donkey anti-mouse IgG HRP. Lanes denotates: 1) pTEM-1 (empty vector), 2) BlaM-1 (pTEM-1::BlaM-1), 3) BPE123::BlaM-1 (pTEM-1::BPE123-BlaM-1) and 4) *E. coli* WP (whole protein obtained from bacteria).

Figure 3.7 Protein translocation assay (TEM-1 assay) to determine translocation of effectors into host cells cytosol by *vir*B-T4SS during bacterial infection. A) Quantification of fluorescence ratio (a shift from green to blue) after RAW264.7 cells were infected with IPTG induced strains *B. melitensis* 16M (WT) and *B. melitensis* 16M (△virB2) expressing TEM-1 fusions of BMEI1482, and VceC (BMEI0948) and BPE123 (BMEII1111) as known controls (16 h.p.i). B) Epifluorescence microscopy of protein translocation assay. RAW26.7 were infected with IPTG induced *Brucella* strains (WT and △virB2) carrying plasmids pTEM-C1 (empty plasmid), N-VceC-2 C.2 (as a N-terminal label control), C-BPE123-T4.1 C.1 (as a C-terminal control), N-BMEI1482-13 C.1 and C-BMEI1482-2 C.1.The results shown are means ± SD from three independent experiments performed in sextuplicates. The one-way ANOVA test coupled with multiple comparison of Kruskal Wallis were used to analyze differences between individual sets of data. Statistically significant differences ($P<0.0001$) are indicated by asterisks (****), as compared to corresponding controls: WT or △virB2.

Figure 3.7 Continued.

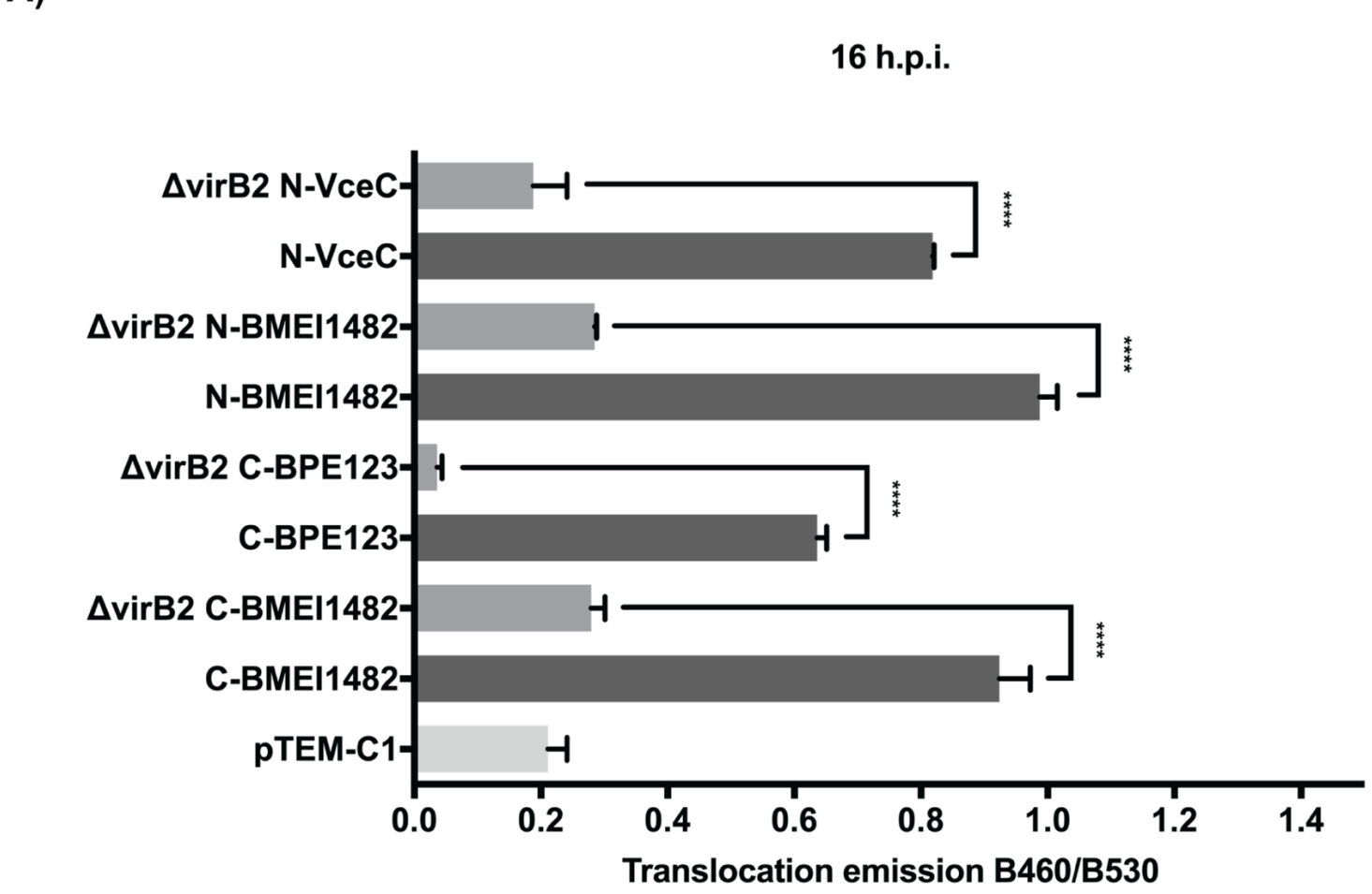

Figure 3.7 Continued.

B)

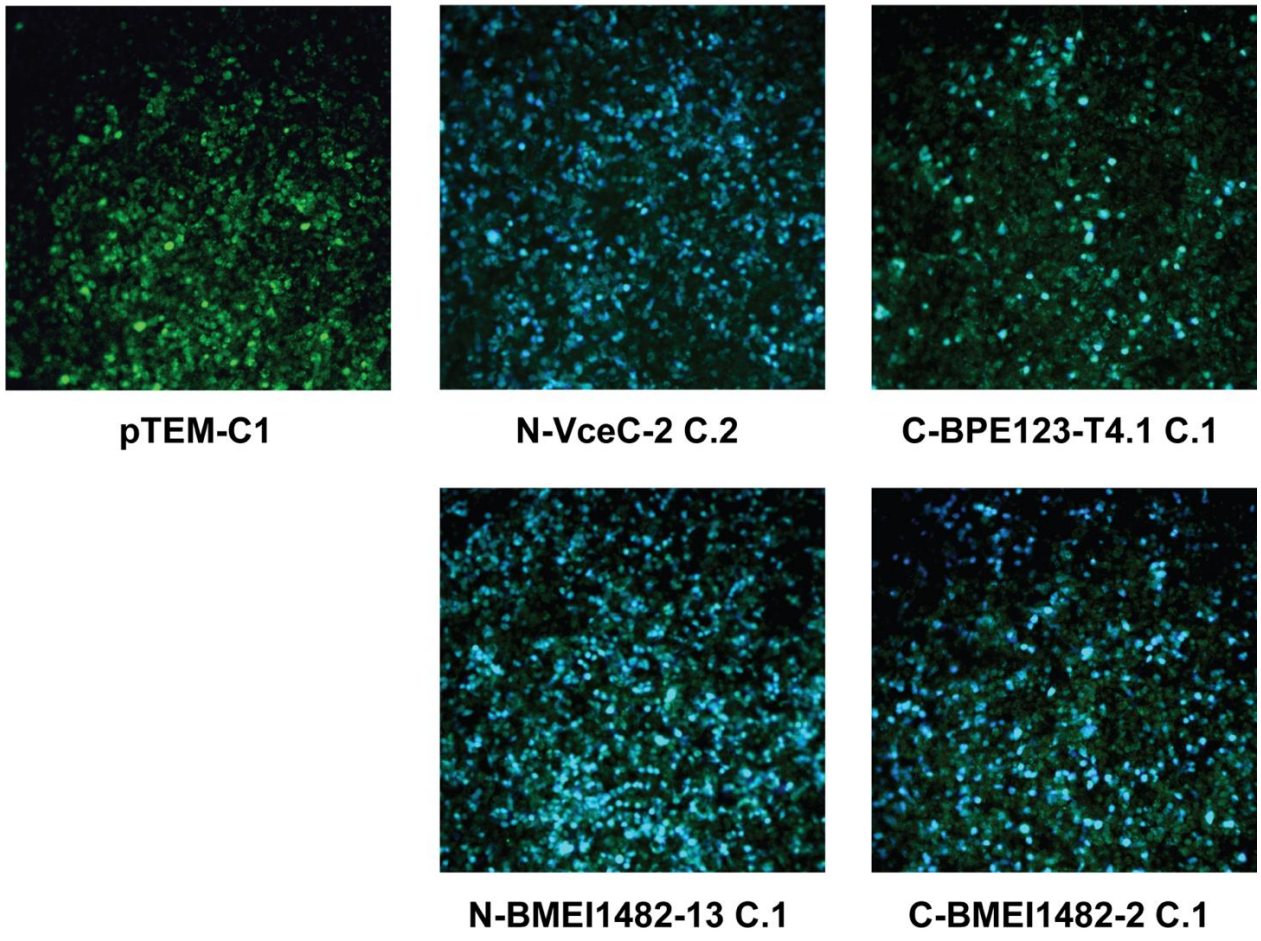

Figure 3.8 Assessment of bacterial counting in bone marrow derived macrophages (BMDMs). A) Schematic representation of BMDMs infection. *B. melitensis* 16M strains: B16M (WT), B16M ΔBMEI1482 and B16M CΔBMEI1482 (ΔBMEI1482::N3XFlagBMEI1482) were used to infect BMDMs at an MOI of 100. Infected cells were lysed at different time points, CFU was determined by serial dilutions and data analyzed. B) Bacterial invasion and replication were measured by CFU counting at 0, 16, 24 and 48 h.p.i. At 0 h.p.i. and 16 h.p.i. no differences were observed among *Brucella* strains (bacterial invasion and replication, respectively). Replication of CΔBMEI1482 was decreased at 24 and 48 h.p.i. The results shown are means ± SD from three independent experiments performed in triplicates. The one-way ANOVA test coupled with multiple comparison of Kruskal Wallis were used to analyze differences between individual sets of data. Statistically significant differences ($P<0.0001$) are indicated by asterisks (****), as compared to corresponding controls: WT or △BMEI1482.

Figure 3.8 Continued.

A)

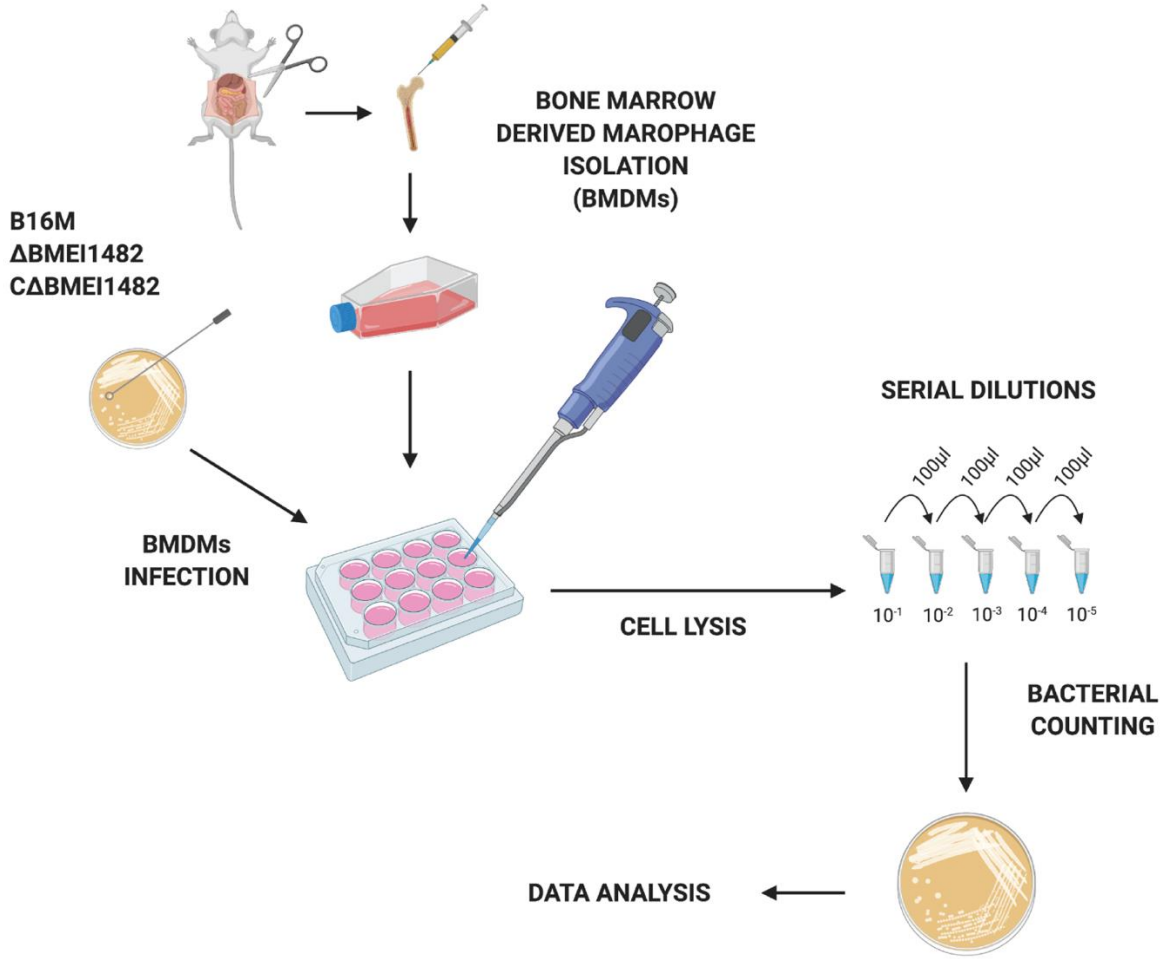

Figure 3.8 Continued.

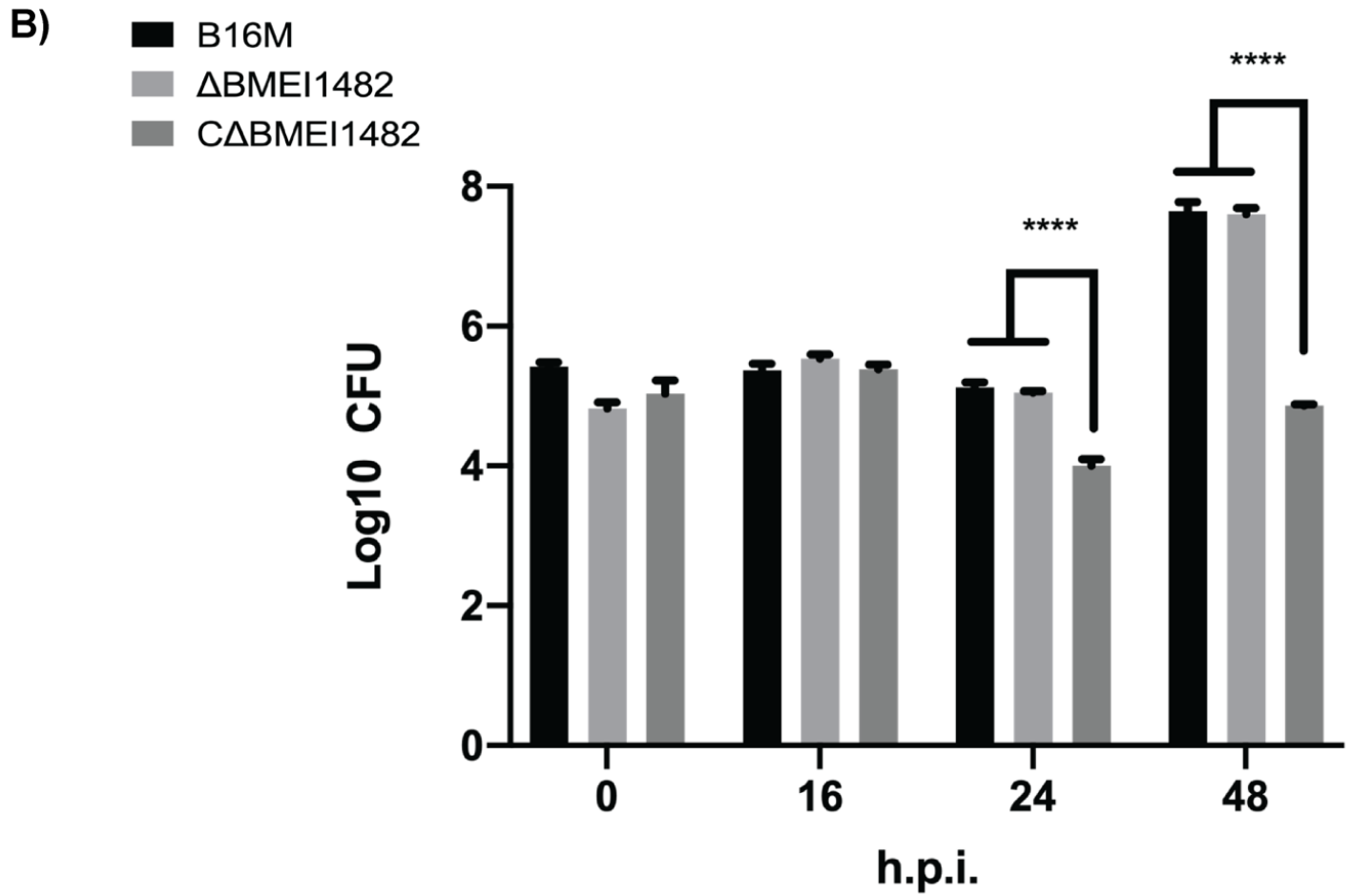

Figure 3.9 Host factors that interact with effector protein BMEI1482. A) Schematic representation of the experimental approach. HEK293Ts cells were transfected with BMEI1482-eGFP and (BMEI0948) VceC-eGFP and eGFP as controls. At 36 h.p.t. samples were harvested using GFP-trap kit and analyzed by mass spectrometry (LC-MS/MS). Data was manually analyzed to eliminate host proteins found in controls. Hits that were found only in BMEI1482-eGFP were manually annotated using uniport database. B) STRING analysis of host proteins that co-immunoprecipitated with BMEI1482-eGFP. STRING analysis reports functional modules (protein-protein associations). Blue circle represents N-glycosylation machinery, OST (oligosaccharyltransferase complex). C) Blot that demonstrates the specific interaction between BMEI1482 and RPN1 and RPN2, OST complex subunits. HEK293Ts cells expressing BMEI1482-eGFP and eGFP were processed for total protein isolation and western blot analysis was performed using mouse anti-RPN1, anti-RPN2 antibodies and anti-eGFP antibodies.

Figure 3.9 Continued.

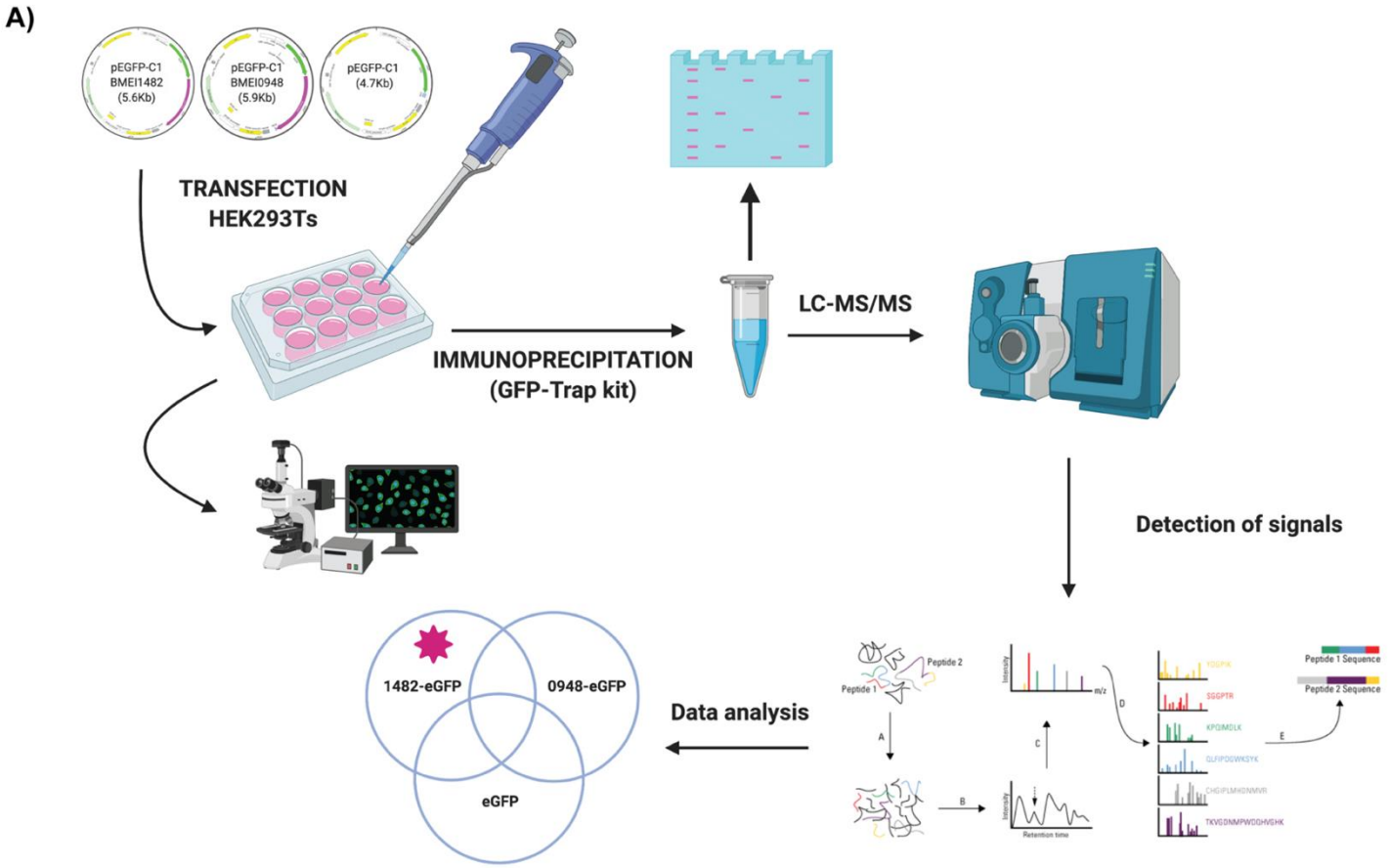

Figure 3.9 Continued.

B)

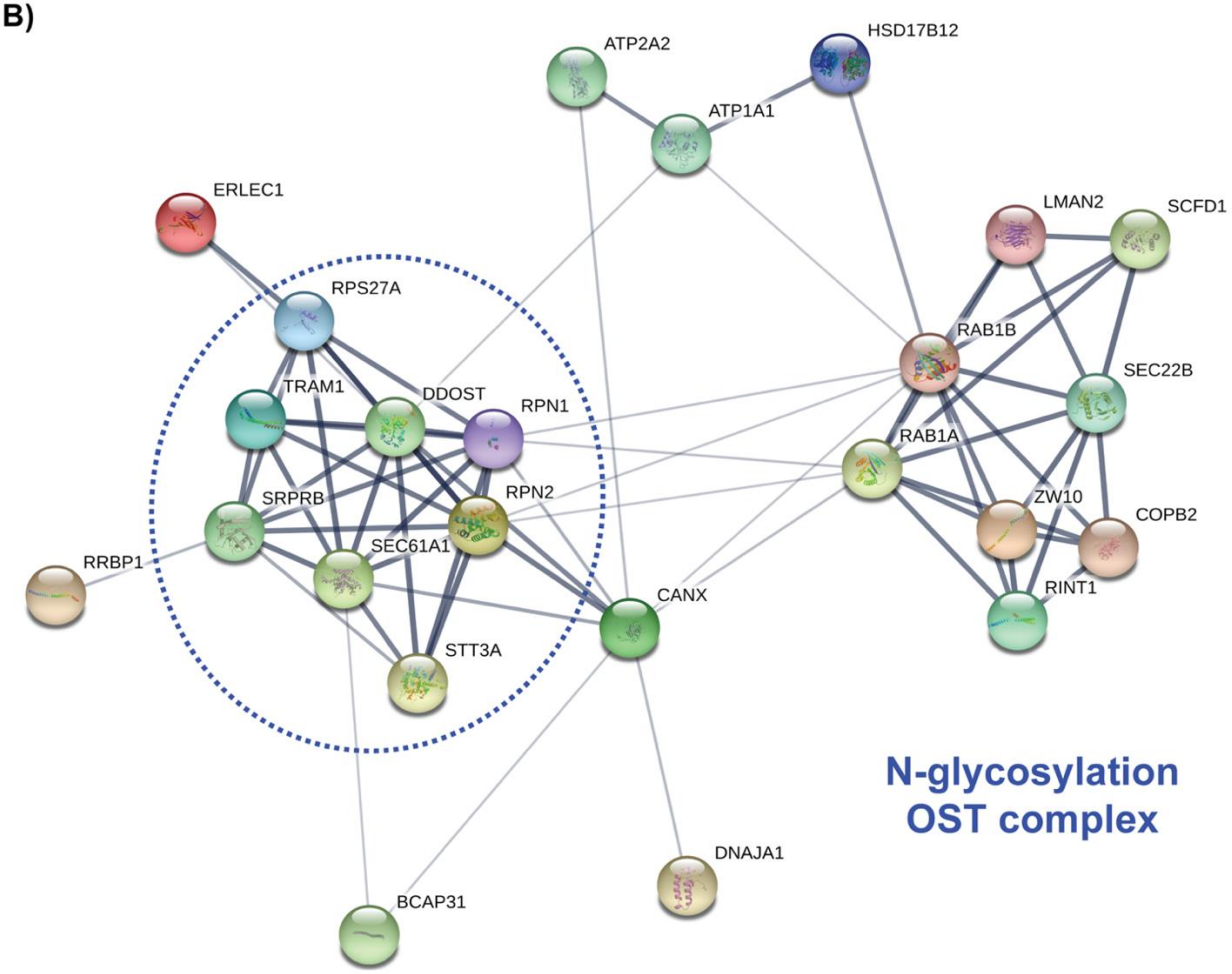

Figure 3.9 Continued.

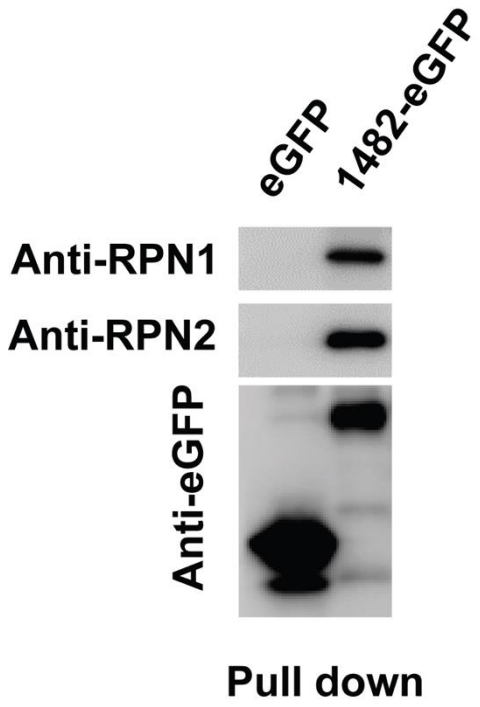

Table 3.2 List of proteins that co-immunoprecipitated with BMEI1482-eGFP.

KDa*	GIN	Uniprot Accession	Description	Score
112.8	ATP1A1	P05023	Sodium/potassium-transporting ATPase subunit alpha-1	316.56
68.5	**RPN1**	P04843	Dolichyl-diphosphooligosaccharide--protein glycosyltransferase subunit	168.47
33.8	**BMEI1482**	Q8YFN8	*Brucella melitensis* (strain 16M) Effector	149.93
44.8	DNAJA1	P31689	DnaJ homolog subfamily A member 1	128.10
122.3	NOMO2	Q5JPE7	Nodal modulator 2	119.83
67.5	CANX	P27824	Calnexin	114.61
34.3	HSD17B12	Q53GQ0	Very-long-chain 3-oxoacyl-CoA reductase	102.66
204.2	ECM29	Q5VYK3	Proteasome-associated protein ECM29 homolog	98.90
17.9	RPS27A	P62979	Ubiquitin-40S ribosomal protein S27a	85.76
69.2	**RPN2**	P04844	Dolichyl-diphosphooligosaccharide--protein glycosyltransferase subunit	83.86
97.1	KPNB1	Q14974	Importin subunit beta-1	78.56
129.9	RTN4	Q9NQC3	Reticulon-4	66.29
61.6	PIGS	Q96S52	GPI transamidase component PIG-S	63.48
45.7	AUP1	Q9Y679	Ancient ubiquitous protein 1	62.20
114.7	ATP2A2	P16615	Sarcoplasmic/endoplasmic reticulum calcium ATPase 2	57.26
22.1	RAB1B	Q9H0U4	Ras-related protein Rab-1B	51.08
98.8	GRIA2	P42262	Glutamate receptor 2	50.85
205.1	NUP210	Q8TEM1	Nuclear pore membrane glycoprotein 210	50.07
102.4	COPB2	P35606	Coatomer subunit beta'	50.00
88.8	ZW10	O43264	Centromere/kinetochore protein zw10 homolog	47.88
72.3	SCFD1	Q8WVM8	Sec1 family domain-containing protein 1	47.26
50.8	**DDOST**	P39656	Dolichyl-diphosphooligosaccharide--protein glycosyltransferase 48 kDa	44.80
22.6	RAB1A	P62820	Ras-related protein Rab-1A	41.23
51.2	HADHB	P55084	Trifunctional enzyme subunit beta, mitochondrial	41.02

Table 3.2 Continued.

KDa*	GIN	Uniprot Accession	Description	Score
80.4	ACSL3	O95573	Long-chain-fatty-acid--CoA ligase 3	40.27
34.9	LRRC59	Q96AG4	Leucine-rich repeat-containing protein 59	39.70
43.0	TRAM1	Q15629	Translocating chain-associated membrane protein 1	38.67
40.2	LMAN2	Q12907	Vesicular integral-membrane protein VIP36	36.58
47.7	LNP	Q9C0E8	Protein lunapark	36.35
25.1	SIGMAR1	Q99720	Sigma non-opioid intracellular receptor 1	36.14
29.7	SRPRB	Q9Y5M8	Signal recognition particle receptor subunit beta	35.73
31.7	AGPAT1	Q99943	1-acyl-sn-glycerol-3-phosphate acyltransferase alpha	35.28
152.4	RRBP1	Q9P2E9	Ribosome-binding protein 1	34.72
59.1	LPCAT1	Q8NF37	Lysophosphatidylcholine acyltransferase 1	33.91
156.2	KTN1	Q86UP2	Kinectin	33.14
122.8	ESYT1	Q9BSJ8	Extended synaptotagmin-1	32.50
54.8	ALDH3A2	P51648	Fatty aldehyde dehydrogenase	31.19
52.6	FAF2	Q96CS3	FAS-associated factor 2	30.67
24.5	SEC22B	O75396	Vesicle-trafficking protein SEC22b	29.50
219.6	THADA	Q6YHU6	Thyroid adenoma-associated protein	28.76
102.3	ESYT2	A0FGR8	Extended synaptotagmin-2	28.55
54.8	ERLEC1	Q96DZ1	Endoplasmic reticulum lectin 1	27.96
49.1	ECSIT	Q9BQ95	Evolutionarily conserved signaling intermediate in Toll pathway, mitochondrial	27.90
27.9	BCAP31	P51572	B-cell receptor-associated protein 31	27.87
90.6	RINT1	Q6NUQ1	RAD50-interacting protein 1	26.04
63.8	MTDH	Q86UE4	Protein LYRIC	25.85
52.2	SEC61A1	P61619	Protein transport protein Sec61 subunit alpha isoform 1	25.49
56.8	CYP51A1	Q16850	Lanosterol 14-alpha demethylase	25.23
80.5	**STT3A**	P46977	Dolichyl-diphosphooligosaccharide--protein glycosyltransferase subunit	22.37

Figure 3.10 Assessment of glycoproteome during bacterial infection of bone marrow derived macrophages (BMDMs). A) Diagram of experimental approach. Total protein was isolated from BMDMs infected with *B. melitensis* 16M strains: B16M (WT), ΔBMEI1482 (gene mutant) and CΔBMEI1482 (gene mutant ectopically expressing N3XFlag-BMEI1482) and analyzed using Lectin array 70 (RayBiotech). B) Heat map of reprogrammed glycoproteome by bacterial strains. Lectin column represents the abbreviation of the lectin used in that row (also explain in RayBiotech manual) and CHO* denotates carbohydrate specificity: 1.-GalNAc: N-Acetylglactosamine, 2.-GlcNAc: N-Acetylglucosamine, 3.-Gal: D-Galactose, 4.-Glc: D-Glucose, 5.-Fuc: L-Fucose, 6.-Lac: Lactose, 7.-Man: Mannose, 8.-Nac: N-Acetylneuraminic acid. Purple and pink colors demonstrate decreased and increased abundance, respectively.

Figure 3.10 Continued.

A)

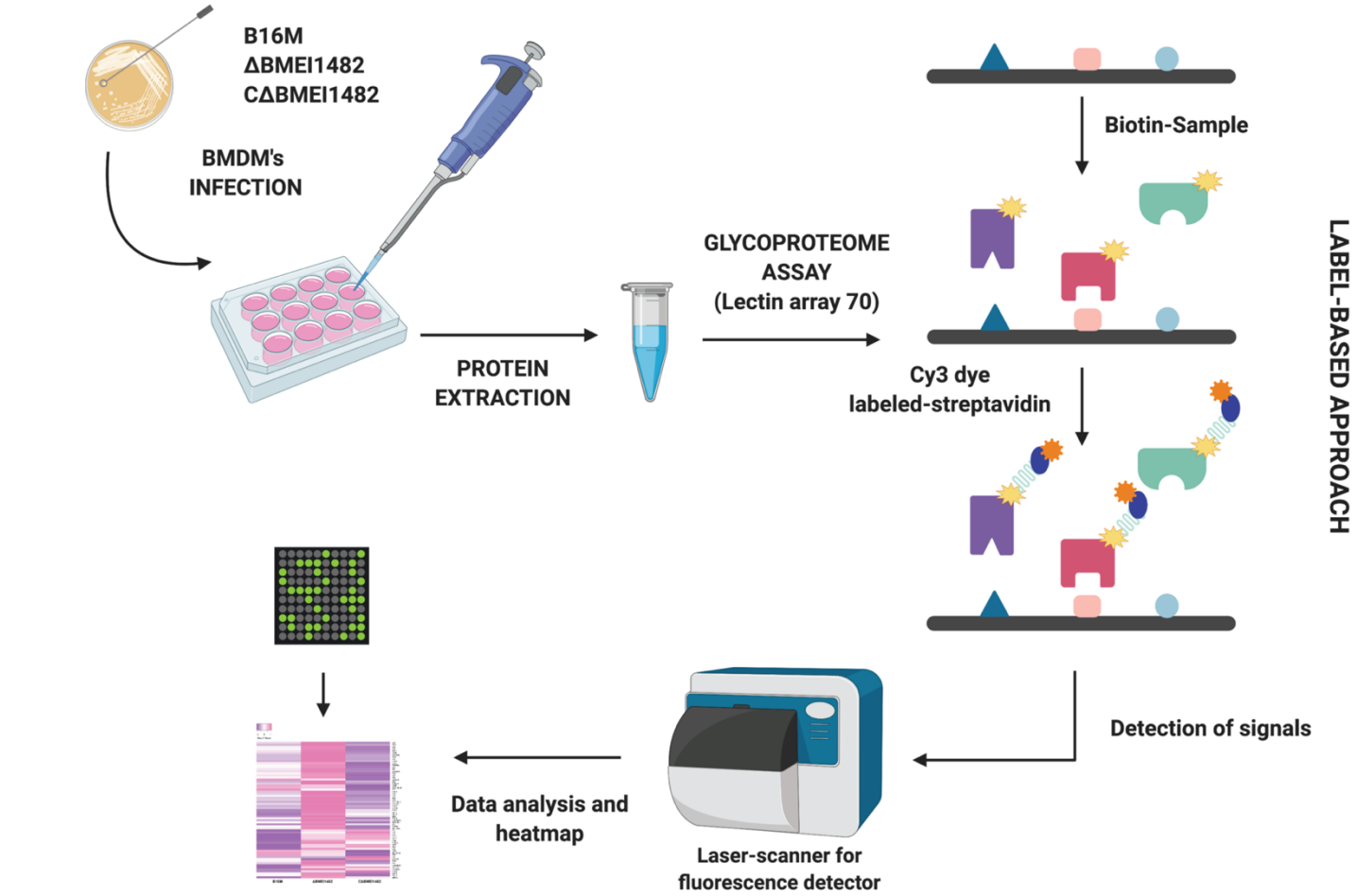

Figure 3.10 Continued.

Figure 3.11 Effector protein BMEI1482 changes host N-glycome abundance. A) Diagram of experimental approach. Total protein was isolated from HEK293Ts cells expressing plasmids BMEI1482-eGFP and empty eGFP using SDC buffer. Samples were treated and analyzed to detect glycan abundance and isomer distribution using LC-MS/MS nanoPGC according to Peng et al., 2019. B) Host (HEK293Ts) N-glycome abundance is significatively decreased during ectopically expression of BMEI1482-eGFP ($P<0.048$). C) Glycan isomer distribution is significantly reprogrammed during BMEI1482-eGFP expression. P values obtained after statistical analysis of each glycan isomer as described in the table. The results shown are means ± SD from six independent experiments performed in triplicates. The student t-test was used to analyze differences between individual sets of data. Statistically significant differences are indicated by asterisks (****), as compared to corresponding controls: eGFP.

Figure 3.11 Continued.

A)

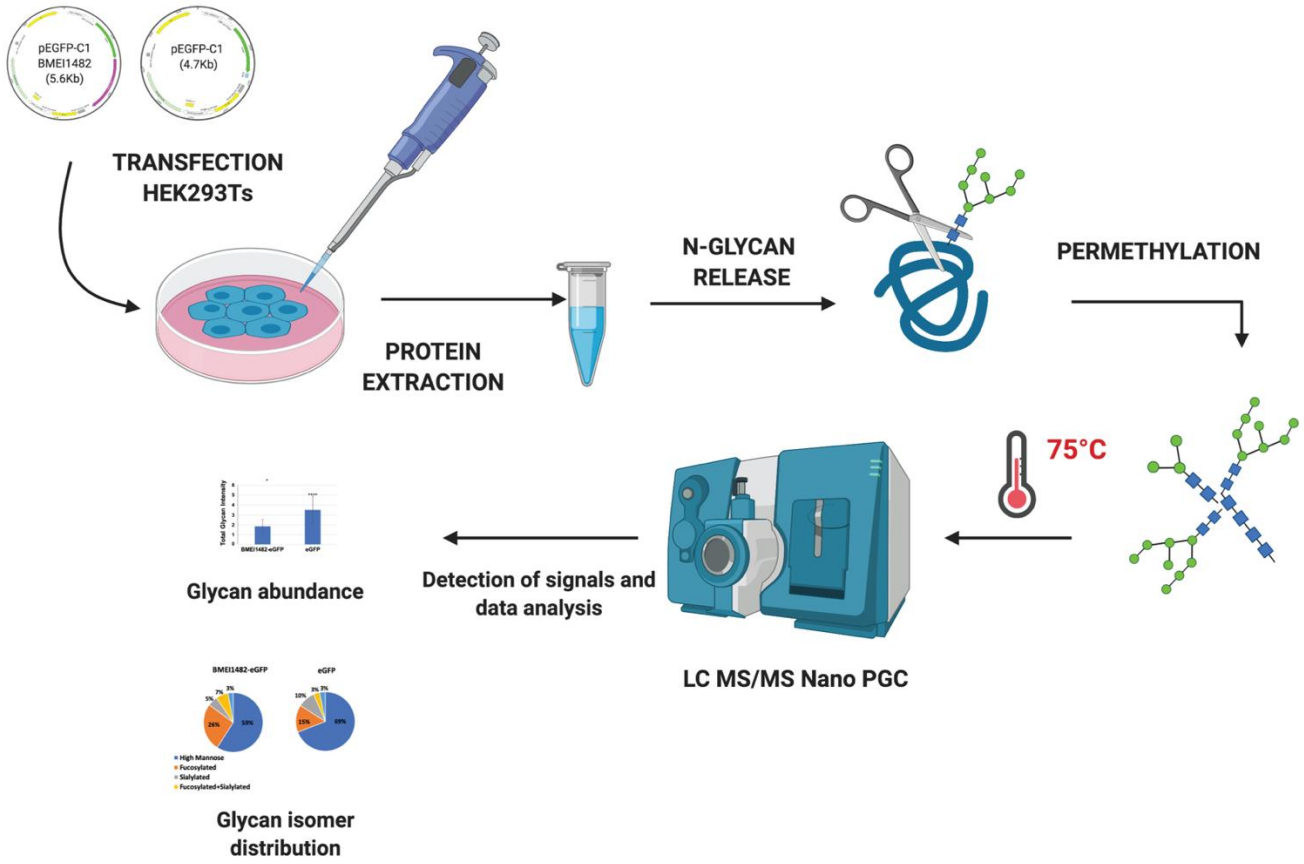

Figure 3.11 Continued.

B)

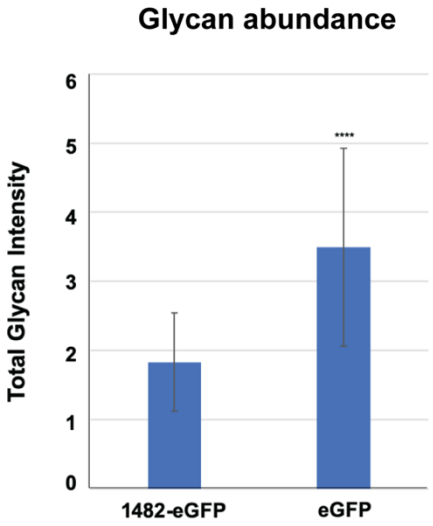

C)

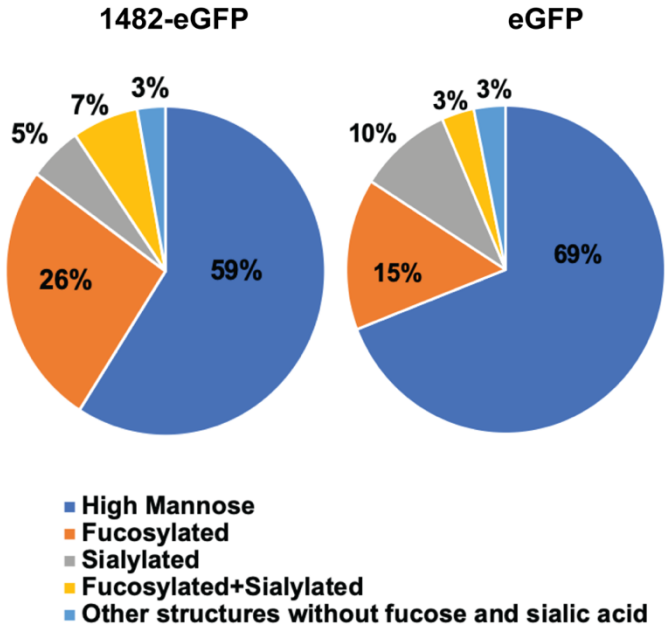

Glycan isomer	P value
High Mannose	0.011
Fucosylated	0.0015
Sialylated	0.0012
Fucosylated + Sialylated	0.0022
Other structures without fucose and sialic acid	0.3052

Figure 3.12 Effector protein BMEI1482 disturbs secretion by retaining cargo at Golgi. A) Diagram of experimental approach, HeLa C1 cells were transfected with plasmids pENTRY-HA BMEI1482, pENTRY-HA and pGalTmCherry. Secretion of cargo was synchronized by treating cells with rapamycin (400 ng/ml). Cells were fixed at different time points and stained with anti-HA antibodies to localize effector protein BMEI1482 by microscopy. B) Representative images of the trafficking of a secreted eGFP-tagged cargo (green) in cells transfected with HA empty vector control. The cells are fixed at indicated time points post rapamycin treatment (400 ng/ml) at 37 °C. The cells were also transfected with GalT-mCherry (red) to mark the Golgi apparatus and immunofluorescent stained with mouse anti-HA antibodies (blue). C) Representative images of the trafficking of a secreted eGFP-tagged cargo (green) in cells transfected with HA-BMEI1482 at indicated time points post rapamycin treatment (400 ng/ml) at 37 °C. The cells were also transfected with GalT-mCherry (red) to mark the Golgi apparatus and immunofluorescent stained with mouse anti-HA antibodies (blue). Scale bars 20 μm. The results shown are means ± SD, significant values (P values) were calculated using either Student's t-test or Mann-Whitney rank sum test as appropriate. Data with a $P< 0.05$ was considered significant. Asterisks (*) and (**) denotate statistical significance with $P< 0.05$ and $P<0.01$, respectively.

Figure 3.12 Continued.

A)

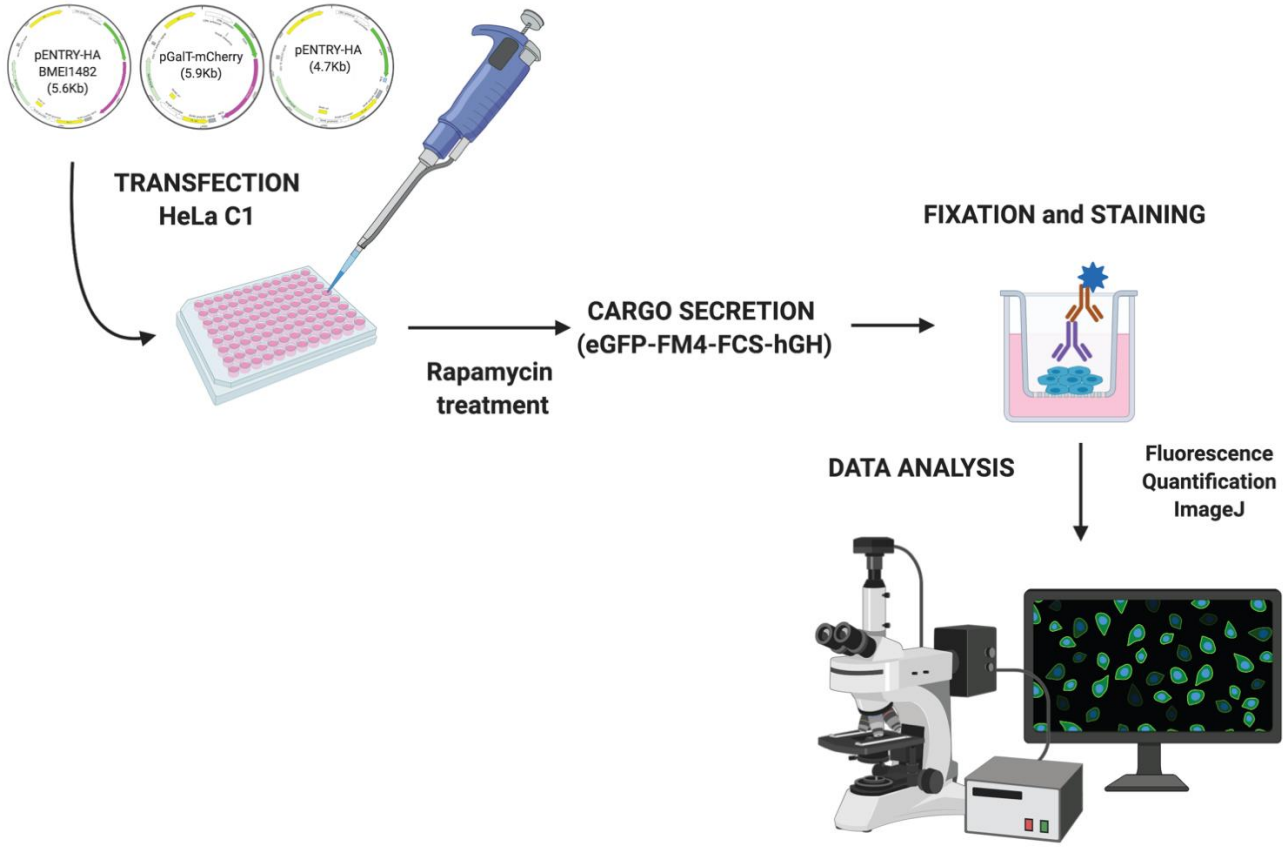

Figure 3.12 Continued.

B)

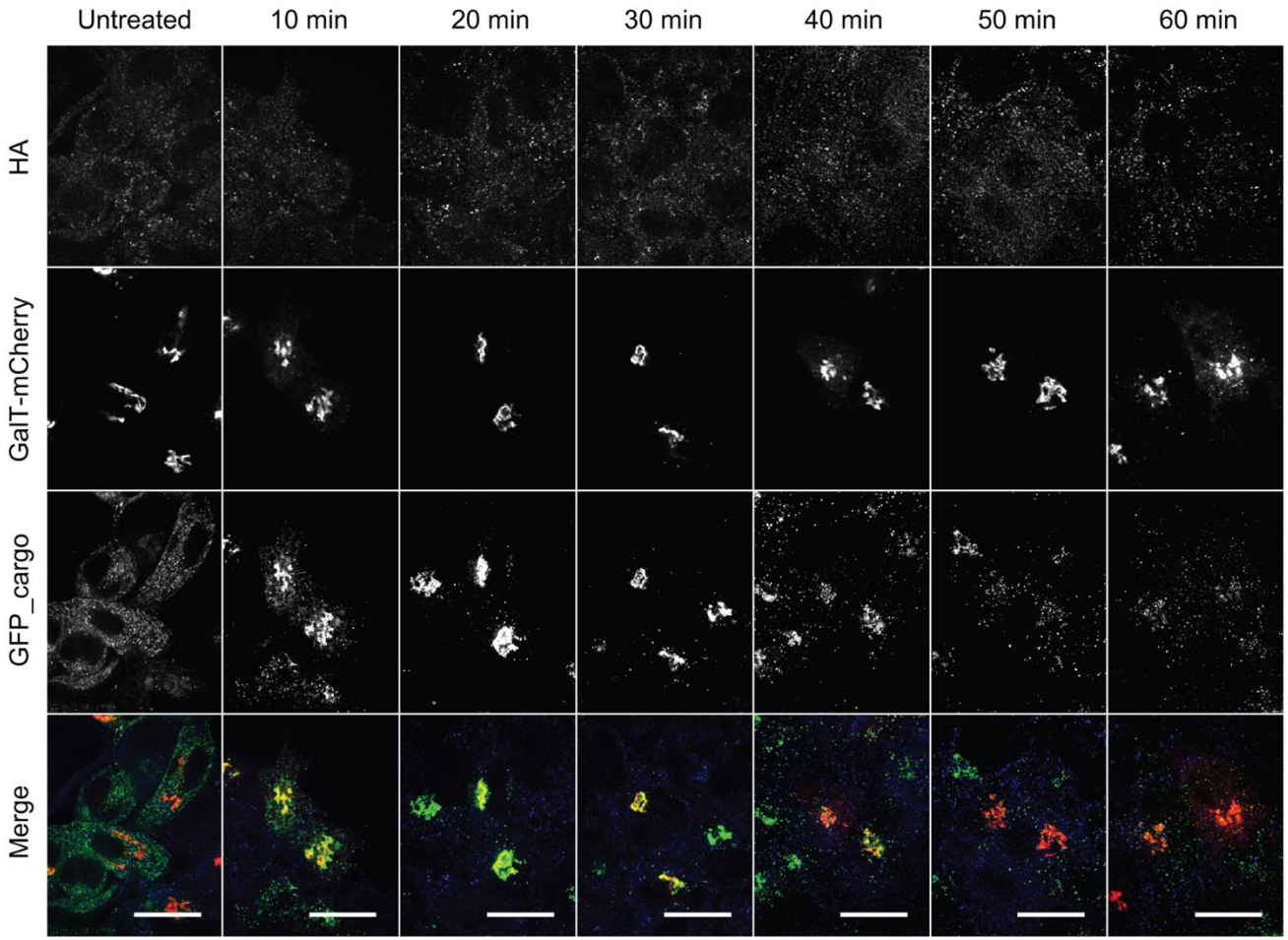

Figure 3.12 Continued.

C)

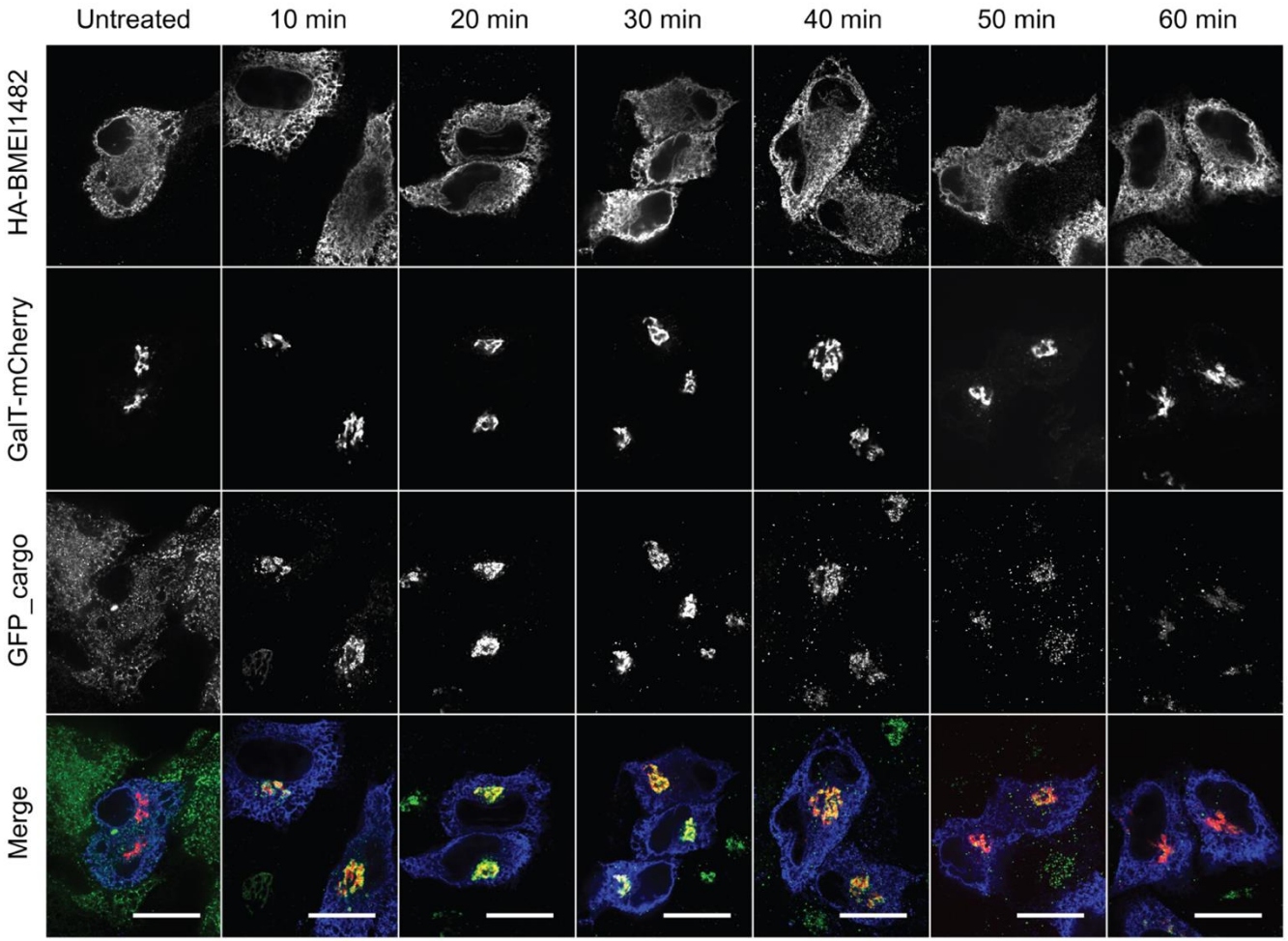

Figure 3.12 Continued.

D)

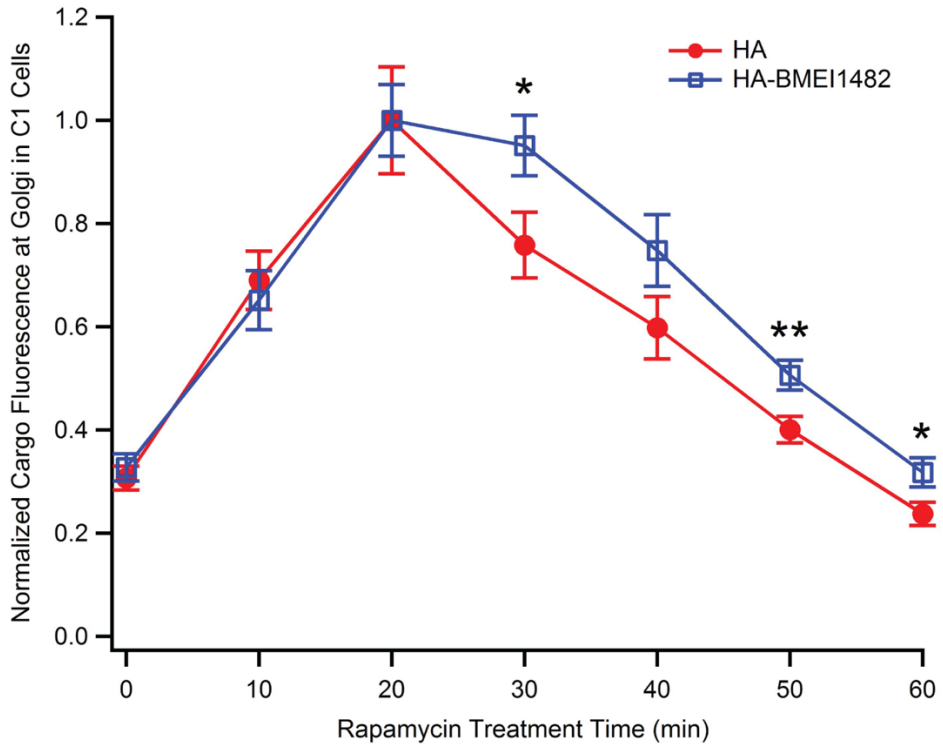

Figure 3.13 Time line representing mice model experimental approach. At day -7, eigth groups of five 6-8 weeks female BALB/c mice were housed. At day 0, blood was collected from all mice groups and then incoulated with 10^6 CFU of *B. melitensis* strains: B16M, ΔBMEI1482 and CΔBMEI1482 (ΔBMEI1482::N3XFlag-BMEI1482, ectopically expression of effector BMEI1482) and PBS1X as control. At days 7 and 14, blood was collected from four mice groups (per day) and tissues (spleen, liver, kidney, brain, heart, lungs and uterus) were collected and processed to determine bacterial CFU counting.

Figure 3.13 Continued.

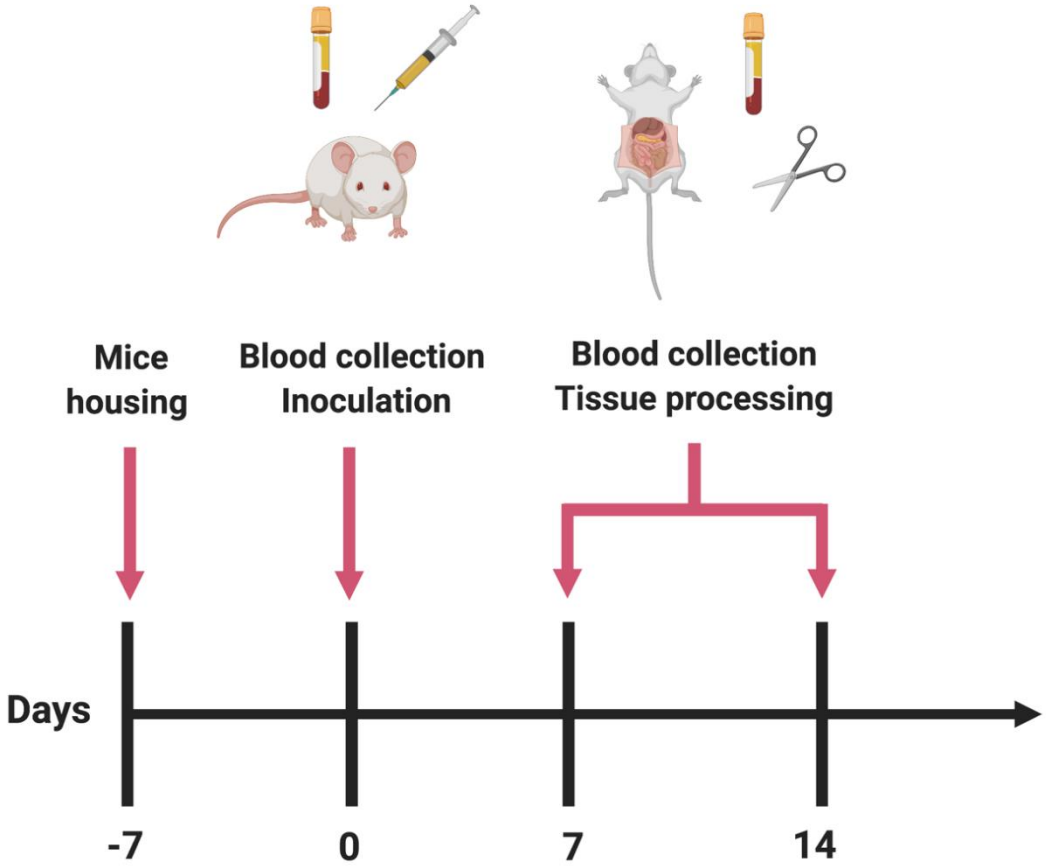

METHODS

- 10^6 CFU of strains:
  -B16M
  -ΔBMEI1482
  -CΔBMEI1482
- Tissue processing:
  -Spleen
  -Liver
  -Kidney
  -Brain
  -Heart
  -Lungs
  -Uterus
- Analyses:
  -Bacterial CFU

Figure 3.14 Bacterial replication in mice model. Groups of five 6-8 weeks BALB/c female mice were inoculated with 10^6 CFU of *B. melitensis* 16M strains: B16M, ΔBMEI1482, CΔBMEI1482 (ΔBMEI1482::N3XFlag-BMEI1482) and PBS1X as control. At 7 and 14 days post-inoculation, mice were euthanized via CO_2 asphyxiation. Tissues were aseptically harvested, weighted and transferred to 1 ml sterile PBS1X for bacterial isolation and counting through homogenization. Recovered bacteria is presented as the Log10 CFU per tissue from serial dilutions plated in triplicate and averaged over five mice. Graphics demonstrate the bacterial replication at 7 days post inoculation. The results shown are means ± SD, significant values (P values) were calculated using either Student's t-test. Data with a $P< 0.05$ was considered significant. Asterisks (**) and (***) denotate statistical significance with $P< 0.002$ and $P<0.0001$, respectively.

Figure 3.14 Continued.

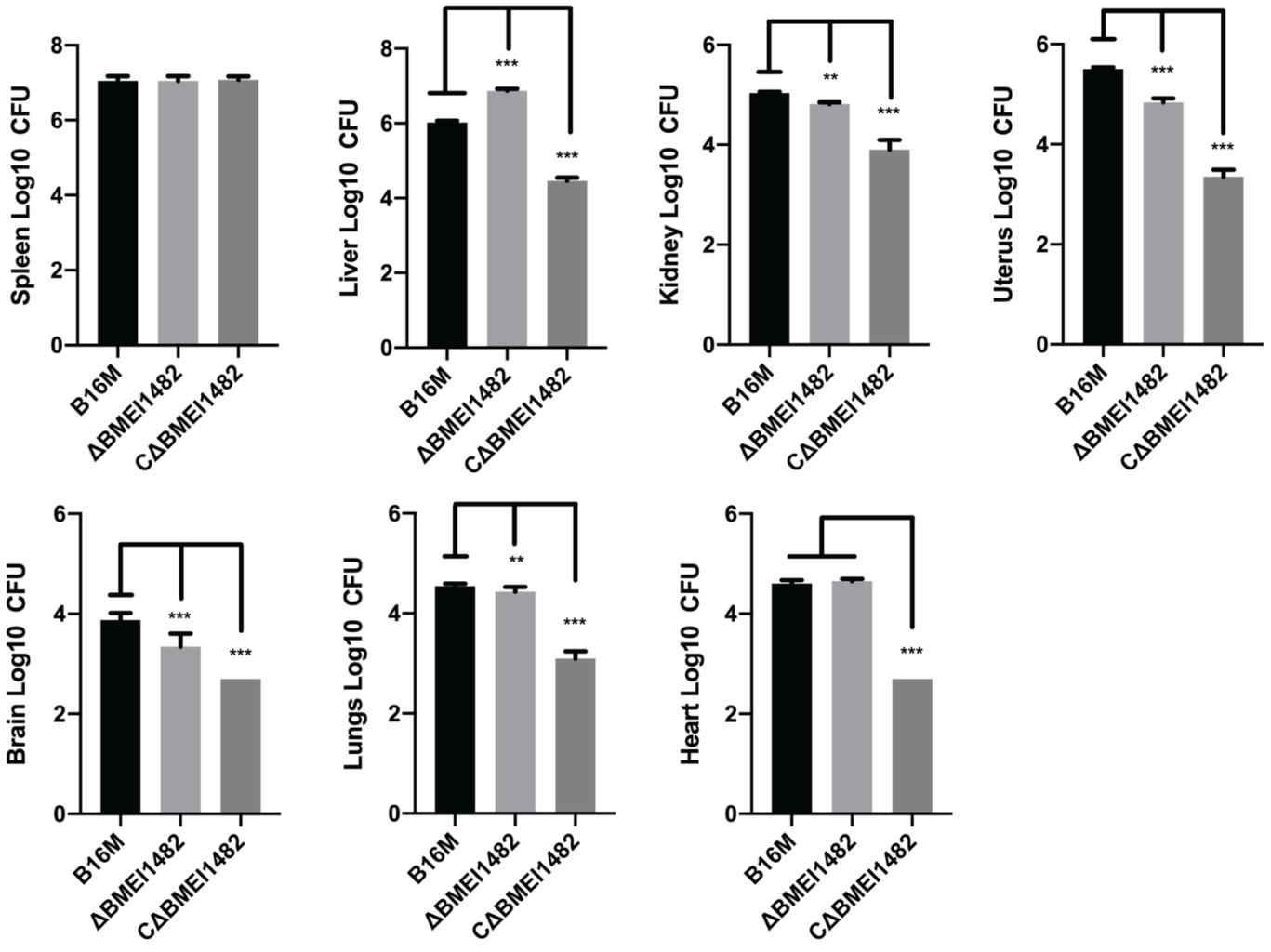

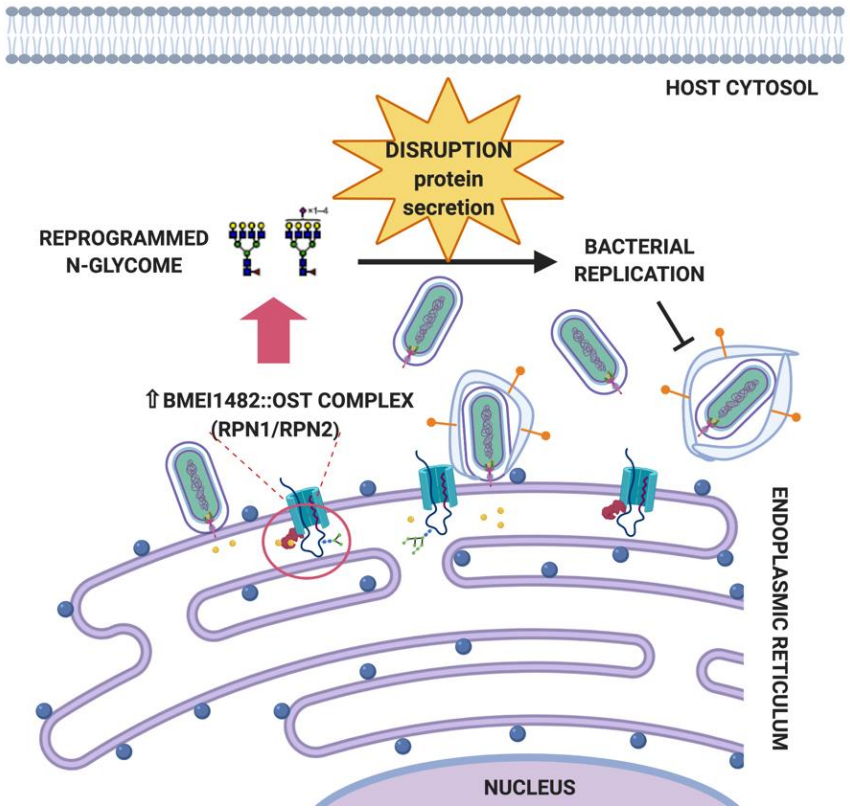

Figure 3.15 Model that demonstrates how effector BMEI1482 (Grhg1) reprograms host N-glycome to sustain bacterial infection. Effector BMEI1482 is translocated by *vir*B-T4SS, interacts with N-glycosylation complex (The OST complex) and disrupts secretory pathway. Effector BMEI1482 specifically interacts with RPN1 and RPN2 subunits of OST complex. It is suggested that during overexpression of effector BMEI1482, the interactions BMEI1482::RPN1 and BMEI1482::RPN2 reprograms host N-glycome that leads into a disruption of secretory pathway (ER stress). Once the host biology is affected bacteria replication is decreased.

3.3. Discussion

B. melitensis is the causative agent of brucellosis, which is a human health threat and a disease of global economic importance. The core mechanism of *Brucella's* infection strategy is to persist in phagocytic cells by expressing genes directly involved in its survival and pathogenesis. Current studies have characterized bacterial interactions with the endocytic and secretory pathways as well as interactions with the ER to sustain a replicative niche (Celli, 2015). Based on these findings, it has been possible to advance the characterization of the *Brucella* life cycle with the goal of understanding the disease.

Elucidating the downstream effect of host molecular mechanisms targeted and manipulated by bacterial effectors is essential to understand the pathogenesis of intracellular bacteria. It is well studied and broadly documented that the host ER and secretory pathways are targeted by *Brucella* for replication (Celli, 2015; Myeni et al., 2013; Qin et al., 2008). In this project, the molecular mechanism of a *Brucella melitensis vir*B-T4SS effector was uncovered. Based on data that demonstrates the effector protein BMEI1482 (a) is secreted by *vir*B-T4SS, (b) contributes to bacterial replication, (c) interacts with the host OST complex, (d) reprograms the host N-glycome and N-glycoproteome, and (e) disturbs the secretory pathway, it is concluded that this bacterium modulates the host N-glycosylation machinery to support its intracellular lifestyle. This finding expands our understanding of interactions between *Brucella* and host cells and provides insights into the molecular mechanisms that control its intracellular life cycle. Based on the observed host N-glycome reprogramming

phenotype of BMEI1482 we named it Grhg1 “Global reprogramming host glycome 1” (Figure 3.15).

The findings presented here raise several questions about the mechanism by which altered global host N-glycosylation influence the intracellular lifestyle of the pathogen. First, changes in N-glycosylation may activate host cell stress responses, including the unfolded protein response (UPR) (Wong et al., 2018), which in turn, control bacterial replication. Several studies have shown that *Brucella* infection of host cells is accompanied by UPR activation (Celli and Tsolis, 2015). In addition, studies have shown that UPR activation promotes intracellular replication (Pandey et al., 2018; Qin et al., 2008). Therefore, it is reasonable to speculate that *Brucella* modulates N-glycosylation to activate the UPR response and promote intracellular replication.

Second, as an intracellular pathogen, *Brucella* must secure its required nutrients from the host. An intriguing hypothesis is that alterations in host cell glycosylation may change the abundance of carbohydrate blocs and oligosaccharides that are available to the pathogen in its replicative niche (the rBCV). Supporting this hypothesis is the observation that *Brucella* infection is accompanied by increases in membrane associated fucose moieties in glycoproteins. It is established that *Brucella* can exploit fucose to express virulence factors involved in intracellular survival and replication (Budnick et al., 2018), thereby suggesting an intriguing model whereby the pathogen reprograms host glycosylation to secure access to this important energy source.

Third, alterations in glycosylation are known to activate the host autophagosome biogenesis program (Adams et al., 2019; Cherepanova et al., 2016; Glick et al., 2010;

Gump and Thorburn, 2011; Lamriben et al., 2016). In addition, several reports have shown that autophagosome biogenesis is important to the intracellular lifestyle of the pathogen (Pandey et al., 2018; Qin et al., 2008). These findings suggest a model whereby *Brucella* exploits changes in glycosylation to promote the biogenesis of an organelle that supports the intracellular lifestyle of the pathogen.

Finally, as a stealthy pathogen, *Brucella* must devise ways of masking its presence in host cells. An interesting hypothesis is that alteration in N-glycosylation may manipulate the host immune response to benefit the pathogen. A similar hypothesis has been proposed by other authors and that has been defined as a "glyco-evasion hypothesis" (Kreisman and Cobb, 2012). Supporting this view is the observation that BMEI1482 interacts with subunits the OST complex. Our immunoprecipitation data allowed us to identify subunits RPN1, RPN2, DDOST and STT3A. The OST complex interacts directly with the translocon and ribosomes, components that perform transfer N-glycans to nascent proteins during co-translational translocation of proteins (Kreibich et al., 1978; Lu et al., 2018; Pfeffer et al., 2017; Shrimal et al., 2013; Turiak et al., 2019; Wilson and High, 2007). The interaction of BMEI1482 with OST subunits may: 1) modulate the transfer of glycans to proteins, 2) change the glycan substrate specificity and 3) reprogram the site-specific N-glycosylation of glycoproteins. Such changes might lead into a reprogrammed host N-glycome with possible immune consequences as observed during infection with other pathogens (Hare et al., 2017; Lu et al., 2015; Park et al., 2016).

The findings presented here may have implications for veterinary and human clinical practices. First, it is well established that glycan moieties can be used as diagnostic markers in wide variety of congenital glycosylation disorders (CDG) or infectious diseases (Kreisman and Cobb, 2012; Lauc et al., 2016; Mohorko et al., 2011). This observation suggests that it may be possible to exploit the altered N-glycome generated in host cells during *Brucella* infection as a diagnostic marker. If possible, this will have several interesting implications. First, it has been notoriously difficult to distinguish species of *Brucella* diagnostically. For example, it has been difficult to distinguish 1) between infections due to bacterial strains *suis, canis* and *abortus* and 2) between vaccinated and infected animals in the field. The obtained data suggest an N-glycome pattern specific to the genetic background of *Brucella melitensis*, suggesting that host N-glycome can be differentially reprogrammed by the bacterial strain.

Finally, developing compounds that prevent *Brucella* alteration of host N-glycosylation may enhance immune recognition and hence have therapeutic value. Toward this end, several studies have shown that glycosylation constitutes an attractive process that can be targeted by diverse drugs, including docetaxel, tunicamycin and NG-1 (Lauc et al., 2016; Lopez-Sambrooks et al., 2016; Wong et al., 2018) In this light, this work may have important pharmaceutical applications.

3.4. Materials and methods

3.4.1. Analysis of BMEI1482 candidate effector

Bioinformatical analyses using PATRIC revealed a hypothetical protein "BMEI1482", that 1) has no homology to already described T4SS effector proteins in *B. abortus* or to reported mutated genes in *Brucella spp*., 2) is present among all three species analyzed (*B. melitensis* 16M and *B. abortus* 2308 and S19) with a few to zero changes at the level of amino acid and nucleic acid sequences among the bacterial strains, and 3) is specific to the *Brucella melitensis* having low homology to other bacterial pathogens with secretion systems (T4ASS, T4BSS) (Figure 2.6).

3.4.2. Construction of plasmids

Primers and plasmids used in this study are described in Table 3.1. Plasmid constructions were analyzed by PCR, double digestion and DNA sequencing, and western blot to confirm plasmid expression when needed. The TEM-1 plasmids expressing β-lactamase and selected effector proteins were developed according to (Myeni et al., 2013) with some modifications. Briefly, to obtain the IPTG inducible backbone plasmid pTEM-1, the LacIq-Ptac fragment was PCR amplified from pKM244 and used to replace the lac promoter of pBBR1MCS-2 by gibson cloning approach (Figure 3.2, Table 3.1). Then, plasmids expressing in frame N-terminal and C-terminal fusions were constructed. BMEI1482 and BlaM genes were PCR amplified from *B. melitensis* DNA and from plasmid pKM244, respectively. Finally, BMEI1482 and BlaM were fused by a second overlapping PCR and cloned into BamHI and SalI digested

pTEM-1 plasmid (Figure 3.3, Table 3.1). The stop codon of BlaM and BMEI1482 were removed to allow the generation of N-terminal and C-terminal in-frame fusions, respectively. The same procedure was followed to construct positive controls VceC (BMEI0948) and BPE123 (BMEII1111) (Figure 3.3, Table 3.1).

To tag the effectors BMEI1482 (Grhg1) and VceC (BMEI0948) with GFP, the PCR amplified fragments were cloned into BglII and SalI digested pEGFP-C1 plasmid. To obtain HA-BMEI1482, the PCR amplified fragment was cloned into pENTRY-HA using gibson assembly (Table 3.1).

The plasmid for in-frame deletion mutant of BMEI1482 was constructed according to (Kahl-McDonagh and Ficht, 2006). Briefly, the following modifications were made: 1) the reverse primer of 5' upstream fragment included 30 nucleotides of sequence complementary to the opposite fragment, 2) the restriction sites BamHI and SalI were included in the forward primer of the 5' upstream fragment and the reverse primer of the 3' downstream fragment of the operon sequence, respectively, and 3) the backbone used was pNPTS138-Km^R. *Brucella* genomic DNA was used to PCR amplify overlapping upstream and downstream fragments from BMEI1482 to run a fusion PCR. The obtained single sequence containing both upstream and downstream fragments of the operon sequence was cloned into XbaI and XmaI digested pNPTS138 to obtain the plasmid pNPTS138-UPBMEI1482DN (Figure 3.4A, Table 3.1).

To construct a plasmid for exogenous expression of BMEI1482, pBBR1MCS-2 was used as backbone to insert *vir*B promoter and 3XFlag label. Briefly, bacterial genomic DNA was used to PCR amplify *vir*B fragment using appropriate primers and to

insert 3XFlag label as well. Then, BMEI1482 was PCR amplified and inserted into BamHI and XhoI digested pBBR1MCS-2-virB-N3XFlag to obtain plasmid pBBRM1MCS-2-virB-N3XFlag-BMEI1482 (Figure 3.5A, Table 3.1).

3.4.3. Bacterial strains and culture

The bacteria used in these experiments included *B. melitensis* 16M (B16M), *B. melitensis* 16MΔ*vir*B2 (B16MΔ*vir*B2), *B. melitensis* ΔBMEI1482 (ΔBMEI1482) strains and CΔBMEI1482). For electroporation *in vitro* and *in vivo* infection experiments, *Brucella* strains were grown on tryptic soy agar (TSA) plates for 72h at 37°C. For *in vitro* infections, *Brucella* strains were inoculated on tryptic soy broth (TSB) with a 37°C overnight shaking incubation to late logarithmic phase. TSB was supplemented with either 1mM IPTG, 50μg/ml of kanamycin or 10% sucrose as needed (TSB-IPTG, TSB-Kan50, TSB-Suc10). For protein translocation assay, B16M and B16MΔ*virB*2 were electroporated with pTEM plasmid series to express β-lactamase-tagged effector proteins (TEM1 fusions). *Brucella* clones harboring pTEM plasmids were selected on TSA plates containing 50μg/ml of kanamycin (TSA-Kan50), and presence of pTEM plasmid was confirmed using PCR adequate primers (Table 3.1).

The in-frame deletion mutant ΔBMEI1482 was obtained by electroporation of B16M strain with pNPTS138-UPBMEI1482DN plasmid. Electroporated bacteria was spread onto TSA-Kan50 and individual clones were replica-plated on both TSA-Suc10 and TSA-Kan50. Clones that presented growth only on TSA-Suc10 were selected to confirm gene deletion by colony PCR. Further bacterial passages were needed to allow

homologous recombination that lead into gene deletion, and frequent PCR analyses coupled with sequencing were performed to confirm mutation. Mutant clones were grown in TSB-Suc10 at 37°C for at least 3 days when needed (Figure 3.4B, Table 3.1).

ΔBMEI1482 strain was electroporated with pBBR1MCS-VirB-N-3XFlag-BMEI1482 to obtain complemented mutant B16MΔBMEI1482::N3XFlagBMEI1482 (Table 3.1). Electroporated bacteria was spread onto TSA-Kan50. Then, individual clones were grown in TSB-Kan50 at 37°C with agitation for 3 days, and appropriate molecular analyses were performed to confirm the presence of the plasmid (Figure 3.5B, Table 3.1).

Escherichia coli DH5α strains used for cloning, plasmid propagation and expression analyses were routinely grown on Luria-Bertani (Difco Laboratories LB Lennox, BD) plates or broth overnight at 37°C, with or without supplemental 50μg/ml kanamycin or 100μg/ml of ampicillin (LB-Kan50 or LB-Amp100).

3.4.4. Electroporation of *Brucella melitensis* strains

For electroporation purposes, *Brucella* were harvested from the surface of confluent plates after 3-4 days of growth at 37^{o}C. The bacteria were pelleted by centrifugation at 5,000g for 15min at 4^{o}C. The cell pellet was washed three times with sterile, ice-cold water by repeating the previous centrifugation, and the pellet was resuspended in 1ml sterile ice-cold water. For electroporation, 70μl of cell suspension was placed into a pre-chilled 1mm gap electroporation cuvette along with 1μg of plasmid in 5-10μl of water. The mixture was electroporated using Bio-Rad Gene Pulser

X-Cell electroporator set at 2.5kV, 250Ω and 50μF. The bacterial suspension was immediately diluted with 1ml warm SOC-B media in the cuvette, then transferred to a sterile microfuge tube and incubated overnight at 37^{o}C with agitation. Next day, the cell suspension was pelleted by centrifugation at 10,000g for 1min, resuspended in a minimum volume of media and spread onto TSA plates supplemented as needed. Plates were incubated at 37^{o}C for at least 3 days or until bacterial growth was observed. Further molecular analyses were done according to plasmid used during electroporation.

3.4.5. Mammalian cells

HeLa, HeLa-M (C1) cell line (Dr. Yuxin Mao Lab) (Gordon et al., 2010)**,** Raw264.7 and HEK293T cell lines were maintained in DMEM supplemented with 10% FBS, sodium pyruvate, nonessential amino acid (NEAA) and 10mM HEPES buffer. Cells were grown to approximately 80% confluency for transfection purposes. Passages were kept to a minimum (<10). For experiments, cell lines were used at concentrations ranging between 5 x 10^4 to 1 x 10^6 cells/well. For gene knock-down selection, cells were grown with 100μg/ml hygromycin B. For synchronization of secretion assay (RUSH system), cells were treated with 400ng/ml rapamycin.

3.4.6. Isolation of mice bone marrow cells and differentiation into macrophages (BMDMs)

Femur and tibia from 5-8 female mice (C57BL/6J), donated by Texas A&M Institute of Genomic Medicine (TIGM), were collected and tissue was cleaned off.

Bones were transferred into sterile 1X PBS supplemented with 2X antibiotic-antimycotic. Then, both ends of bones were cut and a sterile 10ml syringe with a 16G needle was used to blush bone marrow into a sterile 50ml conical tube. To prepare a single cell suspension, media containing bone marrow cells was aspirated using a sterile 10ml syringe with a 22G needle a total of 3-4 times. To get rid of bones and tissue fractions, cells were filtered through a 70 μM cell strainer and centrifuged at 400g for 10min at 4^{o}C, pellet was resuspended in 10ml of 1X RBC lysis buffer and incubated for 8min at room temperature (RT). After lysis, cells were centrifuged at 500g for 5min at RT and supernatant was discarded. Cell pellet was resuspended in 200ml of αMEM media supplemented with 10% FBS, 1x antibiotic-antimycotic and 30ng/ml recombinant mouse M-CSF. Then, 20ml of cell suspension were transferred into 75cm^2 tissue culture flasks and incubated for 2 days at 37^{o}C with 5 % CO_2. After incubation, attached cells were harvested using cold αMEM media and cell scraper, and centrifuged at 900g for 10min at 4^{o}C. Final cell pellet was resuspended in αMEM media supplemented 10% FBS and 30ng/ml MCSF, and cells were plated at a necessary concentration on desired cell culture plate format.

3.4.7. TEM1 protein translocation assay

The translocation of translational fusions between TEM1 and the *Brucella* candidate proteins (Table 3.1) was evaluated by detecting β-lactamase activity in infected Raw 264.7 cells. TEM1 fusions were transformed in *Brucella* by electroporation and their expression of the fusions was verified by Western blot analysis with a primary

anti-β-lactamase antibody (1:1000 dilution) and secondary HRP anti-IgG + IgM (H+L) antibody (dilution of 1:5000). Bacteria were grown in TSB-Kan50 overnight, then treated with 1 mM IPTG for 2h to induce expression of fusion proteins before infection. Then, Raw264.7 cells (6 x 10^4 cells/well) were infected with *Brucella* strains harboring the TEM1 fusions at a MOI of 1000 in presence of 0.1 mM of IPTG throughout the infection. Infected cells were centrifuged at 200g for 5 min to initiate bacterial-cell contact and incubated at 37°C for 30 min. DMEM supplemented with 0.1mM IPTG was replenished and cells were incubated for another 30 min at 37°C, 5%CO_2. At 1 h.p.i., cells were treated with gentamicin (100μg/ml) for 1 h to kill extracellular bacteria. Then, cells were replenished with DMEM with 20μg/ml gentamicin and 0.1 mM IPTG, and incubated at 37°C, 5%CO_2 until the next time point. At 16 h.p.i., cells were washed two times in DMEM and loaded with the fluorescent substrate CCF2/AM LiveBLAzer-FRET B/G loading kit (Cat No. K1032, Invitrogen) in the β-lactamase loading solution supplemented with 15 mM Probenecid (Cat No. P36400, Thermo Fisher Scientific). Cells were incubated in the dark for 90 min at room temperature and then observed under epifluorescence using a NIS element AR 3.0 software-Nikon software. To determine whether effector proteins were translocated in a virB-T4SS dependent manner, translocation efficiencies were compared to a virB-T4SS deficient mutant strain B16MΔ*vir*B2. The presented data are mean values ± SD from three independent experiments performed in triplicate.

3.4.8. Transfections of mammalian cell lines

HeLa and HEK293T cells were transfected using either PolyJet (Cat No. SL100688, SignaGen Laboratories) or Lipofectamine (Cat. No. 11668-019, Thermo Fisher Scientific) mixed with PLUS Reagent (Cat No. 11514015, Thermo Fisher Scientific). Briefly, transfection reaction was prepared by mixing 450µl of plain DMEM (no serum or antibiotic), 10µl of PLUS reagent, 1-10µg of plasmid and 30µl of PolyJet and incubated at RT for 15 min. Cells were washed twice with PBS1X and fresh DMEM 10% FBS media was added. After incubation time, transfection reaction was added dropwise to cells and incubated at 37°C, 5% CO_2. At necessary "hours post-transfection" (h.p.t.) cells were washed twice with 1XPBS and processed accordingly.

3.4.9. Immunoprecipitation and LC-MS/MS- analyses

HEK293T cells transfected with pEGFP-C1-BMEI1482 (Grhg1), pEGFP-C1-BMEI0948 (VceC) (positive control) and pEGFP-C1 (empty vector) were harvested with ice-cold 1XPBS at 36 h.p.t. and immunoprecipitation procedure was followed according to GFP-Trap-MA kit's (Cat No. gtma-10, ChromoTek) manufacturer's instructions with some modifications. Briefly, the cells were lysed for 1h on ice and pipetting every 10min. To equilibrate beads, the washing step with ice-cold dilution buffer was repeated three times. To bind proteins, the tumble end over end incubation was performed for 5h at 4°C and the beads were washed 5 times with dilution buffer. Bound proteins were eluted at room temperature by adding 60µl of 0.2M glycine pH 2.5 followed by a 30sec incubation under constant mixing. Samples were centrifuged,

supernatant was transferred to a new tube and 6µl 1M Tris base pH 10.4 were added for neutralization. Finally, 10µl of eluted sample was used to measure protein concentration using Nano drop (A280 nm) and to mix with 2X SDS-sample buffer to perform SDS-PAGE analysis using Coomassie blue staining. To observe transfection efficiency microscopy was performed on all samples. Samples were sent to UTMB Mass Spectrometry Proteomics Center for LC-MS/MS analyses.

3.4.10. Secretion assay

HeLa-M (C1) cells were transfected with GalT-mCherry and pENTRY-HA-BMEI1482 or pENTRY-HA empty vector and cultured for 20 h. The cells were treated with 400 ng/ml rapamycin at 37°C to allow the secretion of the cargo (eGFP-FM4-FCS-hGH) to occur, and then fixed at the indicated time points. Cells were stained with mouse anti-HA primary and 647nm anti-mouse secondary antibodies. The GFP fluorescence intensity of the cargo at GalT-positive Golgi region was quantified using the ImageJ software. For each time point, fluorescence values were averaged over at least 20 positively transfected cells and then normalized to the mean value at 20min, which has the highest value among all the time points.

3.4.11. Glycomics

BMEI1482-eGFP and eGFP transfected HEK293T cells were washed as described above and harvested using scraper. Cells were centrifuged at 400g for 10min with 4^{o}C and pellet was resuspended in 100µl of 1XPBS. Then, 100µl of 5%SDC were

added and samples were lysed by freeze/thaw method. Briefly, cell samples were incubated at room temperature (25°C) for 30 minutes, then switched to -20°C for one hour. This method was performed three times. Samples were stored at -80°C, until sent to TTU Center for Biotechnology & Genomics. For N-glycome analysis, cell lysate was centrifuged at 21,100 x g for 10 min to collect the supernatant and 2 µL of were taken to measure protein concentration using Micro BCA Protein Assay Kit (Thermo Scientific). The remaining lysate was denatured at 90^{o}C for 15 min prior to PNGase F digestion. PNGase F digestion was performed at 37^{o}C for 18 hrs (3 units enzyme/1 µg protein). Then, formic acid (final concentration of 1%) was added to remove the SDC. After vortexing thoroughly, samples were centrifuged at 21,100 x g for 10 min. Supernatant was transferred to a new tube and dried out. After drying, 1 mL of cold 90% ethanol was added and vortexed. Then, sample (in 90% ethanol) was stood still in a -20^{o}C freezer for 30 min, followed by centrifuging at 21,100 x g for 10 min to remove proteins. After centrifuged, supernatant was collected and dried out. Next, 50 µL of water was added to resuspend sample and then applied to a 500-1000 MWCO dialysis membrane, dialyzed overnight to remove salts and remaining SDC. After dialysis, sample was dried out, then reduced and permethylated as reported previously (Peng et al., 2019) (Peng et al., 2019). Glycomic profiling was performed using an Ultimate 3000 nano LC system (Thermo) coupled to an LTQ Orbitrap Velos mass spectrometer. Data processing was achieved using MultiGlycan software followed by manually checking (Peng et al., 2019).

3.4.12. Mammalian cell culture infections

Bacterial cultures were washed three times with sterile 1XPBS using centrifugation at 5,000 g for 5 min. Final bacterial pellet was resuspended in 1XPBS and used to infect either Raw264.7 or BMDMs at a MOI of 100. The infection was synchronized by a centrifugation of 200g for 5 min and cells incubated at 37°C between 30min and 2h. Extracellular bacteria was killed using fresh DMEM media with 50µg/ml gentamicin and incubated at 37°C for 1 h. To keep later time points of infection, media was removed and replenished using DMEM with 25µg/ml gentamicin and incubated at 37°C for different time point.

After 1 h incubation, cells were washed and treated to evaluate macrophage uptake. To assess bacterial replication, cells were washed and treated after several time points. Briefly, cells from different time points were washed three times with sterile 1XPBS and lysed with 0.5ml of 0.5% (vol/vol) Tween 20 in sterile water. Then, 0.5ml of 1XPBS were added to the mix to prepare serial dilutions and plated on TSA or TSA supplemented with necessary antibiotic marker and incubated at 37°C for at least 3 days. To calculate the bacterial uptake and bacterial replication, the number of bacteria recovered was divided by the number of cells seeded in each well and multiplied by the dilution factor. The assays were performed in triplicate wells and represent the average from three separate experiments.

To obtain samples for glycoproteomic analyses (70-Lectin array-Ray Biotech), BMDMs infections were performed as described by (Pandey et al., 2017, 2018) with some modifications. Briefly, at appropriate time points, infected cells were washed three

times with PBS1X, then cells were resuspended in 80µl of cell lysis buffer (RIPA) [50 mM Tris-HCl, pH 8.0, with 150 mM sodium chloride, 1.0% Igepal CA-630 (NP-40), 0.5% sodium deoxycholate, and 0.1% sodium dodecyl sulfate] (Cat No. R0278-500ML, Sigma-Aldrich) supplemented with protease inhibitor (Cat No. S8830, Sigma-Aldrich) and phosphatase inhibitor cocktails 2,3 (Cat No. P5726-1ML and Cat No. P0044-1ML, Sigma-Aldrich). Cells were incubated in RIPA buffer on ice for 30 min and resuspended by pipetting. The lysate was vortexed for 30 sec and clarified by centrifugation at 5000g for 15 min at 4°C. Samples were removed from BSL3 facility to a reduced containment (BSL2) level for analysis. 10% of one in ten samples were evaluated for growth on solid media (TSA) following incubation at 37°C for at least 3 days. Death certificates were prepared according to protocols reviewed and approved by the Division of Research of Texas A&M Research Compliance and Biosafety and the Texas A&M-Commerce IACUC, in compliance with the CDC Division of Select Agents and Toxins regulations. Protein concentration was determined using a dye-binding method, BCA Protein Assay (Cat No. 23225, Thermo Scientific) and samples were analyzed by RayBiotech®.

3.4.13. Mice infection

Six to eight weeks old BALB/c female mice (purchased from Jackson Labs, Bar Harbor, ME) were acclimated for 1 week prior to infection and randomly divided into three experimental groups (n=30) and one control group (n=4). Each experimental group was inoculated intraperitoneally (i.p.) with a total dose of approximately 10^6 CFUs of B16M, ΔBMEI1482 and CΔBMEI1482 suspended in 100µl of 1XPBS, while the control

group was inoculated with only 1XPBS. Infectious doses were confirmed by plating serial dilutions onto TSA plates and incubated at 37°C for at least 3 days. Groups of five mice per strain were euthanized at 7- and 14- days post-inoculation (d.p.i.) by CO_2 asphyxiation followed by cervical dislocation. Spleens, livers, uterus, heart, lung, kidney and brain were aseptically collected and homogenized in 1ml sterile 1XPBS using Bead Ruptor12 (Cat No. 19-050A, Omni international). Serial dilutions (10-fold) of samples were plated on Farrell's media and grown at 37°C for at least 3 days to determine bacterial colonization by enumeration of colony forming units (CFU) (Figure 3.13). All animal rearing, handling and experimental methods were conducted under protocols (2018-0262) approved by the Texas A&M-Commerce Institutional Animal Care and Use Committee (IACUC) in strict accordance with the recommendations of the Guide for the Care and Use of Laboratory Animals of the National Institutes of Health (NIH). All infections were performed in an Animal Biosafety Level 3 (ABSL3) facility according to protocols reviewed and approved by the Division of Research of Texas A&M Research Compliance and Biosafety and the Texas A&M-Commerce IACUC, in compliance with the CDC Division of Select Agents and Toxins regulations.

3.4.14. Statistical analyses

Results were presented as the mean value ± SEM. One-way ANOVA, Kruskal Wallis multiple comparison, Student's t-test or Mann-Whitney rank sum test were used to detect significant differences ($P < 0.05$ and $P<0.0001$) among treatments.

3.4.15. Compliance statement

All manipulations of *Brucella melitensis* strains were performed in a Biosafety Level 3 facility according to standard operating procedures approved by Research compliance and biosafety of Texas A&M University and in compliance with the CDC Division of Select Agents and Toxins regulations.

4. CONCLUSIONS AND FUTURE PERSPECTIVE

The presented study uncovered the molecular mechanism of a novel effector protein BMEI1482 that is translocated by the *vir*B-T4SS of *B. melitensis* during bone marrow derived macrophage infection. While attributing modes of action to bacterial effector proteins has proven to be a challenging task, the results from this project revealed that BMEI1482 regulates bacterial replication by altering the host N-glycome during infection *in vitro* and/or *in vivo*. In these studies, I used ectopic expression as a tool to gain insight into the mode of action of BMEI1482, and to learn the host cell pathways that were modulated by it. In support of this idea, the ectopic expression of effectors is a broadly used approach in assorted pathosystems, including *Yersinia, Coxiella* and *Legionella* (de Felipe et al., 2008; Lesser and Miller, 2001; Siggers and Lesser, 2008; Weber et al., 2013; Wolters et al., 2015) for testing effector toxicity to eukaryotic host cells as a first step toward gaining insight into biological functions.

The ectopic expression of BMEI1482 decreased bacterial replication during infection, a phenotype that has not been observed during ectopic expression of other *Brucella* effector proteins (Ke et al., 2015). Previous studies reported that *Brucella* rough mutants induce death of macrophages during infection and showed that this phenotype is due to an overexpression of T4SS coupled with an increased secretion of effector proteins (Li et al., 2017). Further mechanistic studies corroborated that overexpression of the T4SS, and its effector proteins, is lethal to host cells by excessively activating the ER stress response through the IRE1α pathway, resulting in the death of macrophages

(Li et al., 2017). Based on these findings, I hypothesize that the decrease in bacterial replication observed upon BMEI1482 ectopic expression is the result of cell death attributed to a toxic effect. To test my hypothesis, it is necessary 1) to determine the expression kinetics of BMEI1482 during a macrophage infection, 2) to confirm the absence of a rough phenotype in a bacterial strain that ectopically expresses BMEI1482, and 3) to demonstrate that levels of ER stress are increased compared to wild type. Specifically, we need to test the hypothesis that overexpression of BMEI1482 drives UPR activation and autophagy biogenesis. The observation that bacterial strains that ectopically express BMEI1482 possess a smooth phenotype and display upregulation in the expression of UPR and autophagy biogenesis transcripts, will support my working hypothesis.

The studies that tried to assign molecular mechanisms to *Brucella* effectors have been limited to demonstrating that an effector-host protein interaction leads to a disruption of the ER secretory pathway (Miller et al., 2017; Myeni et al., 2013). These studies have largely focused on showing that effectors induce the UPR response through the IRE1α-XBP1 arm, one of the three protein quality systems involved in ER homeostasis during protein misfolding (de Jong et al., 2013; Keestra-Gounder et al., 2016; Luizet et al., 2019). The studies proposed that *Brucella* needs to induce ER stress to either tether host vacuoles to the bacterial BCV for nutrition, replication and trafficking or to modulate pro-inflammatory responses to avoid being killed by the host. However, the cell biology of infection and host-pathogen interactions can introduce complexities. During bacterial infection there is a spatiotemporal dimension to the

expression of effectors. In addition, effectors with potential redundant activities may confound experimental interrogation. Finally, some effectors may target a broad range of host factors, further complicating the analysis. Such effector-host interactions are simultaneously 1) working for the benefit of the bacteria, 2) keeping the host alive as a strategy to preserve the intracellular lifestyle of the pathogen and 3) modulating cellular defense mechanisms. Based on these ideas, it is feasible to consider that the three known protein quality control systems: 1) the classical molecular chaperone system, 2) the glycan-dependent molecular chaperone system and 3) the thiol-dependent oxidoreductases, that work simultaneously to maintain cell homeostasis (Adams et al., 2019), have equal chances to be targeted by effector proteins in an attempt to achieve bacterial survival, replication and spreading.

In my project, data obtained from a high-throughput genetic interaction profiling screen obtained by ectopically expression of BMEI1482 in yeast (EMAP approach) (Patrick et al., 2018) coupled with an *in vitro* biochemical approach allowed to uncover a novel cellular pathway targeted by BMEI1482 (the OST pathway). The OST complex was found to be a molecular target of BMEI1482.

The OST complex is responsible for the N-glycosylation of secretory proteins and is part of "the glycan-dependent molecular chaperone system", a protein quality control system. The OST complex transfers preformed glycans to asparagine residues in newly synthesized secretory proteins as part of a co- and post-translational modification system that regulates protein solubility, trafficking, and function (Mohorko et al., 2011). Modulation of the N-glycome is emerging as an important feature by which pathogens

either invade or sustain infection by bacterial pathogens (Kreisman and Cobb, 2012). *Salmonella* changes the host N-glycome, specifically by diminishing sialic acid structures on cell receptors during invasion (Park et al., 2016), *Mycobacterium tuberculosis* increases host cell N-glycan density, changes the N-glycoproteome, upregulates OST complex expression, and down-regulates glycosylation processing enzymes to sustain infection (Hare et al., 2017). Despite these observations, no microbial effector is known to specifically target the OST complex to modulate its activity.

To date, reprogramming of the host N-glycome has not been suggested to promote *Brucella melitensis* intracellular survival or replication. Interestingly, in my study, we demonstrated that the glycoproteome is differentially modulated during wild type *Brucella* infection, a phenotype that is consistent with previous observations in other bacterial pathogens (Hare et al., 2017; Park et al., 2016). Contrary to previous studies, however, our data suggested that the effector BMEI1482 is specifically involved in N-glycome reprogramming, since an absence of BMEI1482 showed an increase in glycoproteome expression while its ectopically expression decreased it. An in-depth glycome analysis showed that specific glycans such as N-acetylgalactosamine, N-acetylglucosamine, galactose and mannose were differentially modulated by BMEI1482. However, considering that lectins detect glycans bound to the entire protein structure, the observed differences in relative florescence glycan signals (RFG) could also be attributed to a proteome up- or down-regulation. In support of this, studies have demonstrated a modulation of host proteome during *Brucella* infection (Rossetti et al., 2009) and the modulated host proteome phenotype has been linked to the host UPR

response (Smith et al., 2013; Taguchi et al., 2015). In addition, reports have shown that a compound-activated UPR response modulates the host proteome, and the host N-glycoproteome (Cherepanova et al., 2016; Wong et al., 2018). In these cases, the phenotypes result from ER stress.

The bacterial replication deficiency observed in BMDMs, coupled with the observed host N-glycoproteome modulation, suggest that wild type expression levels of *B. melitensis* effector BMEI1482 drive the reprogramming of the host glycosylation machinery. Based on these observations, I hypothesize that effector BMEI1482 induces mild levels of protein misfolding through a reprogramming of host N-glycosylation to activate a regulated ER stress response to create a bacterial niche, such as autophagosome for nutrient acquisition and replication. To begin to dissect this possible mechanism, we can pursue several lines of investigation.

First, Mark Lehrman and colleagues (Lu et al., 2018) have developed assays to directly measure OST activity. These assay systems could be used to directly test the transfer efficiency of the glycan substrate ($Glc_3Man_9GlcNAc_2$) by the host OST complex in cells either infected with the pathogen and/or that ectopically express the effector BMEI1482. The observation that OST activity is either increased or decreased in these cells would support our hypothesis that interactions between the OST complex and the effector BMEI1482 modulates glycan transfer. Second, experiments performed with cells treated with chemical compounds, such as tunicamycin, which inhibits the transfer of N-GlcNAc to the OST complex substrates, and subsequently expressing BMEI1482, could show whether the presence of BMEI1482 rescues the otherwise inhibited glycan

transferase activity of the OST complex. A rescued glycan-transferase phenotype will demonstrate that the effector BMEI1482 is involved in an upstream event that transfers glycans to OST complex substrates, suggesting a role in reprogramming host N-glycosylation. Finally, glycoproteome analysis of previously mentioned experiments where either OST activity is affected or rescued by BMEI1482 expression could give insight into the set of proteins that are differentially glycosylated during bacterial infection.

To determine N-glycome abundance and glycan isomer distribution during ectopic expression of BMEI1482 we collaborated with the laboratory of Yehia Mechref (Peng et al., 2019), who used an LC-MS/MS approach to characterize the host cell glycome under various conditions. We observed that BMEI1482 expression decreased the global abundance of the N-glycome. Studies have demonstrated that protein quality control pathways control the accurate and efficient N-glycosylation of proteins, and consequently, correct protein folding (Adams et al., 2019). Defects in the dolichol oligosaccharide assembly pathway or mutations/disruptions in oligosaccharyltransferase subunits cause protein hypoglycosylation, leading into protein misfolding and induction of the UPR pathway (Cherepanova et al., 2016; Denecke and Kranz, 2009; Shrimal et al., 2013; So, 2018; Wong et al., 2018).Accumulation of hypoglycosylated-misfolded proteins activate the UPR sensor proteins IRE1, PERK, and ATF6 to upregulate protein folding machinery to decrease the burden of misfolded proteins while inducing the ER associated degradation response (ERAD) to degrade misfolded proteins and mitigate ER stress (Dewal et al., 2015; Lamriben et al., 2016; Wong et al., 2018). In addition, another

study demonstrated that alteration of the glycosylation pattern interferes with the subcellular trafficking of proteins (Blackburn et al., 2019; Vieira et al., 2019). Based on these observations, I hypothesize that the ectopic expression of BMEI1482 either 1) downregulate the expression of oligosaccharyltransferase subunits involved in glycan transference or 2) downregulate the expression of glycosylation processing enzymes involved in glycan formation. In either case, ER stress via activation of the UPR-IRE1α-XBP1-ERAD response to hypoglycosylated-misfolded proteins will ensue. Both hypotheses are supported by 1) the observed genetic interaction profile obtained from EMAP, 2) the interaction of BMEI1482 with subunits of the OST complex (RPN1/RPN2) and 3) the disruption of the secretory pathway by ectopic expression of BMEI1482. To further test my hypotheses, it would be necessary to determine the expression levels of the oligosaccharyltransferase subunits (OST complex) and glycosylation processing enzymes. Possible treatments involve 1) cells that ectopically express BMEI1482 accompanied by controls VceC (BMEI0948), an effector that does not interact with the OST complex, and empty vector, 2) cells infected, specifically using strains in which the BMEI1482 gene has been deleted, ectopically expression and wild type levels of effector BMEI1482 and 3) cells infected with intracellular pathogens that do not interact with the ER to form a replicative niche (i.e. *Coxiella, Chlamydia*) and that have not been reported to modulate N-glycosylation during infection.

The second part of my hypothesis suggests that the downregulation of oligosaccharyltransferase subunits (OST complex) and glycosylation processing enzymes by wild-type expression levels of BMEI1482 leads into a regulated ER stress-

ERAD response coupled with autophagy that promote bacterial replication by the provision of nutrition. Alternatively, I suggest that ectopically expression of effector BMEI1482 causes an upregulated and sustained ER stress-autophagy that leads to apoptosis (Brumell, 2012; Glick et al., 2010; Gump and Thorburn, 2011). Based on these ideas, the decrease in host N-glycome abundance could be attributed to a decrease in viable cell numbers due to a cytotoxicity effect, as well. To test whether BMEI1482 induces ER stress that specifically activates the UPR-IRE1α-XBP1-ERAD arm, we can measure the IRE1α splicing of XBP1, and the expression of UPR genes and ERAD genes (i.e. chaperones, caspases, pro-inflammatory response, other genes). To learn how this activation is related to the decreased host N-glycome abundance, we can analyze the host N-glycoproteome and N-glycome abundance of cells expressing BMEI1482 and that present an ER stress phenotype. Key treatments could potentially involve 1) ectopic expression of BMEI1482 with controls VceC and empty vectors, 2) bacterial infection using strains in which the BMEI1482 gene has been deleted, ectopic expression and wild type levels, 3) bacterial infection using strains in which VceC has been deleted, and ectopic expression, to discern the specific role of BMEI1482, and 4) bacterial infection using other intracellular pathogens that do not replicative niches in the ER (i.e. *Coxiella, Chlamydia*). An analysis of the results from these treatments could potentially be complemented by an overall host N-glycome abundance analysis.

Another important observation to consider in our analysis is the fact that BMEI1482 reprogrammed the glycan isomer distribution by increasing fucosylated and fucosylated-sialylated isomers and decreasing high mannose and sialylated isomers.

Studies have demonstrated that catalytic subunits (STT3A/STT3B) of the OST complex are glycan specific (Mohorko et al., 2011) and that mutations and or disturbances in STT3A can cause protein hypoglycosylation (Shrimal et al., 2013). In support of this possibility, studies have shown a direct interaction between ribophorins (RPNI and RPNII, accessory subunits of OST complex) and ribosomes (Mohorko et al., 2011). The cytosolic domain of ribophorins provides binding sites for the translating ribosomes and enables co-translational glycosylation of entering polypeptides (Kreibich et al., 1978). It has also been shown that RPNI is involved in the utilization of certain glycosylation sites on defined polypeptides, whereas RPNII is involved in modulation of glycosylation for a proper functional activity of proteins (Honma et al., 2008; (Wilson and High, 2007) Data obtained from our immunoprecipitation experiments coupled with findings from LC-MS/MS studies showed that BMEI1482 interacts with RPNI and RPNII (both subunits of OST complex). Therefore, it is possible to hypothesize that BMEI1482 is either mimicking or modulating RPNI and RPNII activities to reprogram the N-glycan isomer distribution to sustain bacterial nutrition and replication. To test this hypothesis, cells in which the expression of RPNI and RPNII is knocked down and subsequently infected with the pathogen could demonstrate 1) whether the RPNI and RPNII are necessary for bacterial replication, 2) whether BMEI142 expression rescues the affected co-translational glycosylation phenotype and 3) whether BMEI1482 specifically reprograms the host N-glycan distribution. Key controls for these experiments will include ectopic expression of 1) a well-characterized *Brucella* effector such as VceC (BMEI0948) that is involved in the ER stress but does not interact with OST complex and 2) empty vector

controls. Key controls for experiments that require bacterial infection are 1) the use of the effector (BMEI1482) mutant strain, ectopic expression of effector (BMEI1482) bacterial strain, other well studied effector (VceC) mutant strain and the wild type bacterial strain and 2) the use of other intracellular bacteria.

To understand the consequence of the observed glycan isomer distribution by the BMEI1482::OST complex interaction, it is necessary to consider the needs of the bacterium for survival and replication. Studies have shown that *Brucella* has an operon that is activated by fucose to express virulence factors and thereby control bacterial metabolism (Budnick et al., 2018). This activation presumably promotes survival and replication in macrophages and colonization of the spleens of mice (Budnick et al., 2018). Additional studies have shown that surface proteins (SPs) of *Brucella* require the presence of sialic acid on host surface receptors for bacterial adhesion (Castaneda-Roldan et al., 2004; Castaneda-Roldan et al., 2006). On the other hand, high-mannose acts as a tag to facilitate protein processing and folding (Hebert et al., 2005). Mannose structures are processed as proteins fold and traffic in the secretory pathway. Aberrant processing, which may result in the overexpression of high mannose structures on cell surface receptors is characteristic of damaged cells (Adams et al., 2019). Based on these observations, I hypothesize that *Brucella melitensis* is specifically using differential expression of BMEI1482-induced fucosylated and fucosylated-sialylated isomers to activate the bacterial fucose operon and drive the expression of virulence and metabolic factors involved in the survival and replication of the bacterium in host cells. In addition, I hypothesize that the observed BMEI1482-dependent decrease in high-mannose and

sialylated isomers is a downstream effect of ER stress caused by the bacteria to sustain replication. Future studies that examine bacterial carbohydrate metabolism will interrogate these possibilities.

Campylobacter jejuni has a unique N-linked protein glycosylation (pgl) system that regulates virulence. The pgl system is encoded by the pgl operon that consists of 12 genes encoding glycosyltransferases and sugar biosynthetic enzymes to generate a lipid-linked heptasaccharide precursor (Linton et al., 2005; Lu et al., 2015). The pgl system expresses a subunit PglB that transfers glycan onto the target asparagine (Lu et al., 2015). PglB is a structural homologue of the STT3 catalytic subunit of *Saccharomyces cerevisiae* oligosaccharyltransferase complex (Linton et al., 2005; Lu et al., 2015). Genetic mutations in PglB disrupt protein glycosylation and results in diminished *C. jejuni* adhesion and invasion of host cells; consequently, reduced bacterial colonization of mice is observed (Linton et al., 2005; Lu et al., 2015). The authors proposed that Pgl-mediated N glycosylation of *C jejuni* surface proteins may function to protect bacterial proteins from digestion by proteases and promoting bacterial fitness to sustain infection (Linton et al., 2005; Lu et al., 2015). In addition, the authors suggested that the free oligosaccharides generated from the Pgl pathway have a function in bacterial osmotic protection (Linton et al., 2005; Lu et al., 2015).

With these ideas in mind, it is intriguing to speculate that BMEI1482 is transferring glycans to bacterial membrane proteins and/or BVC vacuoles. I propose that the goal of this transferase activity would be either 1) to promote bacterial fitness, by using sugar blocs to express virulence and metabolism factors or 2) to sustain bacterial

infection by mimicking protein-sugar structures of host organelle membranes to evade host killing mechanisms. Further studies that provide high resolution information about the subcellular localization BMEI1482, and analysis of its membrane glycan structure, in infected cells will help answer this question. In addition, studies that interrogate the glycosylation patterns of BCV-containing membrane proteins will enable a better understanding of these processes.

Considering that effector BMEI1482 1) interacts with OST complex, 2) reprograms N-glycome and N-glycoproteome, 3) disturbs secretory pathway and 4) decreases the *B. melitensis* replication in host, a hypothetical working model was developed. I propose that wild-type levels of expression of effector BMEI1482 modulates glycosylation to activate autophagy through an UPR response (IRE1α-XBP1-ERAD). The purpose of the activated autophagy is to recycle hypoglycosylated and misfolded proteins by trimming them into small blocks that are used by *Brucella* for replication. In addition, I propose that ectopically expression levels of effector BMEI1482 decreases *Brucella* numbers due to an exacerbated ER stress response with a sustained autophagy that eventually send signals for apoptosis (Figure 4.1).

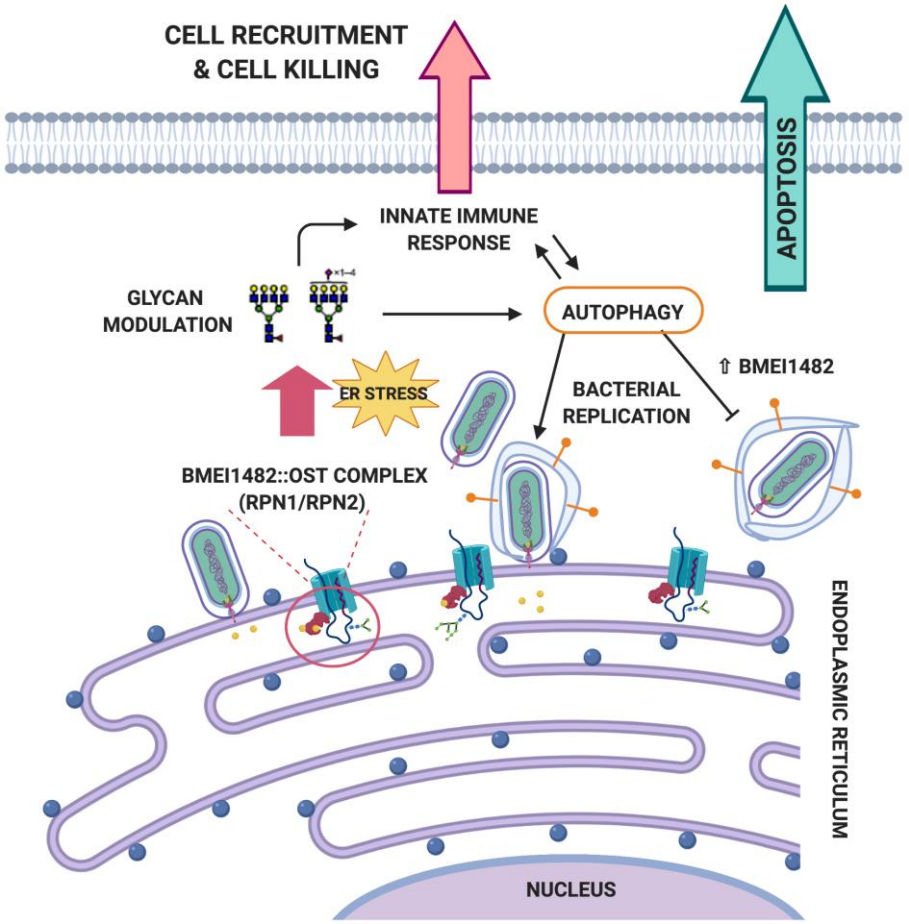

Figure 4.1 Future perspective hypothetical model of how effector BMEI1482 reprograms host N-glycome to sustain bacterial infection. Effector BMEI1482 is translocated by *vir*B-T4SS, interacts with N-glycosylation complex (The OST complex) and disrupts secretory pathway (ER stress). Effector BMEI1482 specifically interacts with RPN1 and RPN2 subunits of OST complex and modulates glycan isomer distribution. For one side, the overexpression of BMEI1482 reprograms the glycan isomer distribution and turns on the immune response signal for detection of infected cells. On the other side, the ER stress caused by BMEI1482::OST complex interaction and glycan isomer reprogramming turns on autophagy to sustain bacterial replication. If overexpression of effector BMEI1482, the autophagy signal is sustained, and apoptosis is turned on. This leads into host cell death which leads into a decreased bacterial number.

REFERENCES

Adams, B.M., Oster, M.E., and Hebert, D.N. (2019). Protein Quality Control in the Endoplasmic Reticulum. Protein J *38*, 317-329.

Alvarez-Martinez, C.E., and Christie, P.J. (2009). Biological diversity of prokaryotic type IV secretion systems. Microbiol Mol Biol Rev *73*, 775-808.

Anderson, D.M., and Frank, D.W. (2012). Five mechanisms of manipulation by bacterial effectors: a ubiquitous theme. PLoS Pathog *8*, e1002823.

Atluri, V.L., Xavier, M.N., de Jong, M.F., den Hartigh, A.B., and Tsolis, R.M. (2011). Interactions of the human pathogenic Brucella species with their hosts. Annu Rev Microbiol *65*, 523-541.

Backert, S., and Meyer, T.F. (2006). Type IV secretion systems and their effectors in bacterial pathogenesis. Curr Opin Microbiol *9*, 207-217.

Blackburn, J.B., D'Souza, Z., and Lupashin, V.V. (2019). Maintaining order: COG complex controls Golgi trafficking, processing, and sorting. FEBS Lett *593*, 2466-2487.

Boschiroli, M.L., Ouahrani-Bettache, S., Foulongne, V., Michaux-Charachon, S., Bourg, G., Allardet-Servent, A., Cazevieille, C., Liautard, J.P., Ramuz, M., and O'Callaghan, D. (2001). The Brucella suis virB operon is induced intracellularly in macrophages. PNAS *99*, 1544-1549.

Brumell, J.H. (2012). Brucella "hitches a ride" with autophagy. Cell Host Microbe *11*, 2-4.

Budnick, J.A., Sheehan, L.M., Kang, L., Michalak, P., and Caswell, C.C. (2018). Characterization of Three Small Proteins in Brucella abortus Linked to Fucose Utilization. J Bacteriol *200*.

Burstein, D., Satanower, S., Simovitch, M., Belnik, Y., Zehavi, M., Yerushalmi, G., Ben-Aroya, S., Pupko, T., and Banin, E. (2015). Novel type III effectors in Pseudomonas aeruginosa. MBio *6*, e00161.

Byndloss, M.X., and Tsolis, R.M. (2016). Brucella spp. Virulence Factors and Immunity. Annu Rev Anim Biosci *4*, 111-127.

Castaneda-Roldan, E.I., Avelino-Flores, F., Dall'Agnol, M., Freer, E., Cedillo, L., Dornand, J., and Giron, J.A. (2004). Adherence of Brucella to human epithelial cells and macrophages is mediated by sialic acid residues. Cell Microbiol *6*, 435-445.

Castaneda-Roldan, E.I., Ouahrani-Bettache, S., Saldana, Z., Avelino, F., Rendon, M.A., Dornand, J., and Giron, J.A. (2006). Characterization of SP41, a surface protein of Brucella associated with adherence and invasion of host epithelial cells. Cell Microbiol *8*, 1877-1887.

Celli, J. (2015). The changing nature of the Brucella-containing vacuole. Cell Microbiol *17*, 951-958.

Celli, J., de Chastellier, C., Franchini, D.M., Pizarro-Cerda, J., Moreno, E., and Gorvel, J.P. (2003). Brucella evades macrophage killing via VirB-dependent sustained interactions with the endoplasmic reticulum. J Exp Med *198*, 545-556.

Celli, J., and Tsolis, R.M. (2015). Bacteria, the endoplasmic reticulum and the unfolded protein response: friends or foes? Nat Rev Microbiol *13*, 71-82.

Charpentier, X., and Oswald, E. (2004). Identification of the secretion and translocation domain of the enteropathogenic and enterohemorrhagic E coli Effector Cif, using TEM-1 B-Lactamase as a new fluorescence-based reporter. J Bacteriol *186*, 5486–5495.

Chen, C., Banga, S., Mertens, K., Weber, M.M., Gorbaslieva, I., Tan, Y., Luo, Z.Q., and Samuel, J.E. (2010). Large-scale identification and translocation of type IV secretion substrates by Coxiella burnetii. Proc Natl Acad Sci U S A *107*, 21755-21760.

Cherepanova, N., Shrimal, S., and Gilmore, R. (2016). N-linked glycosylation and homeostasis of the endoplasmic reticulum. Curr Opin Cell Biol *41*, 57-65.

Collins, S.R., Schuldiner, M., Krogan, N.J., and Weissman, J.S. (2006). A strategy for extracting and analyzing large-scale quantitative epistatic interaction data. Genome Biol *7*, R63.

de Barsy, M., Jamet, A., Filopon, D., Nicolas, C., Laloux, G., Rual, J.F., Muller, A., Twizere, J.C., Nkengfac, B., Vandenhaute, J., *et al.* (2011). Identification of a Brucella spp. secreted effector specifically interacting with human small GTPase Rab2. Cell Microbiol *13*, 1044-1058.

de Felipe, K.S., Glover, R.T., Charpentier, X., Anderson, O.R., Reyes, M., Pericone, C.D., and Shuman, H.A. (2008). Legionella eukaryotic-like type IV substrates interfere with organelle trafficking. PLoS Pathog *4*, e1000117.

de Figueiredo, P., Ficht, T.A., Rice-Ficht, A., Rossetti, C.A., and Adams, L.G. (2015). Pathogenesis and immunobiology of brucellosis: review of Brucella-host interactions. Am J Pathol *185*, 1505-1517.

de Jong, M.F., Rolan, H.G., and Tsolis, R.M. (2010). Innate immune encounters of the (Type) 4th kind: Brucella. Cell Microbiol *12*, 1195-1202.

de Jong, M.F., Starr, T., Winter, M.G., den Hartigh, A.B., Child, R., Knodler, L.A., van Dijl, J.M., Celli, J., and Tsolis, R.M. (2013). Sensing of bacterial type IV secretion via the unfolded protein response. MBio *4*, e00418-00412.

de Jong, M.F., Sun, Y.H., den Hartigh, A.B., van Dijl, J.M., and Tsolis, R.M. (2008). Identification of VceA and VceC, two members of the VjbR regulon that are translocated into macrophages by the Brucella type IV secretion system. Mol Microbiol *70*, 1378-1396.

de Jong, M.F., and Tsolis, R.M. (2012). Brucellosis and the type IV secretion system. Future Microbiol *7*, 47-58.

Delrue, R.M., Deschamps, C., Leonard, S., Nijskens, C., Danese, I., Schaus, J.M., Bonnot, S., Ferooz, J., Tibor, A., De Bolle, X., *et al.* (2005). A quorum-sensing regulator controls expression of both the type IV secretion system and the flagellar apparatus of Brucella melitensis. Cell Microbiol *7*, 1151-1161.

Denecke, J., and Kranz, C. (2009). Hypoglycosylation due to dolichol metabolism defects. Biochim Biophys Acta *1792*, 888-895.

Dewal, M.B., DiChiara, A.S., Antonopoulos, A., Taylor, R.J., Harmon, C.J., Haslam, S.M., Dell, A., and Shoulders, M.D. (2015). XBP1s Links the Unfolded Protein Response to the Molecular Architecture of Mature N-Glycans. Chem Biol *22*, 1301-1312.

Dohmer, P.H., Valguarnera, E., Czibener, C., and Ugalde, J.E. (2014). Identification of a type IV secretion substrate of Brucella abortus that participates in the early stages of intracellular survival. Cell Microbiol *16*, 396-410.

Esmaeili, H. (2014). Brucellosis in Islamic republic of Iran. J Med Bacteriol *3*, 47-57.

Ficht, T.A., and Adams, G.L. (2009). Brucellosis. In Vaccines for Biodefense and Emerging and Neglected Diseases, L.R.S. Alan D.T. Barrett, ed. (London, UK and Amsterdam, The Netherlands: Elsevier), pp. 807-829.

Foulongne, V., Bourg, G., Cazevieille, C., Michaux-Charachon, S., and O'Callaghan, D. (2000). Identification of Brucella suis Genes Affecting Intracellular Survival in an In Vitro Human Macrophage Infection Model by Signature-Tagged Transposon Mutagenesis. Infect Immun *68*, 1297-1303.

Franc, K.A., Krecek, R.C., Hasler, B.N., and Arenas-Gamboa, A.M. (2018). Brucellosis remains a neglected disease in the developing world: a call for interdisciplinary action. BMC Public Health *18*, 125.

Glick, D., Barth, S., and Macleod, K.F. (2010). Autophagy: cellular and molecular mechanisms. J Pathol *221*, 3-12.

Gordon, D.E., Bond, L.M., Sahlender, D.A., and Peden, A.A. (2010). A targeted siRNA screen to identify SNAREs required for constitutive secretion in mammalian cells. Traffic *11*, 1191-1204.

Graham, D.B., Lefkovith, A., Deelen, P., de Klein, N., Varma, M., Boroughs, A., Desch, A.N., Ng, A.C.Y., Guzman, G., Schenone, M., *et al.* (2016). TMEM258 Is a Component of the Oligosaccharyltransferase Complex Controlling ER Stress and Intestinal Inflammation. Cell Rep *17*, 2955-2965.

Grilló, M.J., Blasco, J.M., Gorvel, J.P., Moriyón, I., and Moreno, E. (2012). What have we learned from brucellosis in the mouse model? Veterinary Research *43*, 1-35.

Gump, J.M., and Thorburn, A. (2011). Autophagy and apoptosis: what is the connection? Trends Cell Biol *21*, 387-392.

Hare, N.J., Lee, L.Y., Loke, I., Britton, W.J., Saunders, B.M., and Thaysen-Andersen, M. (2017). Mycobacterium tuberculosis Infection Manipulates the Glycosylation Machinery and the N-Glycoproteome of Human Macrophages and Their Microparticles. J Proteome Res *16*, 247-263.

Herrou, J., and Crosson, S. (2013). Molecular structure of the Brucella abortus metalloprotein RicA, a Rab2-binding virulence effector. Biochemistry *52*, 9020-9028.

Hicks, S.W., and Galan, J.E. (2013). Exploitation of eukaryotic subcellular targeting mechanisms by bacterial effectors. Nat Rev Microbiol *11*, 316-326.

Hong, P.C., Tsolis, R.M., and Ficht, T.A. (2000). Identification of genes required for chronic persitence of B abortus in mice. Infect Immun *68*, 4102-4107.

Hu, S., and Wong, D.T. (2009). Lectin microarray. Proteomics Clin Appl *3*, 148-154.

Kahl-McDonagh, M.M., and Ficht, T.A. (2006). Evaluation of protection afforded by Brucella abortus and Brucella melitensis unmarked deletion mutants exhibiting different rates of clearance in BALB/c mice. Infect Immun *74*, 4048-4057.

Kahsay, R.Y., Gao, G., and Liao, L. (2005). An improved hidden Markov model for transmembrane protein detection and topology prediction and its applications to complete genomes. Bioinformatics *21*, 1853-1858.

Ke, Y., Wang, Y., Li, W., and Chen, Z. (2015). Type IV secretion system of Brucella spp. and its effectors. Front Cell Infect Microbiol *5*, 72.

Keestra-Gounder, A.M., Byndloss, M.X., Seyffert, N., Young, B.M., Chavez-Arroyo, A., Tsai, A.Y., Cevallos, S.A., Winter, M.G., Pham, O.H., Tiffany, C.R., *et al.* (2016). NOD1 and NOD2 signalling links ER stress with inflammation. Nature *532*, 394-397.

Kreibich, G., Freienstein, C.M., Pereyra, C., Ulrich, B.L., and Sabatini, D.D. (1978). Proteins of rough microsomal membranes related to ribosome binding. J Cell Biology *77*, 488-506.

Kreisman, L.S., and Cobb, B.A. (2012). Infection, inflammation and host carbohydrates: a Glyco-Evasion Hypothesis. Glycobiology *22*, 1019-1030.

Krishnan, S., Liu, F., Abrol, R., Hodges, J., Goddard, W.A., 3rd, and Prasadarao, N.V. (2014). The interaction of N-glycans in Fcgamma receptor I alpha-chain with Escherichia coli K1 outer membrane protein A for entry into macrophages: experimental and computational analysis. J Biol Chem *289*, 30937-30949.

Lacerda, T.L., Salcedo, S.P., and Gorvel, J.P. (2013). Brucella T4SS: the VIP pass inside host cells. Curr Opin Microbiol *16*, 45-51.

Lamriben, L., Graham, J.B., Adams, B.M., and Hebert, D.N. (2016). N-Glycan-based ER Molecular Chaperone and Protein Quality Control System: The Calnexin Binding Cycle. Traffic *17*, 308-326.

Larson, C.L., Beare, P.A., Voth, D.E., Howe, D., Cockrell, D.C., Bastidas, R.J., Valdivia, R.H., and Heinzen, R.A. (2015). Coxiella burnetii effector proteins that localize to the parasitophorous vacuole membrane promote intracellular replication. Infect Immun *83*, 661-670.

Lauc, G., Pezer, M., Rudan, I., and Campbell, H. (2016). Mechanisms of disease: The human N-glycome. Biochim Biophys Acta *1860*, 1574-1582.

Lesser, C.F., and Miller, S.I. (2001). Expression of microbial virulence proteins in S cerevisiae models mammalian infection The EMBO journal *20*, 1840-1849.

Li, P., Tian, M., Bao, Y., Hu, H., Liu, J., Yin, Y., Ding, C., Wang, S., and Yu, S. (2017). Brucella Rough Mutant Induce Macrophage Death via Activating IRE1alpha Pathway of Endoplasmic Reticulum Stress by Enhanced T4SS Secretion. Front Cell Infect Microbiol *7*, 422.

Linton, D., Dorrell, N., Hitchen, P.G., Amber, S., Karlyshev, A.V., Morris, H.R., Dell, A., Valvano, M.A., Aebi, M., and Wren, B.W. (2005). Functional analysis of the Campylobacter jejuni N-linked protein glycosylation pathway. Mol Microbiol *55*, 1695-1703.

Loke, I., Kolarich, D., Packer, N.H., and Thaysen-Andersen, M. (2016). Emerging roles of protein mannosylation in inflammation and infection. Mol Aspects Med *51*, 31-55.

Lopez-Sambrooks, C., Shrimal, S., Khodier, C., Flaherty, P.D., Rinis, N., Charest, J.C., Gao, N., Zhao, P., Wells, L., Lewis, T.A., *et al.* (2016). Oligosaccharyltransferase inhibition induces senescence in RTK-driven tumor cells. Nature Chemical Biology *12*, 1023-1030.

Lu, H., Fermaintt, C.S., Cherepanova, N.A., Gilmore, R., Yan, N., and Lehrman, M.A. (2018). Mammalian STT3A/B oligosaccharyltransferases segregate N-glycosylation at the translocon from lipid-linked oligosaccharide hydrolysis. Proc Natl Acad Sci U S A *115*, 9557-9562.

Lu, Q., Li, S., and Shao, F. (2015). Sweet Talk: Protein Glycosylation in Bacterial Interaction With the Host. Trends Microbiol *23*, 630-641.

Luizet, J.-B., Raymond, J., Lacerda, T.L.S., Bonici, M., Lembo, F., Willemart, K., Borg, J.-P., Gorvel, J.-P., and Salcedo, S.P. (2019). Brucella effector hijacks endoplasmic reticulum quality control machinery to prevent premature egress.

Marchesini, M.I., Herrmann, C.K., Salcedo, S.P., Gorvel, J.-P., and Comerci, D.J. (2011). In search of Brucella abortus type IV secretion substrates: screening and identification of four proteins translocated into host cells through VirB system. Cellular Microbiology *13*, 1261-1274.

Marchesini, M.I., Morrone Seijo, S.M., Guaimas, F.F., and Comerci, D.J. (2016). A T4SS Effector Targets Host Cell Alpha-Enolase Contributing to Brucella abortus Intracellular Lifestyle. Front Cell Infect Microbiol *6*, 153.

Mattoo, S., Lee, Y.M., and Dixon, J.E. (2007). Interactions of bacterial effector proteins with host proteins. Curr Opin Immunol *19*, 392-401.

Meyer, D.F., Noroy, C., Moumene, A., Raffaele, S., Albina, E., and Vachiery, N. (2013). Searching algorithm for type IV secretion system effectors 1.0: a tool for predicting type IV effectors and exploring their genomic context. Nucleic Acids Res *41*, 9218-9229.

Miller, C.N., Smith, E.P., Cundiff, J.A., Knodler, L.A., Bailey Blackburn, J., Lupashin, V., and Celli, J. (2017). A Brucella Type IV Effector Targets the COG Tethering Complex to Remodel Host Secretory Traffic and Promote Intracellular Replication. Cell Host Microbe *22*, 317-329 e317.

Mohorko, E., Glockshuber, R., and Aebi, M. (2011). Oligosaccharyltransferase: the central enzyme of N-linked protein glycosylation. J Inherit Metab Dis *34*, 869-878.

Myeni, S., Child, R., Ng, T.W., Kupko, J.J., 3rd, Wehrly, T.D., Porcella, S.F., Knodler, L.A., and Celli, J. (2013). Brucella modulates secretory trafficking via multiple type IV secretion effector proteins. PLoS Pathog *9*, e1003556.

Newton, H.J., Kohler, L.J., McDonough, J.A., Temoche-Diaz, M., Crabill, E., Hartland, E.L., and Roy, C.R. (2014). A screen of Coxiella burnetii mutants reveals important roles for Dot/Icm effectors and host autophagy in vacuole biogenesis. PLoS Pathog *10*, e1004286.

Ninio, S., Celli, J., and Roy, C.R. (2009). A Legionella pneumophila effector protein encoded in a region of genomic plasticity binds to Dot/Icm-modified vacuoles. PLoS Pathog *5*, e1000278.

Nkengfac, B., Pouyez, J., Bauwens, E., Vandenhaute, J., Letesson, J.J., Wouters, J., and De Bolle, X. (2012). Structural analysis of Brucella abortus RicA substitutions that do not impair interaction with human Rab2 GTPase. BMC Biochem *13*, 16.

O'Callaghan, D., Cazevieille, B.C., Allardet-Servent, A., Boschiroli, M.L., Bourg, G., Foulongne, V., Frutos, P., Kulakov, Y., and Ramuz, M. (1999). A homologue of the Agrobacterium tumefaciens VirB and Bordetella pertussis Ptl type IV secretion systems is essential for intracellular survival of Brucella suis. Mol Microbiol *33*, 1210-1220.

Pandey, A., Cabello, A., Akoolo, L., Rice-Ficht, A., Arenas-Gamboa, A., McMurray, D., Ficht, T.A., and de Figueiredo, P. (2016). The Case for Live Attenuated Vaccines against the Neglected Zoonotic Diseases Brucellosis and Bovine Tuberculosis. PLoS Negl Trop Dis *10*, e0004572.

Pandey, A., Lin, F., Cabello, A.L., da Costa, L.F., Feng, X., Feng, H.Q., Zhang, M.Z., Iwawaki, T., Rice-Ficht, A., Ficht, T.A., *et al.* (2018). Activation of Host IRE1alpha-Dependent Signaling Axis Contributes the Intracellular Parasitism of Brucella melitensis. Front Cell Infect Microbiol *8*, 103.

Pappas, G., Papadimitriou, P., Akritidis, N., Christou, L., and Tsianos, E.V. (2006). The new global map of human brucellosis. The Lancet Infectious Diseases *6*, 91-99.

Park, D., Arabyan, N., Williams, C.C., Song, T., Mitra, A., Weimer, B.C., Maverakis, E., and Lebrilla, C.B. (2016). Salmonella Typhimurium Enzymatically Landscapes the Host Intestinal Epithelial Cell (IEC) Surface Glycome to Increase Invasion. Mol Cell Proteomics *15*, 3653-3664.

Patrick, K.L., Wojcechowskyj, J.A., Bell, S.L., Riba, M.N., Jing, T., Talmage, S., Xu, P., Cabello, A.L., Xu, J., Shales, M., *et al.* (2018). Quantitative Yeast Genetic Interaction Profiling of Bacterial Effector Proteins Uncovers a Role for the Human Retromer in Salmonella Infection. Cell Syst *7*, 323-338 e326.

Pei, J., and Ficht, T.A. (2011). Lipopolysaccharide: a complex role in the pathogenesis of brucellosis. Vet J *189*, 5-6.

Peng, W., Goli, M., Mirzaei, P., and Mechref, Y. (2019). Revealing the Biological Attributes of N-Glycan Isomers in Breast Cancer Brain Metastasis Using Porous Graphitic Carbon (PGC) Liquid Chromatography-Tandem Mass Spectrometry (LC-MS/MS). J Proteome Res *18*, 3731-3740.

Pfeffer, S., Burbaum, L., Unverdorben, P., Pech, M., Chen, Y., Zimmermann, R., Beckmann, R., and Forster, F. (2015). Structure of the native Sec61 protein-conducting channel. Nat Commun *6*, 8403.

Pfeffer, S., Dudek, J., Schaffer, M., Ng, B.G., Albert, S., Plitzko, J.M., Baumeister, W., Zimmermann, R., Freeze, H.H., Engel, B.D., *et al.* (2017). Dissecting the molecular organization of the translocon-associated protein complex. Nat Commun *8*, 14516.

Qin, Q.M., Pei, J., Ancona, V., Shaw, B.D., Ficht, T.A., and de Figueiredo, P. (2008). RNAi screen of endoplasmic reticulum-associated host factors reveals a role for IRE1alpha in supporting Brucella replication. PLoS Pathog *4*, e1000110.

Radhakrishnan, G.K., and Splitter, G.A. (2010). Biochemical and functional analysis of TIR domain containing protein from Brucella melitensis. Biochem Biophys Res Commun *397*, 59-63.

Radhakrishnan, G.K., Yu, Q., Harms, J.S., and Splitter, G.A. (2009). Brucella TIR Domain-containing Protein Mimics Properties of the Toll-like Receptor Adaptor Protein TIRAP. J Biol Chem *284*, 9892-9898.

Rossetti, C.A., Galindo, C.L., Lawhon, S.D., Garner, H.R., and Adams, L.G. (2009). Brucella melitensis global gene expression study provides novel information on growth phase-specific gene regulation with potential insights for understanding Brucella:host initial interactions. BMC Microbiol *9*, 81.

Salcedo, S.P., Chevrier, N., Lacerda, T.L., Ben Amara, A., Gerart, S., Gorvel, V.A., de Chastellier, C., Blasco, J.M., Mege, J.L., and Gorvel, J.P. (2013a). Pathogenic brucellae replicate in human trophoblasts. J Infect Dis *207*, 1075-1083.

Salcedo, S.P., Marchesini, M.I., Degos, C., Terwagne, M., Von Bargen, K., Lepidi, H., Herrmann, C.K., Santos Lacerda, T.L., Imbert, P.R., Pierre, P., *et al.* (2013b). BtpB, a novel Brucella TIR-containing effector protein with immune modulatory functions. Front Cell Infect Microbiol *3*, 28.

Salcedo, S.P., Marchesini, M.I., Lelouard, H., Fugier, E., Jolly, G., Balor, S., Muller, A., Lapaque, N., Demaria, O., Alexopoulou, L., *et al.* (2008). Brucella control of dendritic cell maturation is dependent on the TIR-containing protein Btp1. PLoS Pathog *4*, e21.

Schwarz, D.S., and Blower, M.D. (2016). The endoplasmic reticulum: structure, function and response to cellular signaling. Cell Mol Life Sci *73*, 79-94.

Shrimal, S., Ng, B.G., Losfeld, M.E., Gilmore, R., and Freeze, H.H. (2013). Mutations in STT3A and STT3B cause two congenital disorders of glycosylation. Hum Mol Genet *22*, 4638-4645.

Siggers, K.A., and Lesser, C.F. (2008). The Yeast Saccharomyces cerevisiae: a versatile model system for the identification and characterization of bacterial virulence proteins. Cell Host Microbe *4*, 8-15.

Silva, T.M., Costa, E.A., Paixao, T.A., Tsolis, R.M., and Santos, R.L. (2011). Laboratory animal models for brucellosis research. J Biomed Biotechnol *2011*, 518323.

Smith, J.A., Khan, M., Magnani, D.D., Harms, J.S., Durward, M., Radhakrishnan, G.K., Liu, Y.P., and Splitter, G.A. (2013). Brucella induces an unfolded protein response via TcpB that supports intracellular replication in macrophages. PLoS Pathog *9*, e1003785.

So, J.S. (2018). Roles of Endoplasmic Reticulum Stress in Immune Responses. Mol Cells *41*, 705-716.

Starr, T., Ng, T.W., Wehrly, T.D., Knodler, L.A., and Celli, J. (2008). Brucella intracellular replication requires trafficking through the late endosomal/lysosomal compartment. Traffic *9*, 678-694.

Taguchi, Y., Imaoka, K., Kataoka, M., Uda, A., Nakatsu, D., Horii-Okazaki, S., Kunishige, R., Kano, F., and Murata, M. (2015). Yip1A, a novel host factor for the activation of the IRE1 pathway of the unfolded protein response during Brucella infection. PLoS Pathog *11*, e1004747.

Tseng, T.T., Tyler, B.M., and Setubal, J.C. (2009). Protein secretion systems in bacterial-host associations, and their description in the Gene Ontology. BMC Microbiol *9 Suppl 1*, S2.

Turiak, L., Sugar, S., Acs, A., Toth, G., Gomory, A., Telekes, A., Vekey, K., and Drahos, L. (2019). Site-specific N-glycosylation of HeLa cell glycoproteins. Sci Rep *9*, 14822.

Vieira, V., Peixoto, B., Costa, M., Pereira, S., Pissarra, J., and Pereira, C. (2019). N-Linked Glycosylation Modulates Golgi-Independent Vacuolar Sorting Mediated by the Plant Specific Insert. Plants (Basel) *8*.

Vilchez, G., Espinoza, M., D'Onadio, G., Saona, P., and Gotuzzo, E. (2015). Brucellosis in pregnancy: clinical aspects and obstetric outcomes. Int J Infect Dis *38*, 95-100.

von Mering, C., Jensen, L.J., Snel, B., Hooper, S.D., Krupp, M., Foglierini, M., Jouffre, N., Huynen, M.A., and Bork, P. (2005). STRING: known and predicted protein-protein associations, integrated and transferred across organisms. Nucleic Acids Res *33*, D433-437.

Voth, D.E., Broederdorf, L.J., and Graham, J.G. (2012). Bacterial Type IV secretion systems: versatile virulence machines. Future Microbiol *7*, 241-257.

Walter, P., and Ron, D. (2011). The Unfolded Protein Reponse: from stress pathway to homeostatic regulation. Science *334*, 1081-1086.

Walters, S.B., Kieckbusch, J., Nagalingam, G., Swain, A., Latham, S.L., Grau, G.E., Britton, W.J., Combes, V., and Saunders, B.M. (2013). Microparticles from mycobacteria-infected macrophages promote inflammation and cellular migration. J Immunol *190*, 669-677.

Wattam, A.R., Davis, J.J., Assaf, R., Boisvert, S., Brettin, T., Bun, C., Conrad, N., Dietrich, E.M., Disz, T., Gabbard, J.L., *et al.* (2017). Improvements to PATRIC, the all-bacterial Bioinformatics Database and Analysis Resource Center. Nucleic Acids Res *45*, D535-D542.

Weber, M.M., Chen, C., Rowin, K., Mertens, K., Galvan, G., Zhi, H., Dealing, C.M., Roman, V.A., Banga, S., Tan, Y., *et al.* (2013). Identification of Coxiella burnetii type IV secretion substrates required for intracellular replication and Coxiella-containing vacuole formation. J Bacteriol *195*, 3914-3924.

Weber, M.M., and Faris, R. (2018). Subversion of the Endocytic and Secretory Pathways by Bacterial Effector Proteins. Front Cell Dev Biol *6*, 1.

Welch, M.D. (2015). Why should cell biologists study microbial pathogens? Mol Biol Cell *26*, 4295-4301.

Wilson, C.M., and High, S. (2007). Ribophorin I acts as a substrate-specific facilitator of N-glycosylation. J Cell Sci *120*, 648-657.

Wolters, M., Zobiak, B., Nauth, T., and Aepfelbacher, M. (2015). Analysis of Yersinia enterocolitica Effector Translocation into Host Cells Using Beta-lactamase Effector Fusions. J Vis Exp.

Wong, M.Y., Chen, K., Antonopoulos, A., Kasper, B.T., Dewal, M.B., Taylor, R.J., Whittaker, C.A., Hein, P.P., Dell, A., Genereux, J.C., *et al.* (2018). XBP1s activation can globally remodel N-glycan structure distribution patterns. Proc Natl Acad Sci U S A *115*, E10089-E10098.

Zhao, Y., Hu, J., Miao, G., Qu, L., Wang, Z., Li, G., Lv, P., Ma, D., and Chen, Y. (2013). Transmembrane protein 208: a novel ER-localized protein that regulates autophagy and ER stress. PLoS One *8*, e64228.